DIRECT STATISTICAL ANALYSIS OF MISSILE GUIDANCE SYSTEMS VIA CADET (COVARIANCE ANALYSIS DESCRIBING FUNCTION TECHNIQUE)

James H. Taylor, et al

Analytic Sciences Corporation
Reading, Massachusetts

1 August 1974

AD 783098

6 JACOB WAY/READING, MASSACHUSETTS 01867 (617) 944-6850

UNCLASSIFIED
Security Classification

AD 783098

DOCUMENT CONTROL DATA - R & D

(Security classification of title, body of abstract and indexing annotation must be entered when the overall report is classified)

1. ORIGINATING ACTIVITY *(Corporate author)*
The Analytic Sciences Corporation
6 Jacob Way
Reading, Massachusetts 01867

2a. REPORT SECURITY CLASSIFICATION
Unclassified

2b. GROUP

3. REPORT TITLE
DIRECT STATISTICAL ANALYSIS OF MISSILE GUIDANCE SYSTEMS VIA CADET™

4. DESCRIPTIVE NOTES *(Type of report and inclusive dates)*
Final Report through 31 January 1974

5. AUTHOR(S) *(First name, middle initial, last name)*
James H. Taylor
Charles F. Price

6. REPORT DATE	7a. TOTAL NO. OF PAGES	7b. NO. OF REFS
1 August 1974	186	16

8a. CONTRACT OR GRANT NO.	9a. ORIGINATOR'S REPORT NUMBER(S)
N00014-73-C-0213	TR-385-1
b. PROJECT NO.	
c. ONR Task No. NR-215-214	9b. OTHER REPORT NO(S) *(Any other numbers that may be assigned this report)*
d.	

10. DISTRIBUTION STATEMENT
Distribution of this Report is Unlimited.

11. SUPPLEMENTARY NOTES	12. SPONSORING MILITARY ACTIVITY
	THE OFFICE OF NAVAL RESEARCH Vehicle Warfare Technology, Code 411 Arlington, Virginia 22217

13. ABSTRACT

The Covariance Analysis DEscribing Function Technique (CADET™) -- a technique conceived at TASC for the efficient direct statistical analysis of nonlinear systems with random inputs -- is extended in scope to permit the study of a complicated, highly nonlinear model for a tactical missile homing guidance system. Numerous parameter sensitivity studies are performed with selected cases verified by the monte carlo method. The validity of the assumptions underlying the CADET theory is investigated and the impact of possible errors in these assumptions on the accuracy of CADET is assessed. In every realistic situation studied, CADET provided accurate missile performance projections with a small fraction of the computer time required for a comparably reliable monte carlo analysis.

DD FORM 1 NOV 68 1473 REPLACES DD FORM 1473, 1 JAN 64, WHICH IS OBSOLETE FOR ARMY USE.

UNCLASSIFIED
Security Classification

14. KEY WORDS	LINK A		LINK B		LINK C	
	ROLE	WT	ROLE	WT	ROLE	WT
Missile Guidance Systems Covariance Analysis Nonlinear Systems Describing Functions (Random Input)						

TR-385-1

DIRECT STATISTICAL ANALYSIS OF MISSILE GUIDANCE SYSTEMS VIA CADET™

1 August 1974

Prepared Under:

Contract No. N00014-73-C-0213
(ONR Task No. NR-215-214)

for

THE OFFICE OF NAVAL RESEARCH
Vehicle Warfare Technology, Code 411
Arlington, Virginia 22217

Prepared by:

James H. Taylor
Charles F. Price

Approved by:

Arthur A. Sutherland, Jr.
Arthur Gelb

THE ANALYTIC SCIENCES CORPORATION
6 Jacob Way
Reading, Massachusetts 01867

TABLE OF CONTENTS

TABLE OF CONTENTS (Continued)

TABLE OF CONTENTS (Continued)

LIST OF FIGURES

LIST OF FIGURES (Continued)

LIST OF FIGURES (Continued)

LIST OF FIGURES (Continued)

LIST OF TABLES

1. INTRODUCTION

1.1 BACKGROUND

The development of a missile guidance system generally requires several phases, including inception, preliminary design and feasibility studies, decisions concerning implementation of various system functions, and compensation or design modification to obtain the best possible system performance under realistic constraints. In the later stages of development, the mathematical system model used as a basis for generating system performance projections almost inevitably contains nonlinear effects and random disturbances. Nonlinearity is generally associated with nonlinear relations inherent to the laws of physics, unavoidable hardware nonlinearities, and essential design nonlinearities; while random disturbances may include noise (e.g., thermal effects), sensor measurement errors, random target maneuvers, and random initial conditions. When random effects are significant, some statistical measure of system performance is required; often the root-mean-square (rms) miss distance achieved at the time of target interception is used for assessing the capability of a tactical missile.

The traditional approach used to obtain rms miss distance for guidance systems with significant nonlinearities has been the utilization of the monte carlo method. In this technique, a large number of computer simulations (trials) are made using the required nonlinear model with different initial conditions and random forcing functions generated according to the given statistics. The resulting ensemble of simulations provides the basis for making estimates of the true rms miss distance. Associated with the monte carlo method is the problem that a large number of trials is required to provide

confidence in the accuracy of the results; an ensemble as large as 1000 may be needed to obtain an accurate statistical analysis for a nonlinear system. Thus, while the monte carlo method may be useful for performing a few evaluations of a system's performance, it is not a very satisfactory tool for conducting extensive sensitivity and tradeoff studies for different values of the important guidance system parameters, or for conducting detailed studies of nonlinear effects on system performance, due to the large expenditure in computer time required. The purpose of this research is to extend an analytical technique for the direct statistical analysis of nonlinear systems which imposes a considerably smaller computational burden. This method, conceived and currently being developed by TASC, appears exceptionally promising as a means for directly treating nonlinear guidance system statistical behavior. In the sequel it is referred to as the Covariance Analysis DEscribing function Technique (CADET™).

CADET is based on the application of quasi-linearization to permit the application of covariance analysis to generate guidance system performance statistics. Thus, in treating nonlinear systems, describing function theory is used to obtain a quasi-linear approximation for each nonlinearity. The most important factor in the use of quasi-linearization is that one essential property of nonlinear elements is retained: the amplitude sensitivity of the input-output relation. Figure 1.1-1 illustrates the fundamental properties of the random input describing function for an ideal saturation or limiter.

Previous work (Refs. 1 to 3) has demonstrated the capability of CADET to perform rapid statistical analysis of complex nonlinear guidance systems, including the effects of measurement noise, parasitic coupling due to nonlinear boresight error aberration, acceleration command limiting, and highly nonlinear missile airframe dynamics. The research being undertaken in the present program entails the generalization of the basic CADET

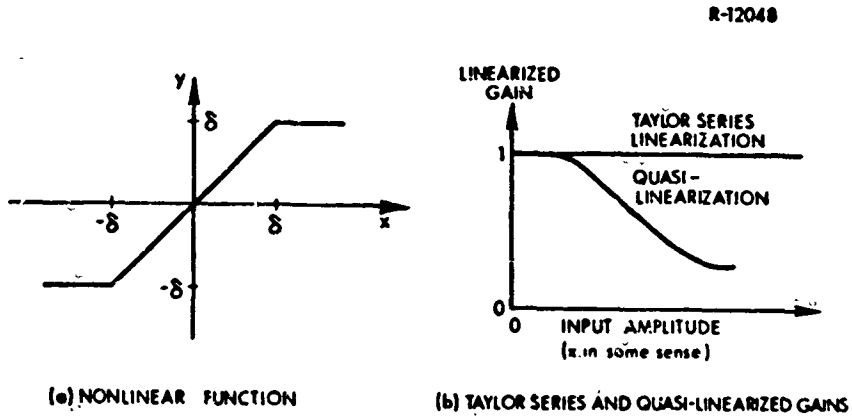

Figure 1.1-1 Illustration of Describing Function Theory: the Random Input Describing Function for a Limiter

concept to render it applicable to a very broad class of missile-target intercept problems. This will establish an essential prerequisite for the systematic investigation of guidance system performance and design -- the ability to efficiently perform detailed studies of the effects of all significant sources of system degradation and to evaluate guidance system modifications that may correct or ameliorate these deficiencies. This type of analysis would be prohibitively expensive in terms of computer time without the computational efficacy inherent to CADET.

While the primary thrust of the development is the extension and refinement of an efficient tool for the statistical evaluation of the performance of missile guidance systems, the overall scope of CADET is evidently much more general. The system model based on a nonlinear state vector differential equation with random inputs is of broad generality, being descriptive of many continuous systems with nondeterministic disturbances. The specific nonlinear effects studied herein are by no means restricted in occurrence to the missile-target intercept problem. It is hoped that the success of the present effort will encourage other applications of the CADET concept.

1.2 OVERVIEW

In order to develop CADET to meet the need for an efficient means for generating performance projections, thereby permitting the effective diagnosis and correction of potential guidance system deficiencies, the following objectives have been chosen for the present study:

- Development of a realistic missile-target intercept model with significant random effects and a number of quite diverse nonlinearities
- Development of a monte carlo simulation capability to provide performance statistics for comparison with CADET results
- Development of CADET methodology to permit the efficient generation of performance statistics for the given system model, based on the computation of describing function approximations for each nonlinearity and the application of covariance analysis to the quasi-linear system
- Verification of the ability of CADET to provide accurate performance projections by comparing the statistical analysis given by CADET with the results of corresponding monte carlo analysis
- Study of the sensitivity of CADET analysis to the assumptions and approximations made, including comparisons of describing functions for different assumed probability density functions and comparisons of histograms generated from monte carlo simulations with the density functions assumed in developing CADET

The first procedure used in developing confidence in the capability of CADET to provide accurate performance statistics is a step-by-step study of nonlinear effects. In every phase of the investigation, the CADET and monte carlo programs for statistical analysis are extended to include identical system dynamic equations, so that performance projections are

exactly comparable. The comparison of CADET and monte carlo performance projections included treating the following effects:

- The basic missile-target intercept model, with nonlinear missile-target kinematic relationships, range dependent error sources in the seeker noise model, acceleration command limiting, and nonlinear guidance law
- Seeker mass imbalance
- Nonlinear friction in the seeker gimbal
- Nonlinear restoring torques acting on the seeker head
- Nonlinear attenuation of boresight error due to the receiver/signal processing nonlinearity

Following the application of CADET to the analysis of guidance system performance, several aspects of the sensitivity problem were considered:

- Sensitivity of random input describing function calculations to changes in the nonlinearity input probability density function
- Methods for calculating approximate quasi-linear gains
- Generation of approximate histograms from data provided by a large number of monte carlo simulations to assess the impact of deviation from the gaussian assumption on CADET analysis

For reasonable initial condition statistics, the CADET-monte carlo comparison proved that CADET results were reliable -- in fact, it appears that the statistics given by monte carlo analysis are not superior to the CADET results until the number of monte carlo trials is in excess of several hundred. While the sensitivity of CADET to underlying assumptions is appreciable in some circumstances, it is gratifying to be able to demonstrate

that this effect is quite small in the present context except in somewhat unrealistic circumstances when nonlinearity inputs are highly nongaussian.

1.3 REPORT OUTLINE

This report is organized according to the following outline: Chapter 2 deals with the significant features of the CADET and monte carlo methods for generating performance statistics in nonlinear systems with random inputs; Chapter 3 treats a general discussion of the guidance system model; details of the initial verification procedure and case studies of the subsidiary nonlinear effects are given in Chapter 4; and the analysis of the sensitivity of CADET calculations to incorrect assumptions concerning nonlinearity input probability density functions is treated in Chapter 5. A summary of the study and general conclusions are provided in Chapter 6. Appendices are included to treat the technical aspects of the system model (Appendix A), random input describing function calculation (Appendix B), and CADET theory and methodology (Appendix C).

2. STATISTICAL ANALYSIS VIA MONTE CARLO AND CADET

2.1 THE MONTE CARLO TECHNIQUE

The monte carlo method for the statistical analysis of the performance of a nonlinear system with random inputs is based on direct simulation to determine the system response to "typical" initial conditions and noise input sample functions generated according to their specified statistics. Thus, the information required for this analysis is the system model, initial condition statistics, and random input statistics. The system model can be given in the form of a state vector differential equation,

$$\dot{\underline{x}} = \underline{f}(\underline{x}) + G\underline{w}(t) \qquad (2.1\text{-}1)$$

where $\underline{f}(x)$ represents the linear and nonlinear dynamic relationships in the system, $\underline{w}$ is an input vector, and the matrix G specifies the input allocation, i.e., each element* g_{ij} of G describes the effect of the input element $w_j(t)$ on the state variable derivative $\dot{x}_i$. The state vector differential equation, Eq. (2.1-1), is portrayed in block diagram notation in Fig. 2.1-1. The initial condition of the state vector is specified by assuming that the state variables are jointly normal with a given mean vector and covariance matrix†,

$$E[\underline{x}(0)] = \underline{m}_0$$
$$E[\underline{x}(0)\,\underline{x}^T(0)] = P_0 \qquad (2.1\text{-}2)$$

*For any matrix G, the quantity g_{ij} denotes the element in the i^{th} row and j^{th} column; similarly, for any column vector $\underline{w}$, w_j denotes the element in the j^{th} row.

†E[ ] denotes the expected value of the bracketed variable.

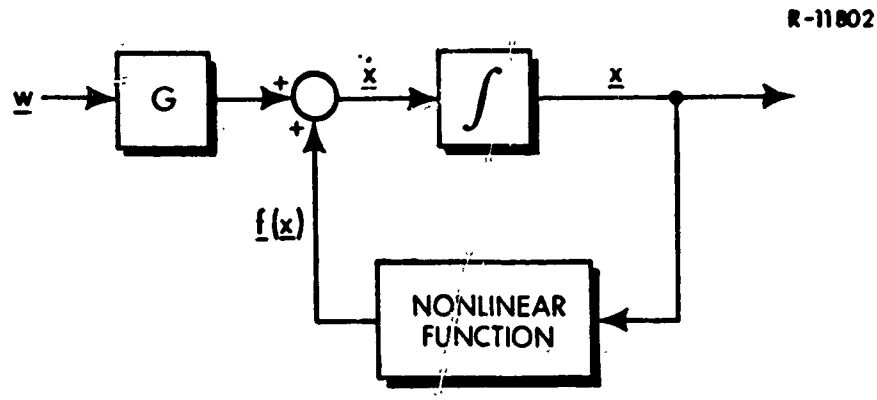

Figure 2.1-1 Nonlinear System Model

The input vector $\underline{w}$ is often assumed to be composed of elements that are independent gaussian white noises, plus an additive mean; thus

$$E[\underline{w}(t)] = \underline{b}(t)$$

$$E[(\underline{w}(t) - \underline{b}(t))(\underline{w}(\tau) - \underline{b}(\tau))^T] = Q(t)\,\delta(t-\tau) \qquad (2.1\text{-}3)$$

where $Q(t)$ is the input spectral density matrix (which is diagonal, due to independence) and the impulse function $\delta(t-\tau)$ indicates that the input vector random components have zero autocorrelation for $t \neq \tau$; i.e., the quantity $\underline{u}(t) = \underline{w}(t) - \underline{b}(t)$ is white noise.

Given the above information, monte carlo analysis requires a large number, say q, of representative simulations of the system response, viz., the q-fold repetition of the following procedure: First, an initial condition vector is chosen according to the statistics indicated above; i.e., a random number generator calculates a random vector $\underline{x}(0)$ based on Eq. (2.1-2). Then a random

initial noise vector is generated, using the statistics given in Eq. (2.1-3)*. These vectors provide the data for evaluation of $\dot{\underline{x}}(0)$ in Eq. (2.1-1) which in turn is used to propagate the solution from t = 0 to t = h according to any standard technique for the digital integration of a state vector differential equation. Then, given $\underline{x}(h)$, simulation continues by the generation of a new value of the input noise vector $\underline{w}(h)$, evaluation of $\dot{\underline{x}}(h)$, numerical integration to obtain $\underline{x}(2h)$ and so on, to the specified terminal time t_f.

Performing q independent simulations yields an ensemble of state trajectories, each denoted $\underline{x}^{(i)}(t; \underline{x}^{(i)}(0), \underline{w}^{(i)}(t))$ to stress the dependence of the trajectory on the random initial condition and noise input sample function:

$$\left.\begin{array}{l} \underline{x}^{(1)}\left(t; \underline{x}^{(1)}(0), \underline{w}^{(1)}(t)\right) \\ \underline{x}^{(2)}\left(t; \underline{x}^{(2)}(0), \underline{w}^{(2)}(t)\right) \\ \vdots \\ \underline{x}^{(q)}\left(t; \underline{x}^{(q)}(0), \underline{w}^{(q)}(t)\right) \end{array}\right\}; \; 0 \le t \le t_f \qquad (2.1\text{-}4)$$

*Neglecting the bias component, we generate a broad-band gaussian noise $u_i(t)$ with spectral density q_i by using a random number generator to obtain an independent sequence of gaussian random numbers $u_{i,k}$, $k = 0, 1, 2, \ldots$ satisfying

$$E[u_{i,k}] = 0$$

$$E[u_{i,k}^2] = q_i/h$$

Then we define $u_i(t)$ by

$$u_i(t) = u_{i,k}, \; kh \le t < (k+1)\,h$$

where h is a small time increment. For h small (1/h much larger than the bandwidth of the system in question), $u_i(t)$ is essentially a gaussian white noise process.

Each satisfies the state vector differential equation (Eq. (2.1-1)) to within the accuracy of the numerical integration method used. The mean $\underline{m}(t)$ and covariance $P(t)$ of the state vector are estimated by averaging over the ensemble of trajectories using the relations

$$\hat{\underline{m}}(t) \triangleq \frac{1}{q} \sum_{i=1}^{q} \underline{x}^{(i)}(t) \cong \underline{m}(t) \tag{2.1-5}$$

$$\hat{P}(t) \triangleq \frac{1}{q-1} \sum_{i=1}^{q} \left(\underline{x}^{(i)}(t) - \hat{\underline{m}}(t)\right)\left(\underline{x}^{(i)}(t) - \hat{\underline{m}}(t)\right)^{T} \cong P(t)$$

where $\hat{\underline{m}}(t)$ and $\hat{P}(t)$ denote the estimated values. The essence of the monte carlo technique is illustrated in Fig. 2.1-2.

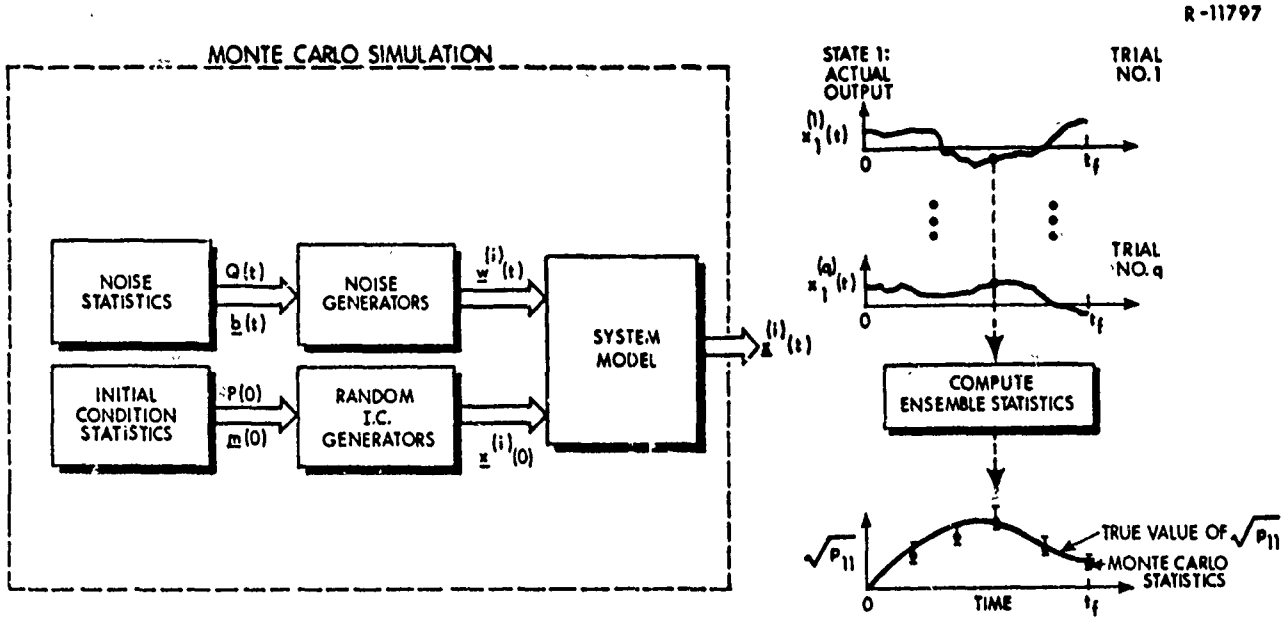

Figure 2.1-2 Schematic Characterization of the Monte Carlo Technique

In order to assess the accuracy of the approximate statistics given in Eq. (2.1-5), it is necessary to consider the statistical properties of the estimates $\hat{\underline{m}}(t)$ and $\hat{P}(t)$. To simplify the notation, consider a scalar random variable y (e.g., the value of some system state variable at some time of interest), and let m and p represent the true values of the mean and variance of y,

$$m = E[y]$$
$$p = E[(y - m)^2] \qquad (2.1\text{-}6)$$

By performing one set of q monte carlo trials, we obtain a single estimate of m and p, which we denote $\hat{m}$ and $\hat{p}$. These estimates are also random variables; that is, if another set of q monte carlo trials were performed independently of the first set, but with the same statistics for the initial conditions and noise inputs, then a different ensemble of simulations results, and different estimates for the mean and variance would be obtained. If q is sufficiently large, then we can invoke the central limit theorem to justify the assumption that the random variables $\hat{m}$ and $\hat{p}$ are gaussian*, and thus that their distributions are completely specified by the following statistics, asymptotically true for large q and given in Ref. 4:

$$E[\hat{m}] = m$$
$$E[\hat{p}] = p$$
$$\sigma_{\hat{m}}^2 \triangleq E[(\hat{m} - m)^2] = \frac{p}{q} \qquad (2.1\text{-}7)$$
$$\sigma_{\hat{p}}^2 \triangleq E[(\hat{p} - p)^2] = \frac{\mu_4 - p^2}{q}$$

*For $q < 20$, it is necessary to assume that $\hat{p}$ has the chi square distribution if y is a gaussian variable (Ref. 5).

where μ_4 is the fourth central moment,

$$\mu_4 = E[(y - m)^4] \tag{2.1-8}$$

For many common probability density functions (pdf's), the fourth central moment is of the form

$$\mu_4 = \lambda p^2 \tag{2.1-9}$$

Table 2.1-1 gives a summary of λ for the pdf's used in this report. In terms of the parameter λ, we can express the standard deviations given in Eq. (2.1-7) in the form

$$\sigma_{\hat{m}} = \sqrt{\frac{p}{q}}$$

$$\sigma_{\hat{p}} = \sqrt{\frac{\lambda - 1}{q}}\, p \tag{2.1-10}$$

The above discussion of the statistics of the gaussian random variable $\hat{p}$ provides the basis for determining a range in the vicinity of $\hat{p}$ such that the true value of p is guaranteed to lie within that range with a specified probability, ψ. This is done by determining the number, n_σ, of standard deviations, $\hat{\sigma}_p$, such that

$$\text{Prob}\,[\,0 \le |p - \hat{p}| \le n_\sigma \sigma_p\,] = \psi \tag{2.1-11}$$

Since $\hat{p}$ is a gaussian random variable, n_σ is the solution to

$$\frac{1}{\sqrt{2\pi}} \int_{-n_\sigma}^{n_\sigma} \exp\left(-\frac{1}{2}\zeta^2\right) d\zeta = \psi \tag{2.1-12}$$

TABLE 2.1-1

SOME COMMON PROBABILITY DENSITY FUNCTIONS

R-11798

DESIGNATION	FUNCTIONAL REPRESENTATION*	GRAPHICAL REPRESENTATION	λ†
EXPONENTIAL	$\frac{1}{\sqrt{2}\sigma}\exp\left(-\frac{\sqrt{2}}{\sigma}\lvert x-m\rvert\right)$, $-\infty < x < +\infty$	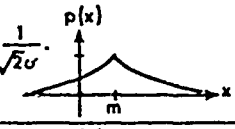	6
NORMAL	$\frac{1}{\sqrt{2\pi}\sigma}\exp\left(-\frac{1}{2}\left(\frac{x-m}{\sigma}\right)^2\right)$, $-\infty < x < +\infty$	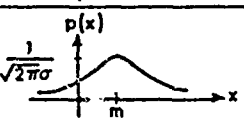	3
TRIANGULAR	$\frac{1}{\sqrt{6}\sigma}\left(1-\frac{\lvert x-m\rvert}{\sqrt{6}\sigma}\right)$, $m-\sqrt{6}\sigma \le x \le m+\sqrt{6}\sigma$	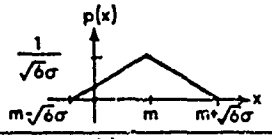	2.4
UNIFORM	$\frac{1}{\sqrt{12}\sigma}$, $m-\sqrt{3}\sigma \le x \le m+\sqrt{3}\sigma$	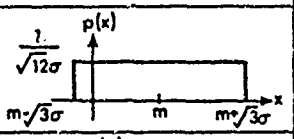	1.8
BIPOLAR (Discrete)	$\frac{1}{2}\delta(x-m-\sigma) + \frac{1}{2}\delta(x-m+\sigma)$	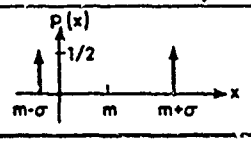	1.0

*Formulated to have mean m and standard deviation σ

† λ is referred to as the "kurtosis" or "excess" of a pdf. (Ref.6)

For example, if the desired probability is 0.95, Eq. (2.1-12) yields $n_\sigma = 1.96$. Other values of n_σ corresponding to different values of ψ can be obtained from probability integral tables (Ref. 6); several representative values are given in Table 2.1-2.

TABLE 2.1-2

CUMULATIVE PROBABILITY WITHIN n_σ STANDARD DEVIATIONS OF THE MEAN FOR A GAUSSIAN RANDOM VARIABLE

n_σ	ψ
1.0	0.6827
1.960	0.9500
2.576	0.9900

To reformulate Eq. (2.1-12) into an inequality for p, we make the substitution for $\hat{\sigma}_p$ indicated in Eq. (2.1-10) into Eq. (2.1-11) to obtain the equivalent statement that

$$\text{Prob}\left[\underline{p} \triangleq \frac{\hat{p}}{1+n_\sigma\sqrt{\frac{\lambda-1}{q}}} \le p \le \frac{\hat{p}}{1-n_\sigma\sqrt{\frac{\lambda-1}{q}}} \triangleq \overline{p}\right] = \psi \qquad (2.1\text{-}13)$$

that is, the true value of p lies between the values $\underline{p}$ and $\overline{p}$ indicated in Eq. (2.1-13) with probability ψ. Alternatively, in terms of the estimated rms value of the variable, $\hat{\sigma}$, we have the comparable result

$$\text{Prob}\left[\underline{\sigma} \le \sigma \le \overline{\sigma}\right] = \psi$$

for $\underline{\sigma}$ and $\overline{\sigma}$ given by

$$\underline{\sigma} \triangleq \sqrt{\underline{p}} = \frac{\hat{\sigma}}{\sqrt{1+n_\sigma\sqrt{\frac{\lambda-1}{q}}}} \triangleq \underline{\rho}\,\hat{\sigma}$$

$$\overline{\sigma} \triangleq \sqrt{\overline{p}} = \frac{\hat{\sigma}}{\sqrt{1-n_\sigma\sqrt{\frac{\lambda-1}{q}}}} \triangleq \overline{\rho}\,\hat{\sigma} \qquad (2.1\text{-}14)$$

The quantities $\underline{\sigma}$ and $\overline{\sigma}$ are referred to as lower and upper confidence limits; the value of ψ expressed as a percent (100ψ) is the degree of confidence. Equation (2.1-14) demonstrates that the standard deviation confidence limits can be obtained from $\hat{\sigma}$ simply by using the multipliers $\underline{\rho}$ and $\overline{\rho}$. The latter are functions only of the parameter λ, the number of monte carlo trials q, and the number of standard deviations n_σ determined by the desired degree of confidence.

The problem of making a reasonable choice of λ, which depends upon the statistics of the random variable y, must be considered before the confidence limit multipliers can be calculated. One option is to determine an approximate value of λ by estimating the fourth central moment using the q sample values of the variable y, and calculating

$$\lambda \cong \hat{\mu}_4 / \hat{p}^2 = \hat{\lambda}$$

The value of λ need not be known exactly, since the confidence limits $\underline{\sigma}$ and $\overline{\sigma}$ are not very sensitive to errors in this parameter. In the absence of reliable information about the higher central moments, it is frequently assumed that y is gaussian; i.e., that $\lambda = 3$. However, if there is reason to believe that the pdf for y has abnormally heavily weighted tails -- as in the case of the exponential distribution in Table 2.1-1 -- then a larger value of λ may be required.

Typical values of $\underline{\rho}$ and $\overline{\rho}$ for $\lambda = 3$ are indicated as functions of the number of monte carlo trials in Fig. 2.1-3, for two values of confidence. As an example of the significance of the confidence interval, if we desire to have 99% certainty that σ is within 10% of the estimated value, $\hat{\sigma}$; i.e.,

$$\text{Prob}\left[0.90\,\hat{\sigma} \le \sigma \le 1.1\,\hat{\sigma}\right] = 0.99 \qquad (2.1\text{-}15)$$

then Fig. 2.1-3 demonstrates that it is necessary to perform 440 trials; 256 trials suffice for 95% confidence.*

Figure 2.1-4 shows the deterioration that occurs in the accuracy of the monte carlo estimated standard deviation for a given level of confidence if λ is greater than three due to y being nongaussian. We discuss an instance where $\lambda \cong 19.5$ in Section 5.3; in this case, even for more than 200 trials, the upper 95% confidence limit is nearly 50% greater than the estimated value of σ.

*Note that the bounds, $\underline{\rho}$ and $\overline{\rho}$, are not symmetric with respect to one; thus the point at which $\overline{\rho}$ crosses 1.1 determines the value of q for which Eq. (2.1-15) is satisfied.

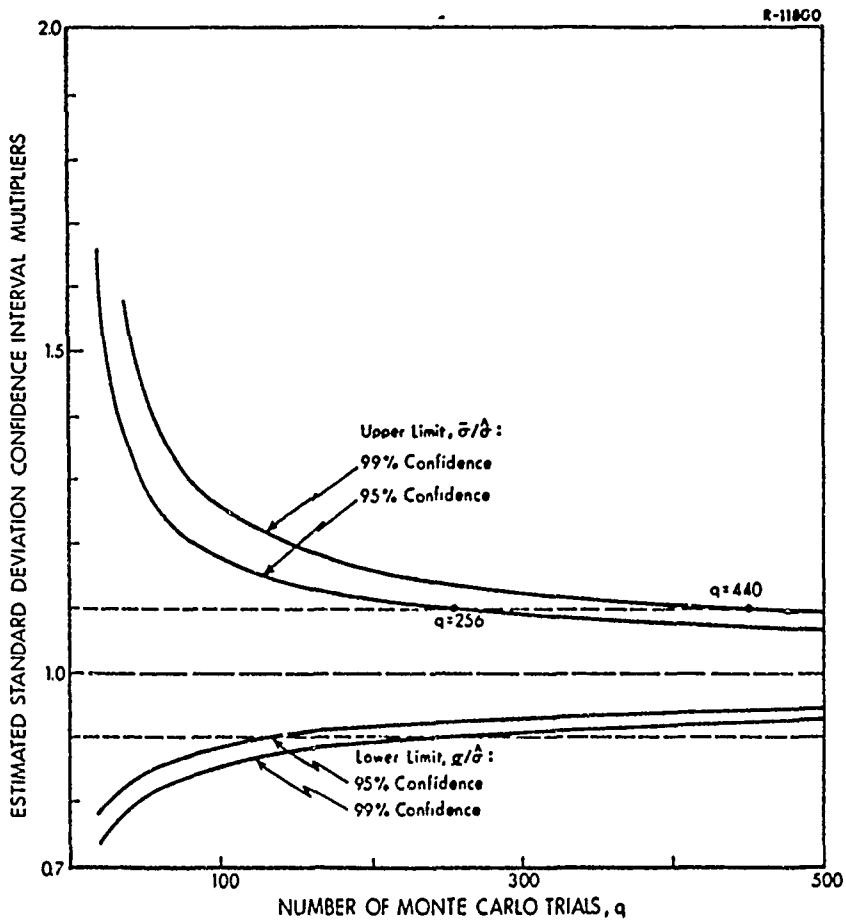

Figure 2.1-3 Typical Confidence Interval Multipliers for the Estimated Standard Deviation of a Gaussian Random Variable ($\lambda = 3$)

The confidence interval calculation for the estimated mean is quite direct, since $\sigma_{\hat{m}}$ (Eq. (2.1-9)) is not a function of the mean. The same value of n_σ is obtained for the desired degree of confidence (e.g., $n_\sigma = 1.96$ for 95% confidence), and value of $\bar{p}$ given in Eq. (2.1-13) is used in deriving the result that

$$\text{Prob}\left[\underline{m} \leq m \leq \overline{m}\right] = \psi$$

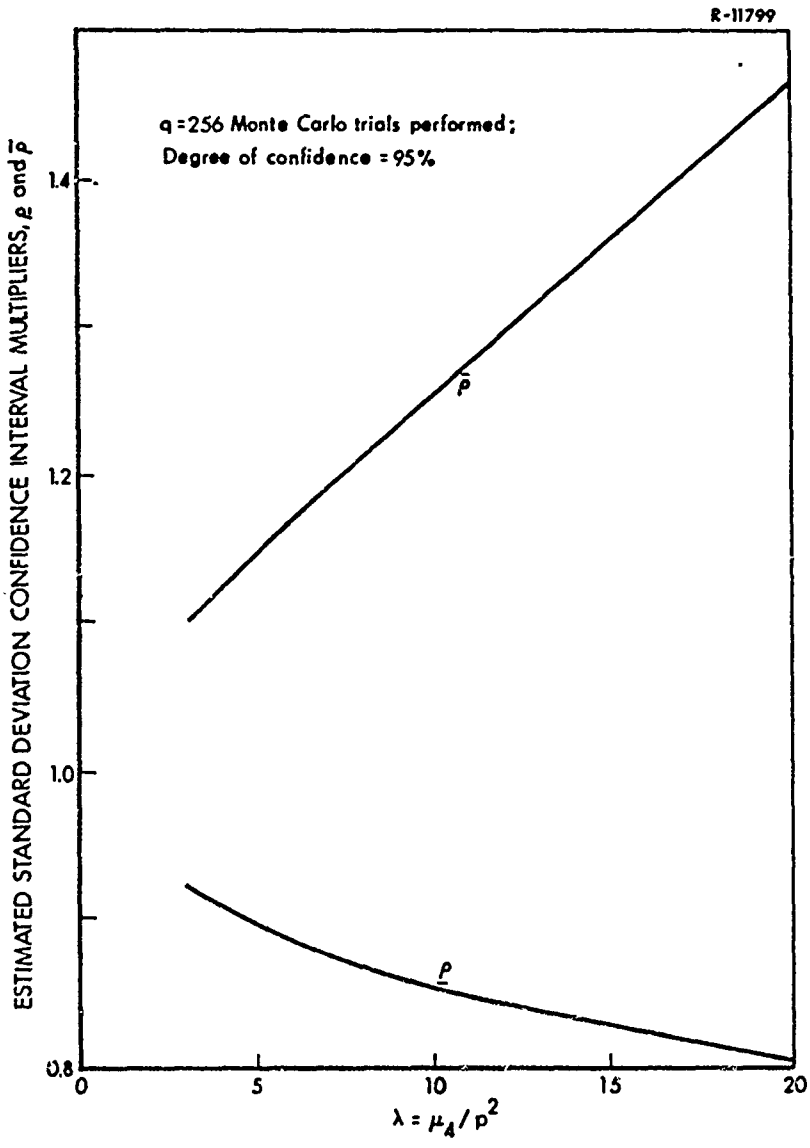

Figure 2.1-4 Effect of λ on Confidence Interval Limits

for $\underline{m}$ and $\overline{m}$ given by

$$\underline{m} = \hat{m} - n_\sigma \sqrt{\frac{\bar{p}}{q}}$$

$$\overline{m} = \hat{m} + n_\sigma \sqrt{\frac{\bar{p}}{q}} \qquad (2.1\text{-}16)$$

Here, we see that $\underline{m}$ and $\overline{m}$ cannot be readily expressed in terms of a multiple of $\hat{m}$.

The confidence limit concept developed above provides a statistical measure of the accuracy of the estimated mean and standard deviation of a random variable obtained by using the monte carlo method. It is only possible to assess the accuracy of such estimates in a probabilistic sense; e.g., for 256 trials, we can assert that an estimated standard deviation (rms value) is within 10% of the true value, with probability 0.95 (with 95% confidence).

2.2 THE COVARIANCE ANALYSIS DESCRIBING FUNCTION TECHNIQUE (CADET)

Covariance analysis, where it is applicable, provides a direct, exact technique for the statistical evaluation of the performance of dynamic systems with random inputs, permitting the propagation of the mean component and covariance matrix of the system state vector as functions of time. This technique does not require the generation of a large ensemble of representative state trajectories and the computation of the ensemble statistics. The latter approach --the monte carlo method -- is both time consuming (in terms of computer time) and approximate; we have seen in Section 2.1 that several hundred sample state trajectories may be required in order to obtain reasonably accurate statistics for systems in which the state variables are nearly gaussian; for nonlinear systems in which variables may be highly nongaussian, one thousand or more simulations could be required to achieve an acceptable level of confidence in the accuracy of the results. The direct approach is thus distinctly preferable to the monte carlo technique.

The fundamental bases of covariance analysis are the differential equations governing the evolution of the mean vector and covariance matrix with time. Corresponding to the state vector differential equation given by Eq. (2.1-1) with the input vector specified by Eq. (2.1-3), we have the differential equations (Ref. 7)

$$\dot{\underline{m}} = E[\underline{f}(\underline{x})] + G\underline{b}(t)$$

$$\dot{P} = E[\underline{f}\,\underline{r}^T] + E[\underline{r}\,\underline{f}^T] + GQ(t)G^T \qquad (2.2\text{-}1)$$

where

$$E[\underline{x}(t)] = \underline{m}(t)$$

$$\underline{r}(t) = \underline{x}(t) - \underline{m}(t) \qquad (2.2\text{-}2)$$

$$P(t) = E[\underline{r}(t)\,\underline{r}^T(t)]$$

The first and second moments of the system response are completely determined by the integration of the indicated vector and matrix differential equations (Eq. (2.2-1)) when the initial conditions, $\underline{m}(0)$ and $P(0)$, are specified.

The form of the differential equations for the statistics of $\underline{x}(t)$ is particularly convenient in the case of linear systems; given

$$\underline{f}(\underline{x}) = F\underline{x}$$

Eq. (2.2-1) reduces to

$$\dot{\underline{m}} = F\underline{m} + G\underline{b}$$

$$\dot{P} = FP + PF^T + GQG^T \qquad (2.2\text{-}3)$$

These linear differential equations can be solved using standard numerical integration techniques.

The nonlinear covariance equations can be represented in the same format as Eq. (2.2-3) by definition of two auxiliary matrices, N_m and N_r, given by

$$N_m \underline{m} = E[\underline{f}(\underline{x})]$$
$$N_r P = E[\underline{f}(\underline{x})\, \underline{r}^T] \tag{2.2-4}$$

so Eq. (2.2-1) may be written

$$\dot{\underline{m}} = N_m \underline{m} + G\underline{b}$$
$$\dot{P} = N_r P + P N_r^T + G Q G^T \tag{2.2-5}$$
$$\triangleq 2\,\mathrm{sym}\,[N_r P] + \tilde{Q}$$

where sym [ ] indicates the symmetric part of the indicated matrix, and $\tilde{Q}$ is the spectral density matrix of $G(\underline{w} - \underline{b})$. The dependence of N_m and N_r on the statistics of the state vector, which is implicit in the expectation operations in Eq. (2.2-4), is due to the existence of nonlinearities in the system. Without nonlinear effects, the propagation of the mean and covariance is "uncoupled," as shown in Eq. (2.2-3).

The matrices N_m and N_r given in Eq. (2.2-4) must be determined before we can proceed to solve Eq. (2.2-5). A direct approximate method of accomplishing this is to use describing function theory to linearize the system nonlinearities; the resulting generalization of linear covariance analysis is then called CADET -- Covariance Analysis DEscribing function Technique. This procedure, presented in detail in Appendix C, entails assuming the form of the nonlinearity input and calculating describing functions which provide a quasi-linear approximate input-output relation for each nonlinearity. For the problem at hand, the system input vector $\underline{w}(t)$ is taken to be a gaussian random process plus a

bias, and it is useful to assume that the state variables also have mean components and random parts that are jointly normal. While this assumption is strictly true only for linear systems, it is often approximately valid in nonlinear systems. Although the output of a nonlinearity with a gaussian input is generally nongaussian, it is known from the central limit theorem that random processes tend to be made gaussian when passed through low-pass linear systems ("filtered"). Hence if there are a few stages of linear dynamics between nonlinearities, the input to each nonlinearity should be nearly gaussian. The essential requirement of CADET is that the state variables must be nearly jointly normal. From a practical viewpoint, the gaussian hypothesis serves to simplify the CADET methodology by permitting each nonlinearity to be treated in isolation, with N_m and N_r formed from the individual random input describing functions (ridf's) for each nonlinearity, as discussed in Appendix C. Since ridf's have been extensively catalogued in Ref. 8, the implementation of CADET is a straightforward procedure for a broad class of nonlinear systems. We also note that under the gaussian assumption, the random input describing functions can be calculated directly from the mean vector, $\underline{m}$, and the covariance matrix, P, of the system state vector. Thus, we write N_m and N_r in the form

$$N_m = N_m(\underline{m}, P)$$

$$N_r = N_r(\underline{m}, P)$$

Relations of this form permit the direct evaluation of the ridf's at each integration step in the propagation of $\underline{m}$ and P by numerical techniques according to Eq. (2.2-5), as illustrated in Fig. 2.2-1.

To demonstrate the ease with which CADET can be mechanized under the gaussian assumption, we consider a single nonlinearity and illustrate the steps involved in performing statistical analysis via CADET. Assume that only the nonlinearity $f_j(x_k)$ occurs in the differential equation for x_j,

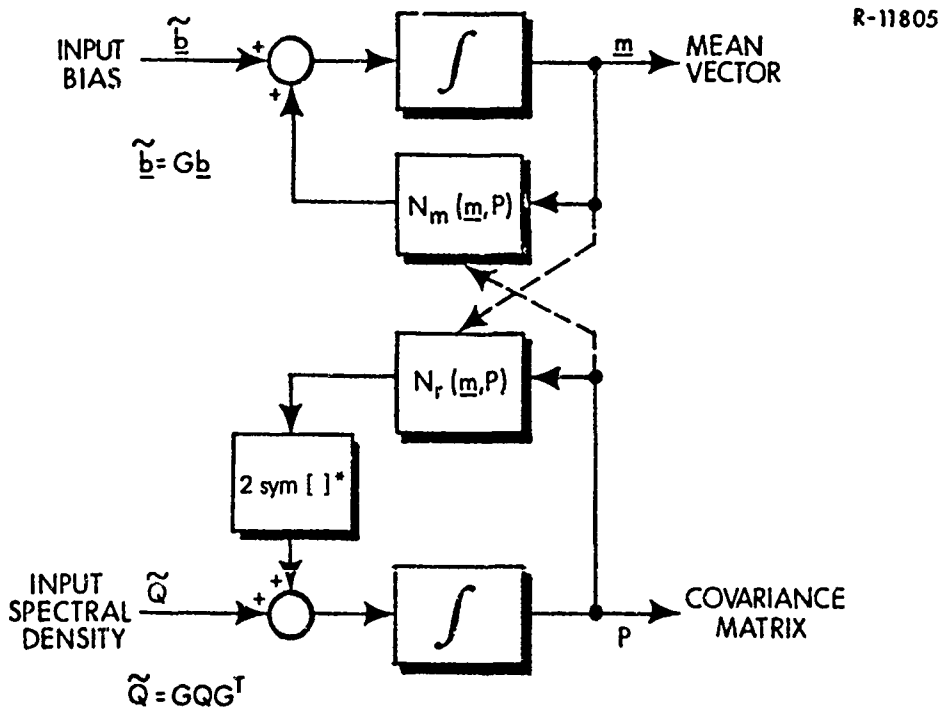

Figure 2.2-1 Nonlinear Covariance Analysis -- CADET

$$\begin{bmatrix} \dot{x}_1 \\ \vdots \\ \dot{x}_j \\ \vdots \\ \dot{x}_n \end{bmatrix} = F\underline{x} + \begin{bmatrix} 0 \\ \vdots \\ f_j(x_k) \\ \vdots \\ 0 \end{bmatrix} + G\underline{w}(t) \qquad (2.2\text{-}6)$$

where we have explicitly separated the linear portion of the dynamics from the nonlinearity. The random input describing function approximation to $f_j(x_k)$ is shown schematically in Fig. 2.2-2. The input x_k is first separated into its mean and random components, m_k and r_k, which are then multiplied by the scalar quasi-linear gains, n_{rk} and n_{mk}; the latter are selected to minimize the mean square error between the linear approximation $n_{rk}r_k + n_{mk}m_k$ and $f_j(x_k)$. The gain n_{rk} is added to the element f_{jk} of the matrix F in determining N_r; similarly

*The indicated symmetry operator yields $2\,\mathrm{sym}[N_rP] = N_rP+PN_r^T$ where the symmetry of P is taken into account.

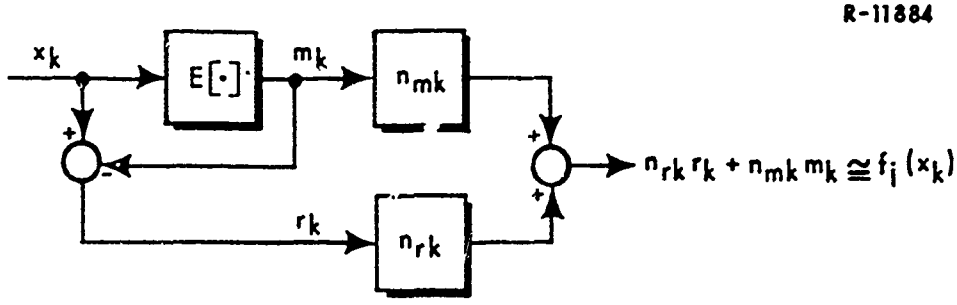

Figure 2.2-2 Random Input Describing Function Approximation of $f_j(x_k)$

n_{mk} is added to the same element of F to give N_m. Thus, the j^{th} rows of N_r and N_m are given by

$$[N_r]_j = [f_{j1}, f_{j2}, \ldots, (f_{jk} + n_{rk}), \ldots, f_{jn}]$$

$$[N_m]_j = [f_{j1}, f_{j2}, \ldots, (f_{jk} + n_{mk}), \ldots, f_{jn}]$$

A comparison of quasi-linearization with the classical Taylor series or small-signal linearization technique provides a great deal of insight into the success of the ridf in capturing the essence of nonlinear effects. Small-signal linearization for a scalar nonlinear element f(x) is based on the identification of a nominal operating point x_o and the evaluation of the slope of the nonlinearity at that value; then the approximation is made that

$$f(x) \cong f(x_o) + f'(x_o)(x - x_o) \qquad (2.2\text{-}7)$$

which represents the first two terms of a Taylor series expansion about the given operating point, as illustrated in Fig. 2.2-3 for the example, $y = x^3$. While this is a useful approach if excursions from the nominal are small, the validity of the Taylor series approximation is questionable when x is a random variable which can exhibit large variations about its mean value.

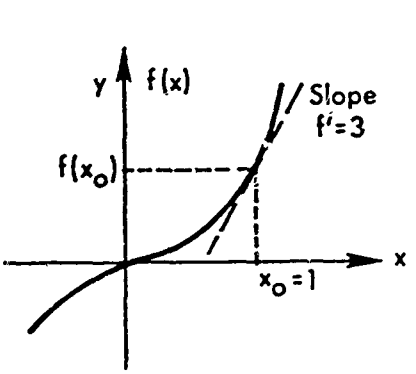

Figure 2.2-3 Taylor Series Linearization of $y=x^3$ about $x_o=1$

By contrast, the quasi-linear representation of a nonlinearity is sensitive to the input amplitude in some sense; in the case of random inputs, the statistics $m_x = E[x]$ and $p_x = E[(x-m_x)^2]$ provide the measure of input amplitude. For the example $y=x^3$, where x is a gaussian random process, we calculate the describing functions according to Eqs. (C.2-4) and (C.2-5),

$$n_r = 3(p_x + m_x^2)$$

$$n_m = 3p_x + m_x^2$$

and the nonlinearity is approximated by

$$x^3 \cong (3p_x + m_x^2)\, m_x + 3(p_x + m_x^2)\,(x - m_x) \qquad (2.2\text{-}8)$$

Comparing Eqs. (2.2-7) and (2.2.8), we see that the describing function gains depend on both the mean and variance of x, as indicated in Fig. 2.2-4, while the coefficients in the Taylor series approximation do not.

Finally, some comments about the generality of CADET are in order. Many approximate techniques for treating nonlinear systems are applicable only to low order systems (with two or three state variables at most) with one

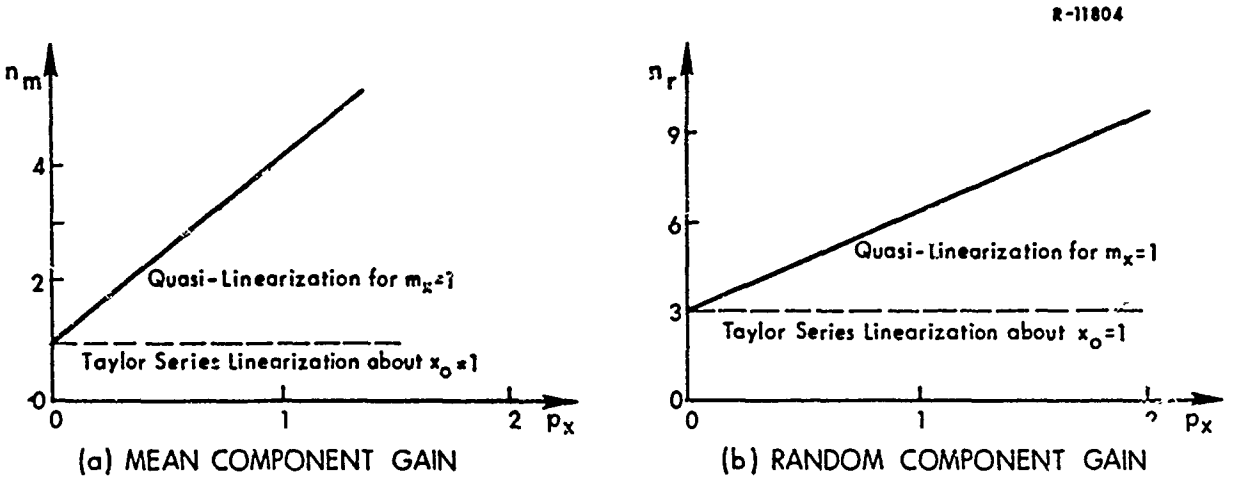

Figure 2.2-4 Quasi-Linearization of $y=x^3$ for Unity Input Mean

nonlinearity. By contrast, describing function techniques can be used for systems with any number of nonlinearities, leading to a quasi-linear system model that can then be handled using the CADET methodology. There is no limit on the number of state variables in the system model; in fact, CADET tends to be more accurate as the ratio of the number of states to nonlinear elements increases, thus improving the validity of the gaussian assumption.

2.3 COMPARISONS AND PHILOSOPHY OF APPLICATION

In comparing CADET and monte carlo methods for use in obtaining performance projections for nonlinear systems with random inputs, there are several significant similarities. Both techniques are applicable to nonlinear system models with an arbitrary number of states and nonlinearities, and we often rely on the gaussian assumption in assessing the accuracy of the performance statistics obtained. In both cases, any departure from normality can be compensated for to a certain extent; in CADET, nongaussian pdf's can be used in calculating describing functions, while in monte carlo simulation the fact that the confidence limits increase for nongaussian random variables (Fig. 2.1-4) can be counteracted by increasing the number of trials performed. The

principal trade-off between the two methods is in efficiency versus generality (versatility). The monte carlo simulation ensemble of q representative state trajectories (Eq. (2.1-2)) can be used not only as a data base for calculating estimated performance statistics $\hat{\underline{m}}(t)$ and $\hat{P}(t)$ at instants of time of interest, but also for estimating higher order moments, and for generating histograms which are approximate pdf's for the variables under consideration (of course, at an additional cost in terms of data processing). CADET, on the other hand, provides approximate values for $\underline{m}(t)$ and $P(t)$ in a single numerical integration of the quasi-linear covariance equations (Eq. (2.2-5)), usually in a small fraction of the computer processing time required for accurate monte carlo analysis. Depending on the number of state variables and nonlinearities, and on the desired accuracy (which determines the number of monte carlo trials required), it may be possible to perform from ten to thirty distinct CADET studies at the same computational expense required for one monte carlo analysis.

One of the primary purposes of the statistical analysis of tactical missile system performance is the evaluation of guidance effectiveness with variations in random input levels, initial conditions statistics, system parameter values and secondary nonlinear effects such as seeker mass imbalance, acceleration command limiting, etc. Due to the multiplicity of these factors, it is evident that the analysis will generally be done repeatedly. As a consequence, efficiency is an important consideration; this point is a strong argument in favor of CADET. On the other hand, the versatility of monte carlo simulation provides a self-check capability; i.e., the q representative state trajectories can be used to estimate higher moments and the pdf's of the state variables, which in turn leads to an assessment of the accuracy of the monte carlo analysis. This is a feature lacking in CADET which makes it advisable to rely upon monte carlo simulation in a monitoring capacity, since it is always possible to obtain accurate performance projections by increasing q sufficiently.

The effective use of CADET and monte carlo analysis in concert can be demonstrated in a hypothetical trade-off study where two parameters, say α_1 and α_2, are to be varied over certain ranges to obtain optimal performance in some sense (perhaps to obtain minimum rms terminal miss distance). As shown in Fig. 2.3-1, a few points in the parameter plane are chosen for careful CADET-monte carlo comparison (verification of CADET); then extensive performance curves are generated using CADET, from which the optimal values of α_1 and α_2 are chosen. If desired, the vicinity of the point of optimally can be studied using a few selected values of α_1 and α_2 and performing the required monte carlo simulations. Similar approaches can be used in studying sensitivity to nonlinear and random effects.

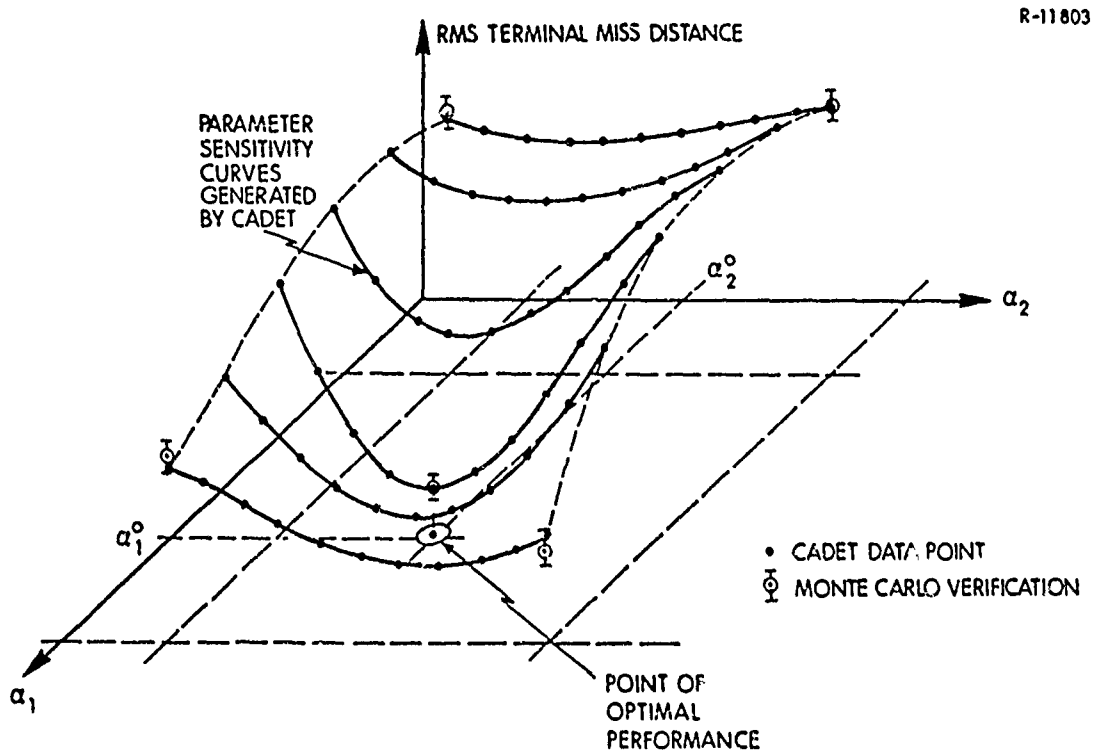

Figure 2.3-1 Illustration of CADET and Monte Carlo Analysis in a Parameter Trade-Off Study

The overall philosophy of CADET usage, based on the strong points of both CADET and monte carlo simulation, is illustrated in Fig. 2.3-2. The initial verification procedure is generally undertaken for the "nominal system," i.e., for the system with nominal parameters values, and is of necessity more meticulous. Thus several hundred monte carlo trials may be performed, and if there is reason to believe that the system is highly nonlinear -- so that the system variables may be quite nongaussian -- it may be necessary to investigate higher order moments or histograms to decide whether more trials are needed in order to obtain a reliable statistical analysis. Once this phase has been completed satisfactorily, the CADET parameter sensitivity studies can then be performed. Observe that the preliminary careful but time-consuming monte carlo study (perhaps with the indicated self-check procedure and increase in the number of trials) is always required if accurate performance statistics are to be obtained from monte carlo simulation with high confidence. The subsequent use of the monte carlo statistics to verify CADET requires minimal computer time (if any), and that comparison paves the way for the ensuing efficient study of various effects via CADET. In the latter studies, it is rarely necessary to perform as detailed a monte carlo analysis as is required in the initial verification procedure, so as few as 20 to 50 monte carlo trials may suffice to demonstrate that CADET has accurately captured the effect in question. This approach mirrors the development of CADET that has been carried out in the present study.

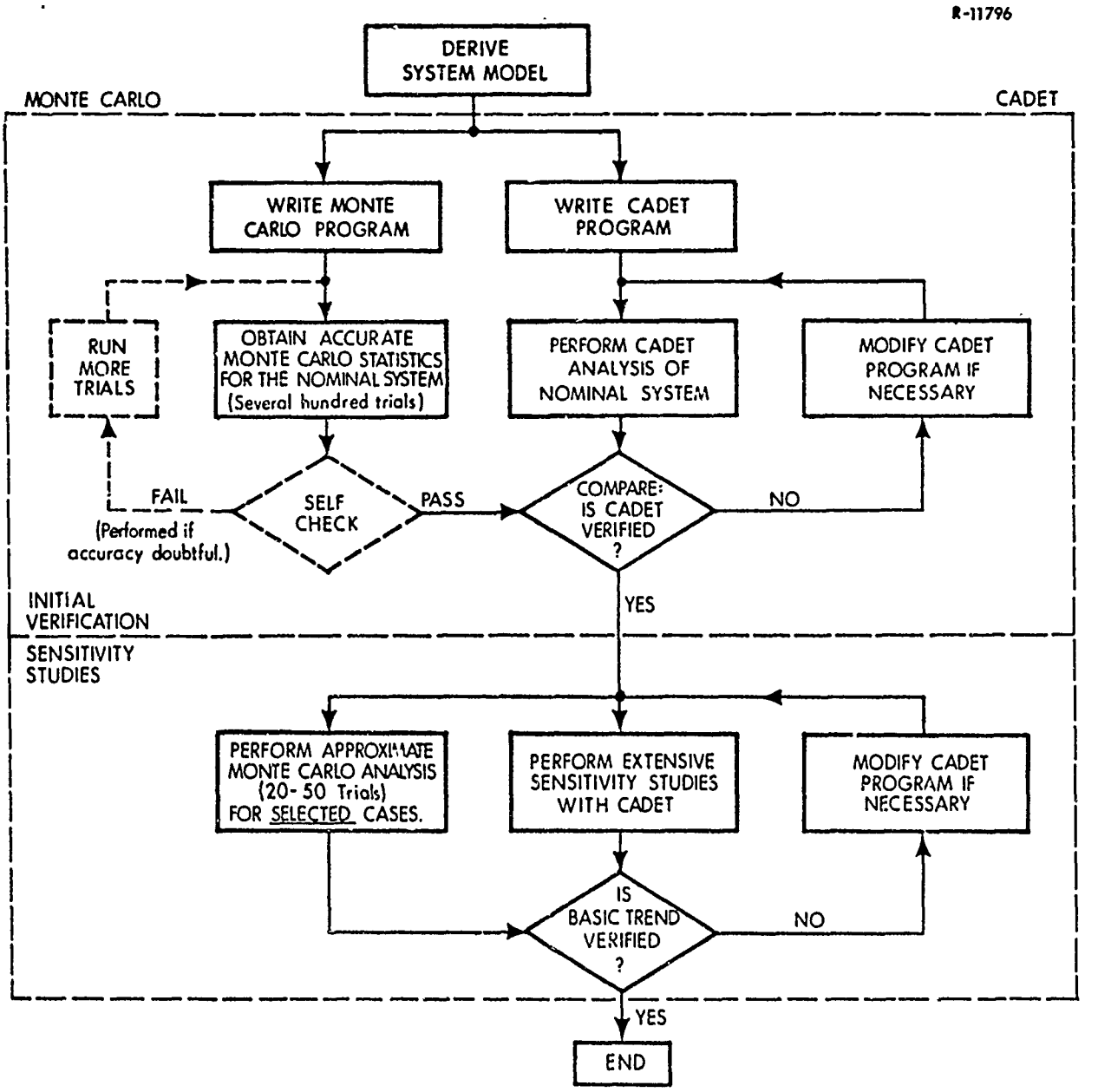

Figure 2.3-2 Philosophy of CADET Application

3. MISSILE-TARGET INTERCEPT MODEL DEVELOPMENT

3.1 INTRODUCTION

Previous development of CADET as an efficient tool for undertaking the statistical analysis of tactical missile guidance system performance has focused on the planar missile-target intercept problem. At each stage, the model has been made more general by the inclusion of more of the system dynamics (addition of more system states) and the consideration of more nonlinear effects and random disturbances. The initial work (Ref. 1) treated only one important nonlinearity -- acceleration command limiting -- and one noise input -- a random target maneuver. A second, more extensive application of CADET (Ref. 2) included three nonlinear effects and four random inputs, two of which had a deterministically time-varying rms value. A third investigation (Ref. 3), which complements and in some respects parallels the present effort, involves a very detailed application of CADET to a specific tactical missile -- the SAM-D. A brief synopsis of the system models considered in the various research programs is provided in Table 3.1-1.

The purpose of the present study is to significantly extend the verified capability of CADET to provide rapid, accurate assessments of tactical missile performance. We have generalized the previous missile-target intercept models by adding a variety of nonlinear effects and random inputs which have heretofore not been treated and which can have a significant impact on the effectiveness of the tactical missile -- as quantified by the rms miss distance between the missile and target at terminal time. The specific equations that represent the dynamics of the missile and target are developed in Appendix A; in this chapter, we provide a brief summary of the effects studied. The verification that CADET

TABLE 3.1-1

OVERVIEW OF MISSILE-TARGET INTERCEPT STUDIES

Model Subsystem	STUDY 1 (Ref. 1)	STUDY 2 (Ref. 2)	STUDY 3 (Ref. 3)	STUDY 4 (Present)
Missile-Target Kinematics	• Deterministic down-range separation • Linear cross-range separation dynamics	• Deterministic down-range separation • Nonlinear cross-range separation dynamics	Same as Study 2	Nonlinear down-range and cross-range dynamics
Target Acceleration	First-order Markov	First-order Markov	First-order Markov; deterministic evasive maneuver	First-order Markov
Autopilot-Airframe	Linear, single pole	Linear, three poles	Same as Study 2	Same as Study 2
Guidance Law	Linear proportional guidance with • First-order noise filter • Acceleration command limiting	A. Linear proportional guidance, same as Study 1 B. Proportional with Kalman noise filter C, D. Linear optimal with Kalman noise filter E. Nonlinear optimal with Kalman noise filter [All with acceleration command limiting]	Options B, C, D of Study 2	Proportional guidance with • First-order noise filter • Nondeterministic closing velocity with uncertainty • Secant compensation • Acceleration command limiting
Seeker Dynamics and Error Sources	None	• Time-varying noise sources • Linear radome aberration • First-order dynamics	• Time-varying noise sources • Nonlinear radome aberration • First-order dynamics	• Range-dependent noises • Receiver/signal-processing characteristic • Seeker mass imbalance • Seeker gimbal friction • Seeker head restoring torques • Inverse tangent LOS angle computation • Third-order dynamics
Number of States	4	10	14	17
Nonlinearities Verified by Monte Carlo	1	3	6	16
Random Inputs	1	4	4	5

can indeed provide accurate performance projections with these effects taken into account is presented in Chapters 4 and 5.

3.2 MISSILE-TARGET KINEMATICS

In Fig. 3.2-1 we portray the graphical definition of the coordinate frame and variables involved in describing the motion of the missile and target. In deriving the equations of motion, it is assumed that the missile and target velocity vector magnitudes are constant, or, equivalently, that the missile and target acceleration vectors are normal to the velocity vectors. These conditions, neglecting the effects of drag and assuming that the angle of attack is small, are representative of many missile-target engagement situations during the critical last few seconds.* Thus, the lateral acceleration of either vehicle simply produces a rotation of the corresponding velocity vector, given by

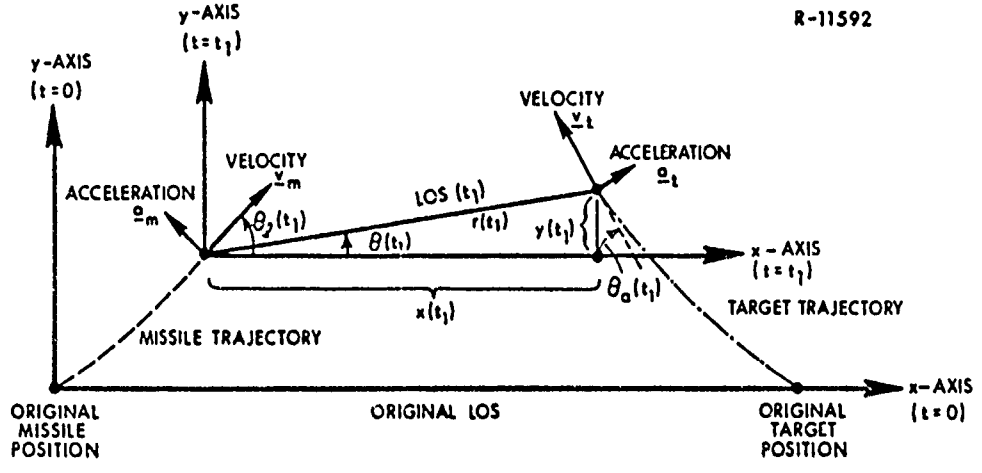

Figure 3.2-1 Missile-Target Planar Intercept Geometry

*The application of CADET to cases where angle of attack and drag variations are important is currently being considered in a continuation of the study described in Ref. 3.

$$\dot{\theta}_\ell = \frac{1}{v_m} a_m$$

$$\dot{\theta}_a = \frac{1}{v_t} a_t \qquad (3.2\text{-}1)$$

The equations describing the motion of the target with respect to the missile center of gravity (governing the cross- and down-range missile-target separation, x and y respectively) are found by projecting the velocity vectors onto the axes shown in Fig. 3.2-1; in terms of the velocity magnitudes v_m and v_t,

$$\dot{x} = - v_m \cos(\theta_\ell) - v_t \cos(\theta_a)$$

$$\dot{y} = - v_m \sin(\theta_\ell) + v_t \sin(\theta_a) \qquad (3.2\text{-}2)$$

Equation (3.2-2) represents the essential nonlinearities inherent to the missile-target kinematic relationship.

3.3 TARGET LATERAL ACCELERATION MODEL

An important source of missile guidance system error is target maneuverability. We assume that the target lateral acceleration magnitude, a_t, is a first-order Markov process, modelled as a zero-mean gaussian white noise* passed through a single stage of low-pass filtering, as depicted in Fig. 3.3-1.†

*The five white noise inputs to the system are simply denoted w_j, $j = 1, 2, \ldots, 5$, for convenient reference.

†Although the transfer function representation is formally restricted to use in completely linear systems, we use it as a compact notation for depicting linear subsystems in our model. While general practice is to replace the variables w_5 and a_t with the formal Laplace transforms, say $W_5(s)$ and $A_t(s)$, we continue to indicate linear subsystems inputs and outputs by their time domain representation to avoid a cumbersome dual notation for all variables.

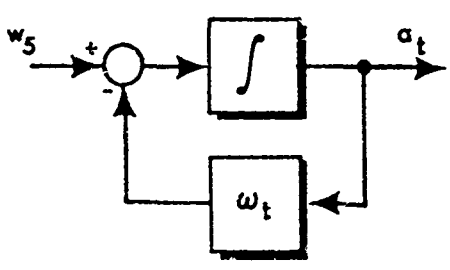

(a) DIFFERENTIAL EQUATION REPRESENTATION

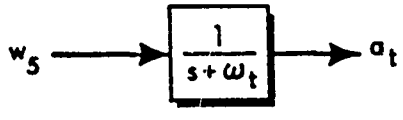

(b) TRANSFER FUNCTION FORMULATION

Figure 3.3-1 Band-Limited Gaussian Noise Model for Target Lateral Acceleration

By adjusting the values of target maneuver bandwidth, ω_t, and rms level, a wide range of target maneuver characteristics can be represented. A constant rms level of lateral acceleration over the entire terminal homing phase is assumed,

$$E[a_t^2(t)] \equiv \sigma_t^2 \tag{3.3-1}$$

Thus we choose the initial condition and gaussian white noise statistics to satisfy

$$E[a_t^2(0)] = \sigma_t^2$$

$$E[w_5(t)\, w_5(\tau)] = 2\omega_t \sigma_t^2 \delta(t-\tau) \triangleq q_5 \delta(t-\tau) \tag{3.3-2}$$

where q_5 is the spectral density of this white noise input.

3.4 AUTOPILOT - AIRFRAME MODEL

We use a linear time-invariant autopilot-airframe model, under the assumptions that:*

- Missile velocity is constant (drag effects are negligible over the period of time considered).
- Altitude remains nearly constant.
- The center of pressure, mass and inertia of the missile are constant.
- Lift force is linearly related to changes in angle of attack about some trim condition and to control fin deflection.
- Control fin actuator dynamics are linear.
- Fin effectiveness is independent of angle of attack.

The airframe equations of motion are then based on a set of missile aerodynamic coefficients identified with the vehicle short-period dynamics with values typical of a tactical missile in the terminal homing phase. We choose the autopilot feedback compensation gains to achieve a suitable compensated airframe response (Appendix A, Section A.4). The outputs of the airframe model are missile lateral acceleration, a_m, and missile body angular rate, $\dot{\theta}_m$; in transfer function form, they are related to the acceleration command, a_c, provided by the guidance law, by

$$a_m = \frac{720 - 0.865\,s - 1.87\,s^2}{720 + 275\,s + 18.3\,s^2 + s^3}\; a_c$$

$$\dot{\theta}_m = \frac{0.24 + 0.642\,s}{720 + 275\,s + 18.3\,s^2 + s^3}\; a_c$$

*Application of CADET to a complex, nonlinear airframe model is being considered in a continuation of the work described in Ref. 3.

which corresponds to a dominant pole at s = - 3.16 and secondary poles at s = - 7.56 ± 13.0j.

3.5 GUIDANCE LAW MODEL

The present study utilizes a nonlinear model of the classical proportional guidance law, described in Section A.5. In principle, it is desired to develop a missile lateral acceleration that has a component normal to the line-of-sight (LOS) which is proportional to the product of closing velocity and LOS angular rate. In practice, it is not possible to obtain either the closing velocity or the LOS angular rate exactly for generating an acceleration command. A noisy measurement of LOS angular rate, denoted by η in Fig. 3.5-1, is provided by the missile seeker, which is treated in Section 3.6. In the guidance law model, a single stage low-pass filter is included to reduce the effect of measurement noise in η; the filter output is denoted by $\hat{\dot{\theta}}$. Measurements of closing velocity (range rate) will also contain errors, which are represented by the uncertainty variable e_v. The latter is a first-order markov process,* modelled in the same form shown in Fig. 3.3-1. The resulting model for the acceleration command is given by

$$a'_c = n' \hat{\dot{\theta}} \left[v_m + e_v + v_t \frac{\cos(\theta_a + \theta)}{\cos(\theta_\ell - \theta)} \right] \qquad (3.5\text{-}1)$$

where the constant n' is designated the navigation ratio. The guidance law is completed by noting that this unconstrained acceleration command must generally be limited in magnitude in order to prevent exceeding the structural capacity of the airframe and to avoid the possibility that the missile might go

*A constant or bias error, e_{vb}, is obtained by suitably choosing the initial condition, $e_v(0) = e_{vb}$, and mean value of the input, $b_4 = E[w_4] = \omega_4 e_{vb}$.

into a stall. Thus the actual acceleration command, a_c, is represented as the output of a limiter whose input is a'_c.

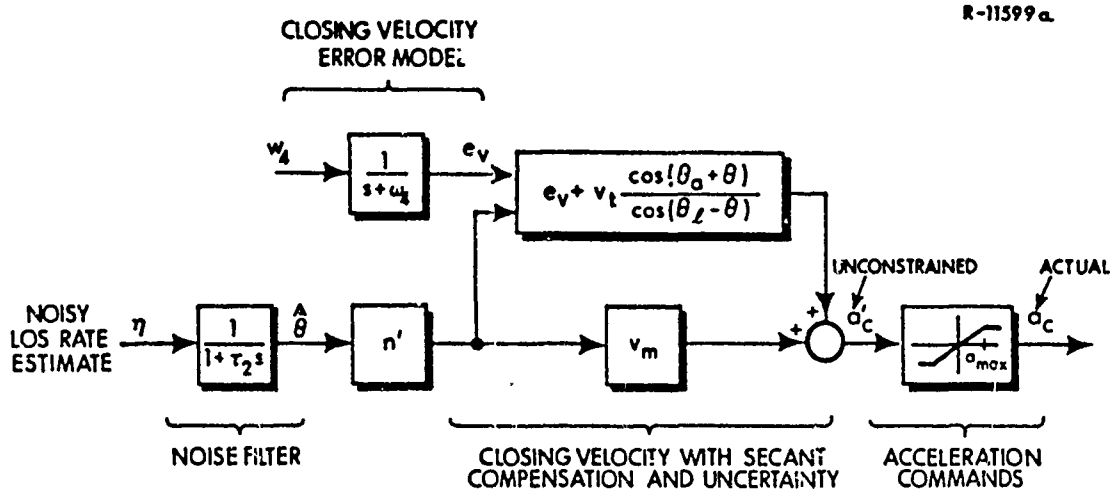

Figure 3.5-1 Guidance Law Model

3.6 THE SEEKER SUBSYSTEM

The basic function of the seeker is to track the target and provide the guidance package with an estimate of the LOS angular rate. There are a significant number of important error sources which can lead to a marked deterioration in the seeker performance. We can categorize them as noise sources, boresight error distortion effects, and seeker head disturbance torques; there are several specific mechanisms that give rise to errors of each type.

- Noise sources:

  Target amplitude and angular scintillation noise
  Receiver noise
  Seeker servo noise
  External jamming

- Boresight error distortion sources:

  Aberration
  Receiver/signal processing characteristics

- Disturbance torque sources:

  Seeker mass imbalance
  Seeker gimbal friction
  Seeker head restoring torques

The seeker noise model includes three fundamental types of additive random inputs: those that have an effective rms level that varies directly with the missile-target range, or range proportional noise, including such effects as receiver noise and distant external stand-off jamming; those exhibiting a constant effective rms level, or range independent noise, such as target amplitude scintillation and seeker servo noise; and those with an effective rms level that varies inversely with the range, or inverse range proportional noise, such as target angular scintillation. These sources are modelled as wide-band independent gaussian noises (filtered gaussian white noise) with appropriate nonlinear gains to give the desired range dependence, as portrayed in Fig. 3.6-1. The present study provides the first CADET application in which the range dependent components of the seeker noise have been modelled as nonlinear functions of state variables. In previous models, the missile-target separation was taken to be linearly decreasing to zero at the nominal terminal time, t_f.

The boresight error distortion model includes both aberration caused by the passage of incident radiation through a protective cover prior to detection, and boresight error limiting due to a signal processing nonlinear characteristic which may be introduced to circumvent the null and spurious sidelobe response inherent to the restricted beamwidth of the antenna or detector. The aberration is generally a complicated effect, expressed as an angular error, θ_{ab}, added to the seeker look angle, θ_{look}, the latter being the angle between

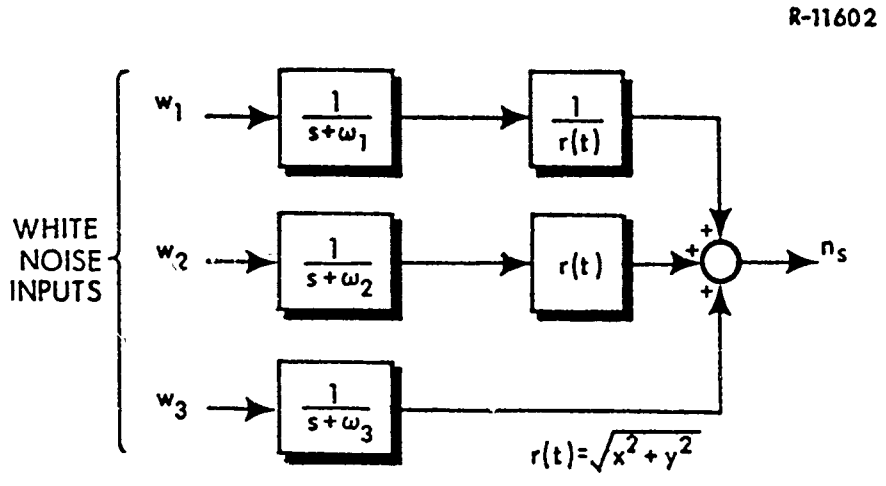

Figure 3.6-1 Nonlinear Seeker Noise Model

the line-of-sight to the target and the missile body axis defined in Fig. 3.6-2. The aberration effect is treated extensively in Ref. 3 (refer also to Fig. A.6-2), and thus is not considered in detail here. A description of the model employed for the nonlinear receiver characteristic is given in Section A.6. A functional diagram of the boresight error model is portrayed in Fig. 3.6-3.

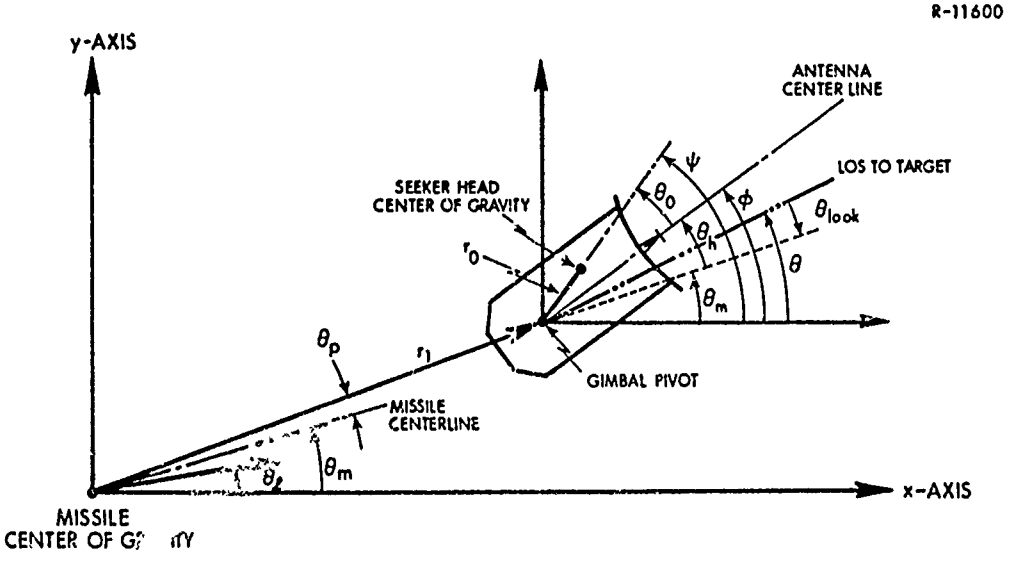

Figure 3.6-2 Seeker Head Configuration

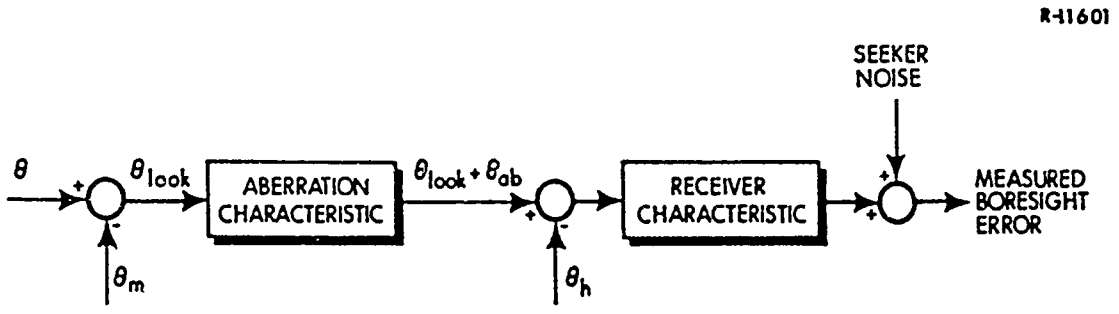

Figure 3.6-3 Boresight Error Distortion Model

The seeker track loop, shown in Fig. 3.6-4, is designed to maintain the measured boresight error near zero. A control torque, T_c, is generated which has a component proportional to the boresight error, and suitable dampling is assured by means of rate feedback provided by a rate gyro mounted on the seeker head. A compensator of the proportional plus integral form is included in the track loop to remove the effect of steady state disturbance torques. The characteristics of the control loop dynamics are discussed in detail in Sections A.6 and A.7.

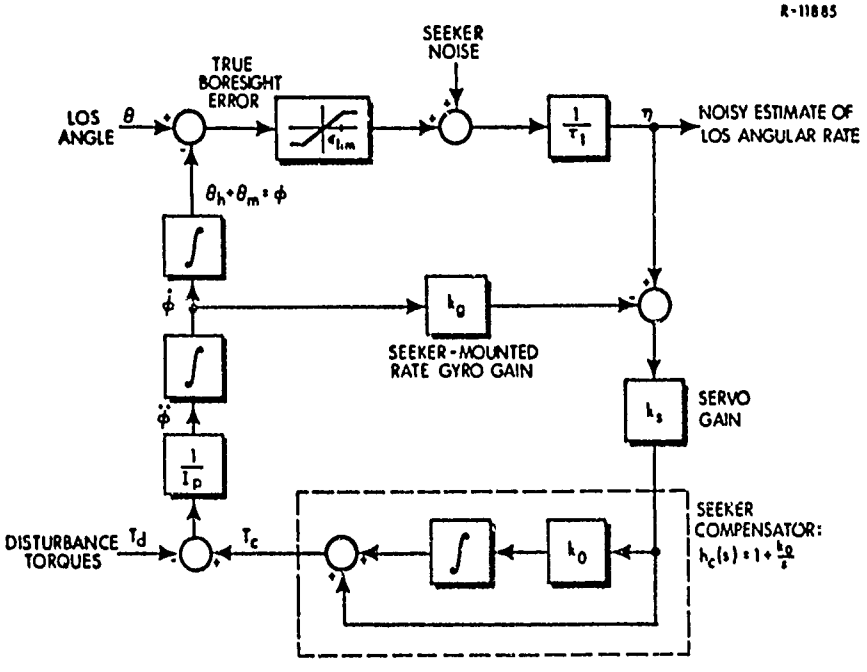

Figure 3.6-4 Seeker Track Loop Model

The seeker head disturbance torque model, depicted in Fig. 3.6-5, shows the three effects under consideration. The most complex nonlinear phenomenon is an effective torque due to seeker mass imbalance, T_m, with three components; one proportional to missile body angular acceleration, another to the square of the missile body angular rate, and the third to the missile lateral acceleration, as derived in Section A.6. Another nonlinearity represents an applied torque T_r, due to restoring torques acting on the seeker head (caused either by wiring harnesses or by restraining springs provided to prevent large seeker head angular excursions). Generally, this is a "hard spring" effect, i.e., the restoring torque will be negligible for small values of seeker head angle, but as θ_h increases, the restoring torque will increase more rapidly, in a nonlinear manner, as depicted in Fig. 3.6-5. This effect is represented here by a power law nonlinearity, viz.

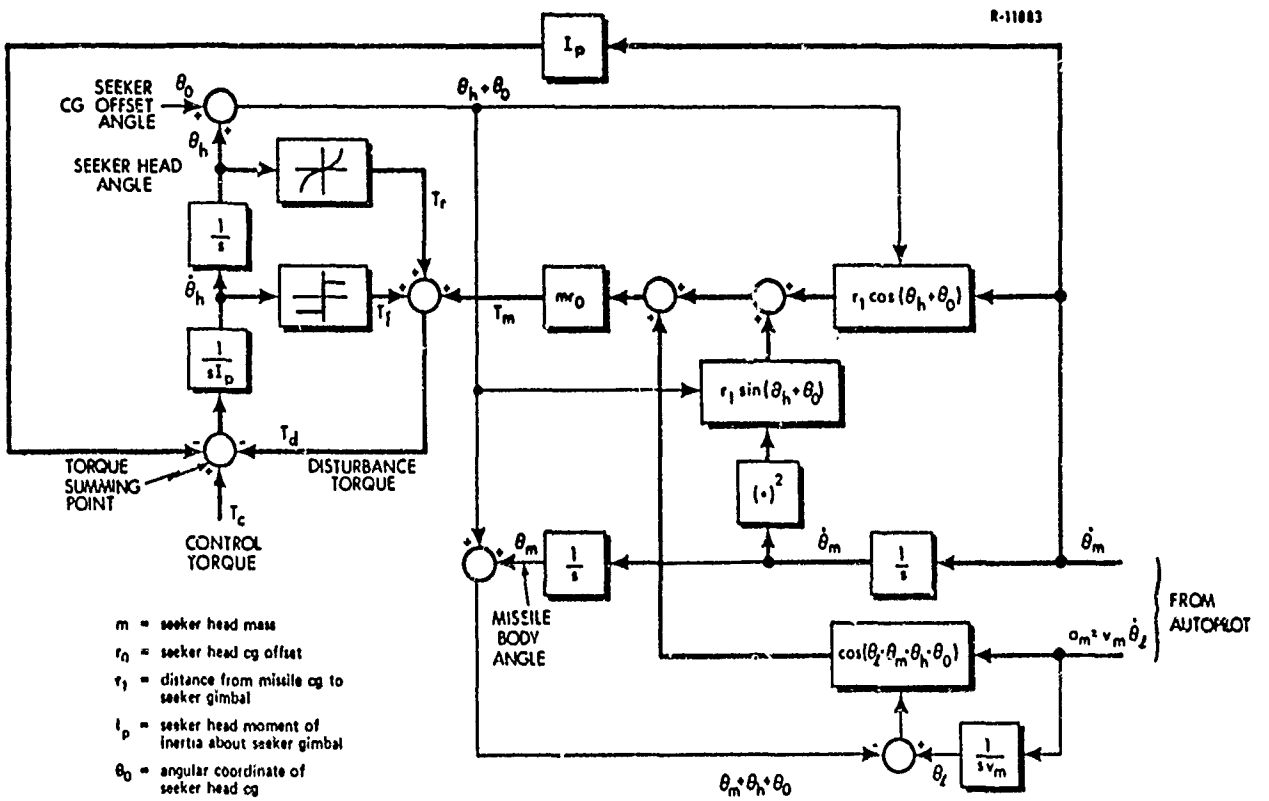

Figure 3.6-5 Disturbance Torque Model

$$T_r = f_1(\theta_h) = k_1 \left| \frac{\theta_h}{\theta_{lim}} \right|^{\kappa} \text{sign}(\theta_h) \qquad (3.6\text{-}1)$$

where κ is an integer. A final nonlinearity is introduced to describe the friction torque, T_f; in particular, we consider the "dry" or coulomb type of friction which produces a counter torque that is constant in value, having the sign of the seeker angular rate,

$$T_f = f_2(\dot{\theta}_h) = k_2 \text{ sign } (\dot{\theta}_h) \qquad (3.6\text{-}2)$$

Coulomb friction can cause limit cycles to appear in the seeker track loop, producing a deterioration in the missile guidance system performance.

3.7 SUMMARY

In Fig. 3.7-1 the complete missile-target intercept model is portrayed with all of the subsystems described in the previous sections appropriately interconnected. All of the system variables are depicted except angle of attack, control fin deflection and the seeker compensation state, which are encompassed in the linear dynamics represented by the transfer functions $g_1(s)$, $g_2(s)$, and $(1+k_0/s)$. The functions $f_1(x_1)$, $f_2(x_2)$ and $f_3(\epsilon)$ represent effects due to nonlinear restoring torques acting on the seeker head, nonlinear friction in the seeker gimbal, and the receiver characteristic, respectively. The first two are described in Eqs. (3.6-1) and (3.6-2). The last function is the standard limiter operating on measured boresight error, as illustrated in Fig. 3.6-4. All other effects are described by the specific functional relations shown.

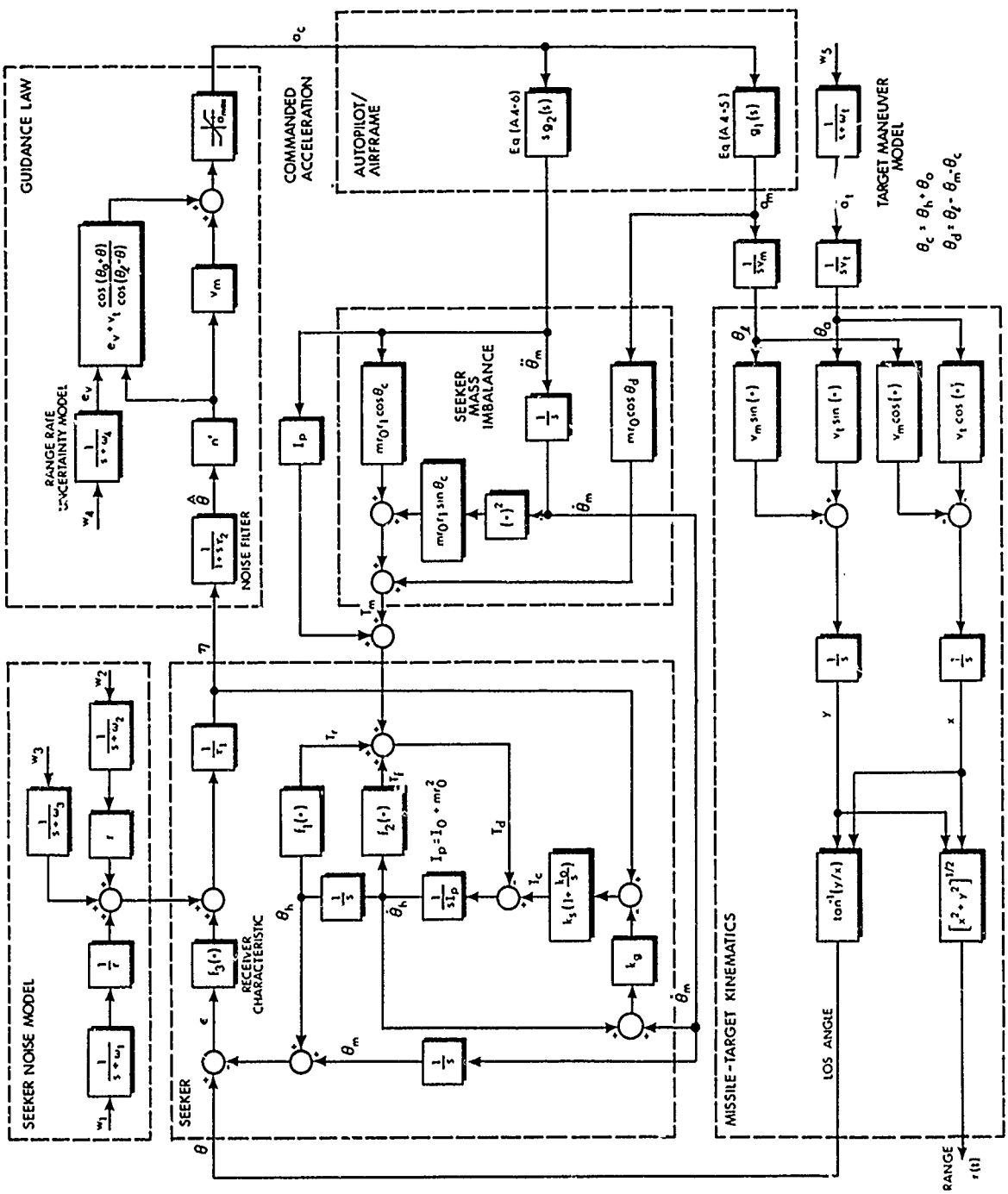

Figure 3.7-1 Overall Missile-Target Intercept Model

4. CADET AND MONTE CARLO STUDIES OF NONLINEAR EFFECTS

4.1 CADET-MONTE CARLO COMPARISONS FOR THE BASIC SYSTEM

In extending the validity of CADET as a missile system analysis tool, we first consider the basic system model, which includes the following nonlinear effects:

- Range-dependent seeker noise sources (Fig. 3.6-1)
- Proportional navigation law with secant compensation (Fig. 3.5-1)
- Acceleration command limiting (Fig. 3.5-1)
- Missile-target kinematics (Section 3.1)
- Inverse tangent calculation of LOS angle

The basic system model incorporates nine distinct nonlinearities, listed in Section A.8, as compared with previous investigations (Refs. 1 to 3) where the same effects were approximated by only three nonlinearities and several linear time-varying gains.

In all studies, the three components of the wide-band seeker noise (100 rad/sec bandwidths) are always specified such that they have an equal effective rms level at about the midpoint of the terminal homing phase. To be more precise, the spectral densities of the three white noise inputs w_1 to w_3 in Fig. 3.6-1 are chosen to achieve rms values of the noise states x_{14}, x_{15} and x_{16} that satisfy

$$q_1 = \sigma_o^2 \times 10^4 \longrightarrow \sigma_{14} = 0.7071\,\sigma_o \text{ rad-ft}$$

$$q_2 = \sigma_o^2 \times 10^{-12} \longrightarrow \sigma_{15} = 0.7071 \times 10^{-8}\sigma_o \text{ rad/ft}$$

$$q_3 = \sigma_o^2 \times 10^{-4} \longrightarrow \sigma_{16} = 0.7071 \times 10^{-4}\sigma_o \text{ rad} \qquad (4.1\text{-}1)$$

where we have used the relation indicated in Eq. (3.3-2). The dimensionless parameter σ_o is designated the seeker noise factor. The three components of the range dependent seeker noise,

$$n_s = x_{14}/r(t) + x_{15}r(t) + x_{16}$$

thus have rms levels given approximately by $\sigma_{14}/r(t)$, $\sigma_{15}\,r(t)$ and σ_{16}, respectively, which are equal for $r(t) = 10,000$ ft. With the nominal parameter values indicated in Table 4.1-1, $r(t)$ achieves this value at about $t = 2.5$ sec in a terminal homing phase of about six seconds duration.

For all of the studies that follow, the fundamental measure of system performance is rms miss distance; this is defined to be the rms cross-range missile-target separation at the mean terminal time, t_f. The mean terminal time, defined as the instant when the mean down-range separation, m_x, goes through zero, is a variable in this study; its value without random disturbances or initial conditions is 6 sec, while the presence of noise sources or a nonzero rms target maneuver level typically increases t_f by a few hundredths of a second. This effect is a direct result of relaxing the assumption of constant closing velocity that was made in earlier work (Refs. 1 and 2).

In every case considered in this chapter, one or several of the system parameters are allowed to vary from the nominal, and the effects of this change on the missile guidance system performance are analyzed via

TABLE 4.1-1

NOMINAL SYSTEM PARAMETERS
(Refer to Fig. 3.7-1)

SEEKER PARAMETERS	Seeker head mass, m		0.15 oz-sec^2/in
	Seeker head moment of inertia about cg, I_0		0.1 in-oz-sec^2/rad
	Seeker head cg offset, r_0		0 in
	Angle of seeker head cg offset, θ_0		0 rad
	Distance, missile cg to seeker gimbal, r_1		40 in
	Servo gain, ks		6 in-oz-sec/rad
	Rate gyro gain, kg		1
	Integral compensator gain, k_0		0
	Track loop time constant, τ_1		0.12 sec
	Restoring torque, $f_1(x_1)$		0 in-oz
	Gimbal friction, $f_2(x_2)$		0 in-oz
GUIDANCE LAW PARAMETERS	Noise filter time constant, τ_2		0.3 sec
	Navigation ratio, n′		4
	Acceleration command limit, a_{max}		250 ft/sec^2
AUTOPILOT/ AIRFRAME TRANSFER FUNCTIONS	$g_1(s) = \frac{c_3 s^2 + c_2 s + c_1}{s^3 + c_3 s^2 + c_2 s + c_1}$;	c_1	720 sec^{-3}
		c_2	275 sec^{-2}
		c_3	18.3 sec^{-1}
	$g_2(s) = \frac{d_2 s + d_1}{s^3 + c_3 s^2 + c_2 s + c_1}$;	d_1	0.24 rad/ft-sec^2
		d_2	0.642 rad/ft-sec
		e_1	720 sec^{-3}
		e_2	-0.865 sec^{-2}
		e_3	-1.87 sec^{-1}
VEHICLE VELOCITIES	Missile velocity magnitude, v_m		3000 ft/sec
	Target velocity magnitude, v_t		1000 ft/sec
RANDOM INPUT BANDWIDTHS	Seeker noise source bandwidths, $\omega_1, \omega_2, \omega_3$		100 rad/sec
	Target maneuver bandwidth, ω_t		0.2 rad/sec
	Range rate uncertainty bandwidth, ω_4		100 rad/sec
NOISE STATE RMS LEVELS	Range rate uncertainty level, σ_{12}		0 ft/sec
	Target acceleration level, σ_{13}		50 ft/sec^2
	Seeker noise factor (Eq. (4.1-1)), σ_0		1
STATE VARIABLE INITIAL CONDITION STATISTICS	Mean heading error, m_8		0 deg
	RMS heading error, σ_8		1 deg
	Mean down-range separation, m_{11}		24,000 ft
	RMS down-range separation, σ_{11}		0 ft

CADET. A few of the resulting performance projections are compared with monte carlo studies to provide a basis for assessing the accuracy of CADET in capturing the effect under consideration. Since the nominal case is to be used as the starting point for all subsequent studies of nonlinear effects and parameter variations, it takes on a significance that makes it advisable to perform a monte carlo verification using a large number of trials.

One comparison of the results of CADET and monte carlo analysis for the nominal case is shown in Fig. 4.1-1. A second case with a reduced acceleration command limit, $a_{max} = 150\ ft/sec^2$, is also portrayed; the latter curve demonstrates the significant deterioration in the missile guidance system performance that results from reducing the missile maneuverability. This nonlinear effect has been treated in previous studies; Fig. 4.1-2, taken from Ref. 2, indicates the typical variation in rms miss distance with changing missile acceleration limit.

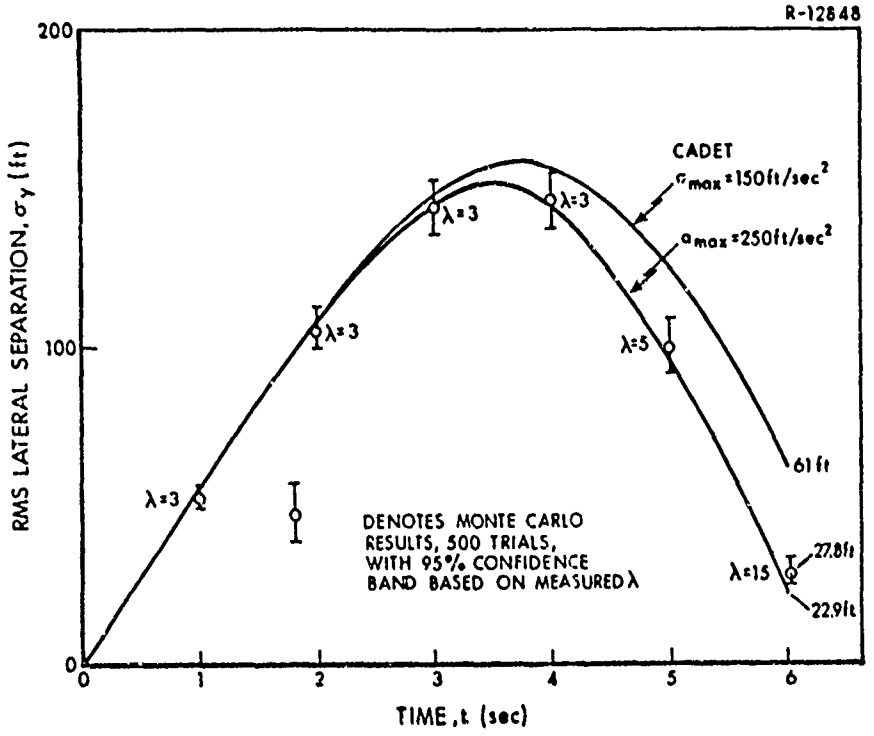

Figure 4.1-1 Effect of Acceleration Command Limiting on Basic System Performance

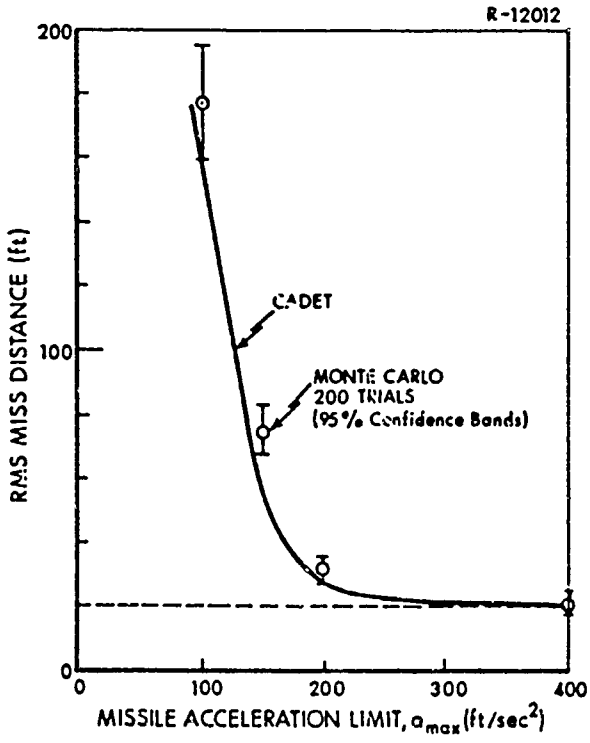

Figure 4.1-2 Acceleration Command Limit Study (Ref. 2)

Returning to the nominal case (a_{max} = 250 ft/sec^2 in Fig. 4.1-1), we note that the CADET result (the smooth curve, exhibiting an rms miss distance of 22.9 feet at 6 sec) lies within, or close to, the 95% confidence band of the corresponding monte carlo data throughout the engagement. The width of the confidence band provides a measure of the theoretical reliability of the monte carlo data, based on the number of trials performed and an estimate of λ (kurtosis; refer to Section 2.1).

The fact that the monte carlo estimate of the rms lateral separation, $\hat{\sigma}_y$, is a random variable that converges to the true value slowly as the number of trials increases is depicted in Fig. 4.1-3, where we show the value of $\hat{\sigma}_y$ versus the number of trials performed, q. The case shown in Fig. 4.1-3a corresponds to the estimation of rms lateral separation two seconds before intercept, when the probability density function is nearly gaussian ($\lambda \cong 3$). The accuracy of the result obtained by performing 500

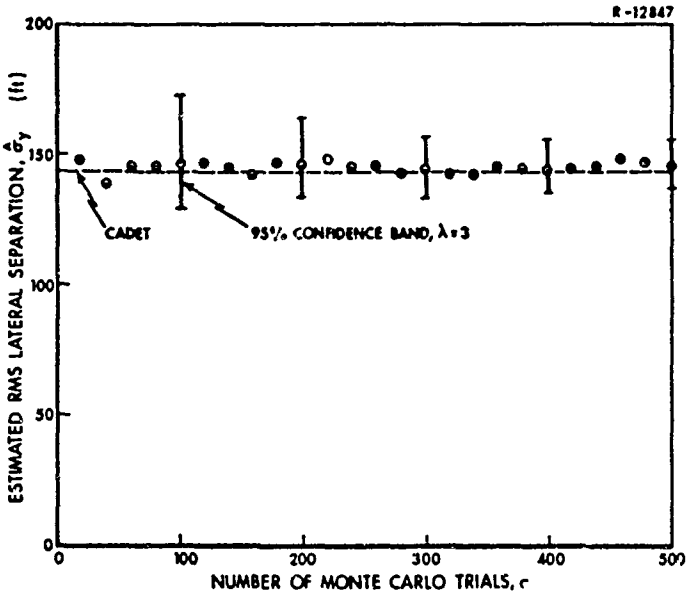

(a) t = 4 sec

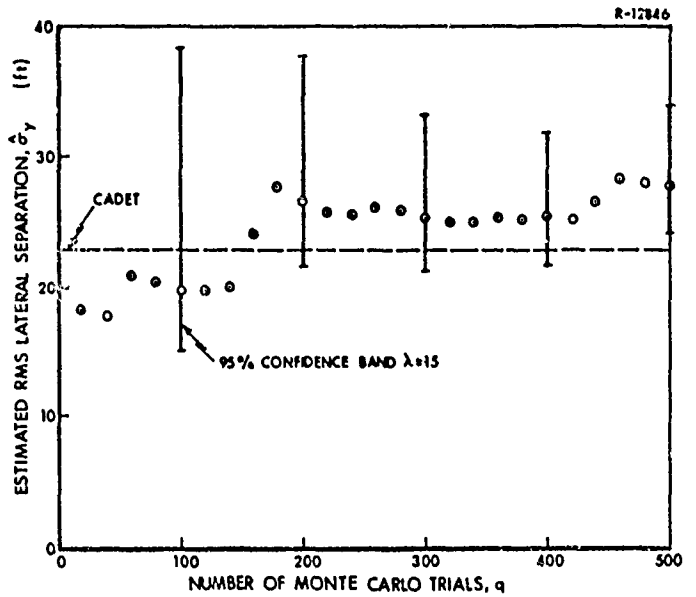

(b) t = 6 sec

Figure 4.1-3 Comparison of CADET and Monte Carlo rms Lateral Separation for the Nominal Case

monte carlo trials is quantified by

$$\Pr\left[137.7 \text{ ft} \leq \sigma_y(4) \leq 156.0 \text{ ft}\right] = 0.95$$

Near the terminal time, however, the density of y is found to be significantly

nongaussian; on the basis of the monte carlo study, it is estimated that the kurtosis is approximately 15. Thus the estimate of the rms miss distance, $\hat{\sigma}_y(6)$, necessarily is less certain than when y is gaussian. The large value of λ is due to nonlinearity in the system which gives rise to a small but significant probability that the miss distance may be very large (see also Section 5.3); whenever a trial is performed which results in such a pathological miss there is a large "transient" in the estimated rms miss distance. This phenomenon is observed between trials 140 and 180 and between trials 420 and 460 in Fig. 4.1-3b.

The agreement of CADET and the monte carlo analysis is excellent as long as y is reasonably gaussian; at the end of the engagement, CADET appears to have underestimated the rms miss distance by ten to fifteen percent. This study provides a graphic demonstration of the fact that several hundred or even a few thousand monte carlo trials are required to obtain an estimate of rms miss distance that is more accurate than the result given by CADET. Taking the five sets of 100 trials separately*, the value of $\sigma_y(6)$ varies from 19.72 to 35.88 ft; thus the use of only 100 trials is inadequate for determining the absolute accuracy of CADET. On the basis of this quite typical behavior, we generally consider that the CADET result is well verified whenever it lies close to or within the 95% confidence band.

The present study of the nominal case also shows that CADET can yield a very accurate analysis of the mean value of the down-range separation,

*The first 100 trials shown in Fig. 4.1-3b yielded $\sigma_y(6) \cong \sigma_1 = 19.72$ ft, the second set (trials 101 to 200) resulted in $\sigma_y(6) \cong \sigma_2 = 32.08$ ft, and subsequent sets yielded $\sigma_3 = 22.25$ ft, $\sigma_4 = 25.67$ ft, and $\sigma_5 = 35.88$ ft. To aggregate the statistics for various sets of trials, it is necessary to average the variances:

$$\sigma^2_{200} = v_{200} = \frac{1}{2}(\sigma^2_1 + \sigma^2_2), \ldots, \qquad \sigma^2_{500} = v_{500} = \frac{1}{5}(\sigma^2_1 + \ldots \quad \sigma^2_5)$$

m_x, when the terminal time is not deterministic. In Fig. 4.1-4, it is demonstrated that the CADET analysis is well verified by the monte carlo results. The mean terminal time given by CADET, 6.026 sec, is in almost exact agreement with the monte carlo figure.

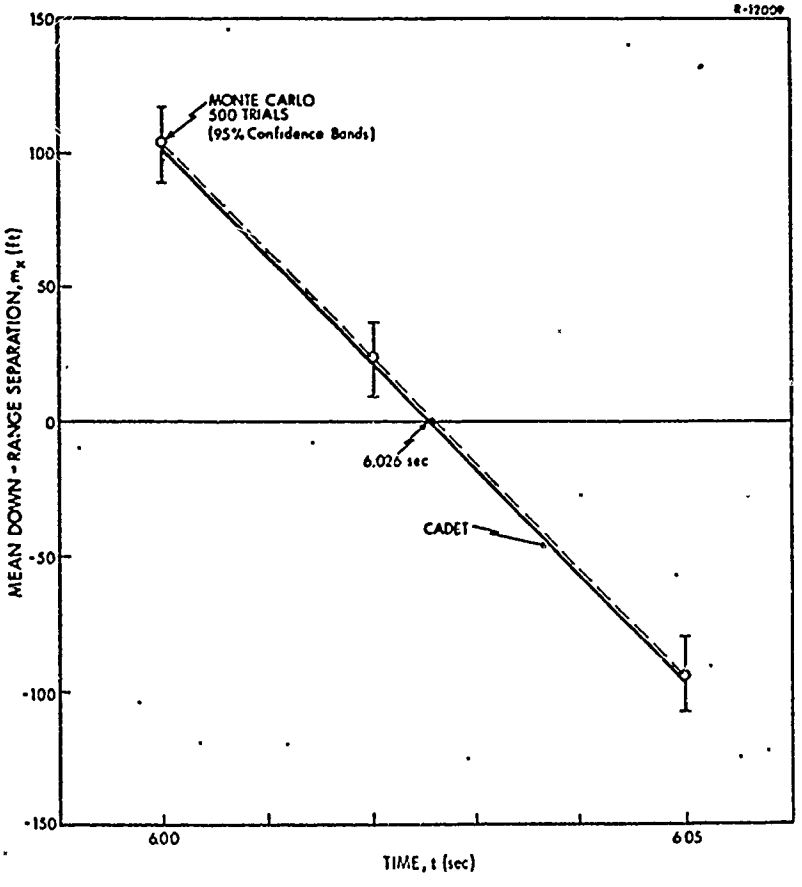

Figure 4.1-4 Mean Down-Range Missile-Target Separation Near the Mean Terminal Time

The remaining two components of the missile-target separation are of secondary importance. The mean lateral separation, m_y, computed by CADET and the monte carlo method, is shown in Fig. 4.1-5a. We note that CADET gives the exact result for the mean of y, viz. $m_y \equiv 0$ throughout the

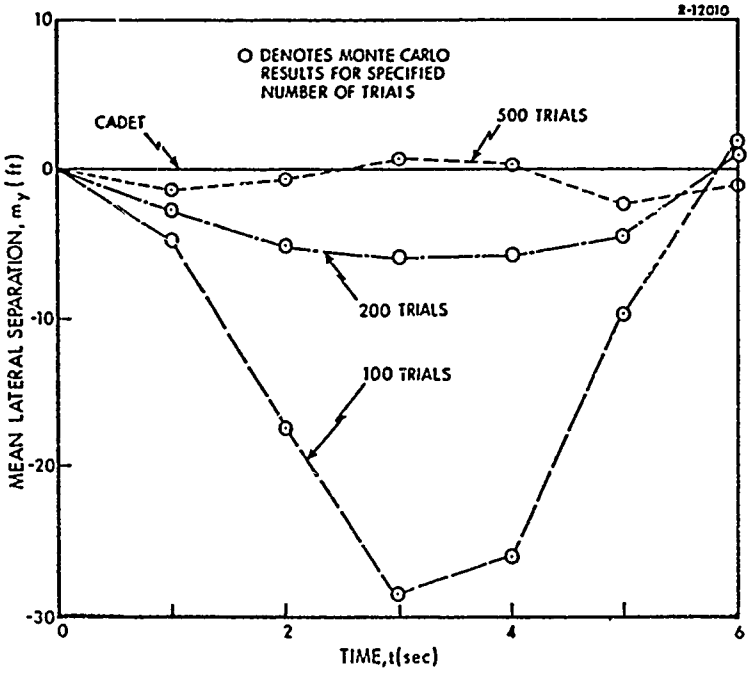

(a) CADET AND MONTE CARLO STUDY OF MEAN LATERAL SEPARATION

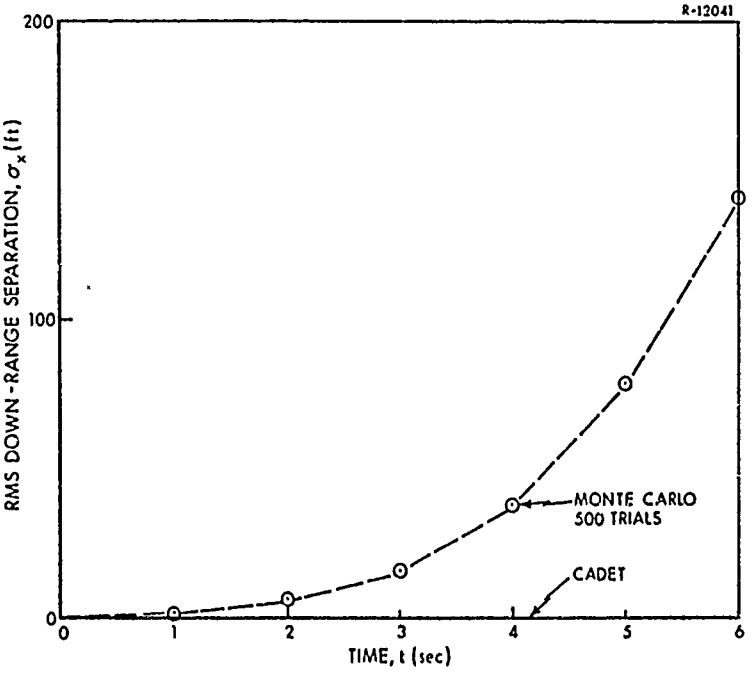

(b) CADET AND MONTE CARLO STUDY OF RMS DOWN-RANGE SEPARATION

Figure 4.1-5 Mean Lateral Separation and rms Down-Range Separation in the Nominal Case

engagement, * while the monte carlo results converge to a zero mean quite slowly. However, CADET incorrectly indicates that x has no random component ($\sigma_x \equiv 0$) as shown in Fig. 4.1-5b, which is not true; it is observed, however, that σ_x is negligible except in the last few hundredths of a second of the terminal homing phase. The lack of a random component of x in the CADET analysis is due to the even symmetry of the nonlinearities cos (θ_a) and cos (θ_ℓ) that constitute the two contributions to $\dot{x}$; any even function with a zero mean input has a random input describing function gain that is identically equal to zero.

Figure 4.1-6 indicates the sensitivity of the miss distance to changes in the noise level for the basic system configuration. The more stringent

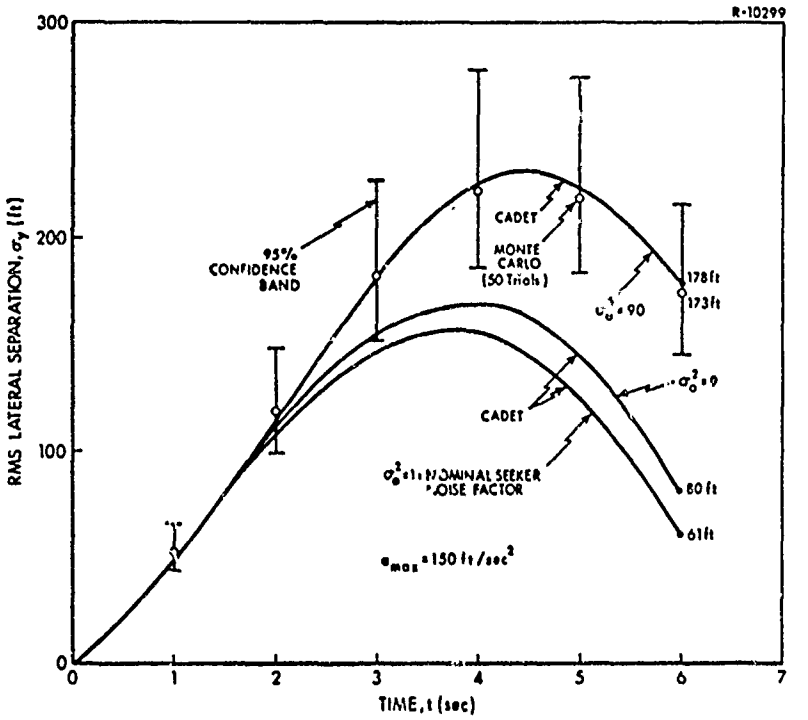

Figure 4.1-6 Effect of Seeker Noise Level on the Basic System Performance

*This can be demonstrated by noting that there are no mean components in the initial conditions except for x(0) = 24,000 ft, and no bias components in the random disturbances, so the basic guidance loop nonlinearities have odd symmetry and all variables except range have zero means for all time.

acceleration command limit, a_{max} = 150 ft/sec^2, was retained in this investigation. For a seeker noise factor of $\sigma_o^2 = 90$, a significant deterioration in the rms miss distance is observed, and the CADET analysis is well verified by the monte carlo results.

The above investigation of the capability of CADET to provide an accurate measure of tactical missile performance verifies the applicability of CADET to the basic system model, thus paving the way for studies of other effects.

4.2 SEEKER MASS IMBALANCE

In this study, it is assumed that the seeker head center of gravity (cg) is offset from the gimbal pivot point by a distance r_0, and located at an angle θ_0 with respect to the antenna centerline (refer to Fig. 3.6-2). This cg offset results in an effective disturbance torque of significant complexity. Two types of nonlinearities that have not previously been studied are required to model the effect of mass imbalance. These are the product of one variable with a trigonometric function of another variable ($v_1 \cos v_2$), and the square of a variable times a trigonometric function of a second variable ($v_1^2 \sin v_2$).

The sensitivity shown in Fig. 4.2-1 corresponds to the situation where the seeker head cg is directly in front of the gimbal point -- $\theta_0 = 0$ deg. Without seeker dynamic compensation, described in Section 3.6, a pronounced deterioration in the missile guidance system performance is noted with very small values of cg offset. Even for an offset of one thousandth of an inch, Fig. 4.2-1 indicates that the rms miss distance is nearly twice the nominal value. The introduction of proportional plus integral compensation to remove the effect of steady state disturbance torques (Section A.7)

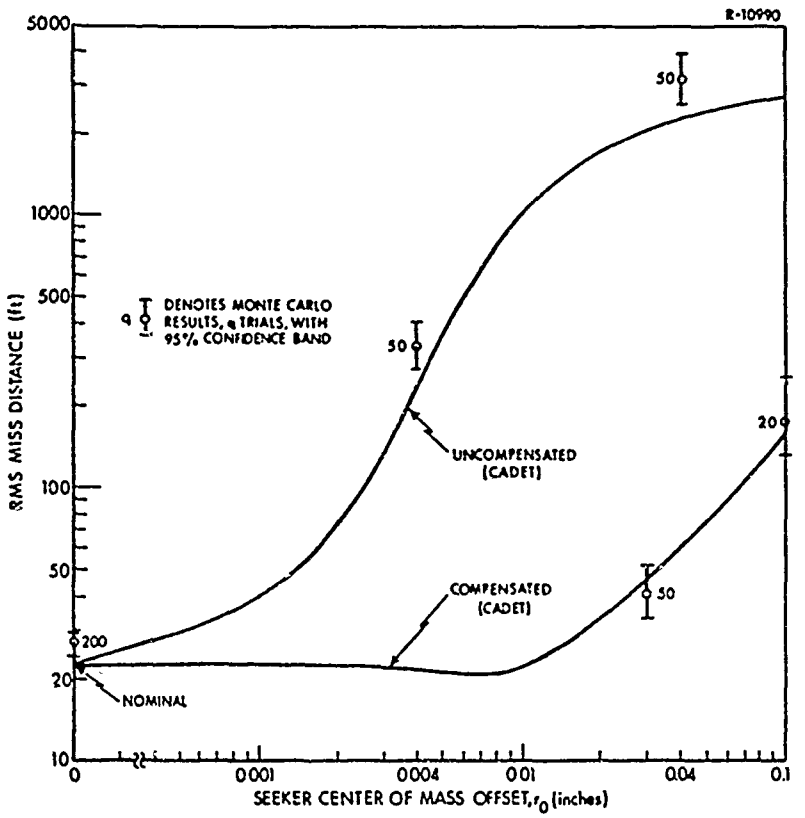

Figure 4.2-1 Effect of Seeker Mass Imbalance on Guidance Accuracy

markedly improves the guidance system performance. In both the uncompensated and compensated cases, the monte carlo results* are in good agreement with the CADET analysis, even when extremely large miss distances are incurred. Thus CADET gives an accurate assessment of the effect of seeker mass imbalance.

*The confidence bands plotted in Fig. 4.2-1 and subsequent figures are based on the gaussian assumption ($\lambda \cong 3$). In the previous section it is demonstrated that the actual confidence bands are probably larger; it is not possible to obtain a useful estimate of the kurtosis with fewer than one hundred monte carlo trials, however, so no attempt is made to consider this factor.

The effect of the angular coordinate of the cg location, θ_0, was studied for a single value of cg offset (0.03 in) and with the seeker assumed to be compensated. The CADET analysis indicates only a slight difference in rms miss distance for θ_0 = 180 deg compared with the case θ_0 = 0 deg, as shown in Fig. 4.2-2. With the cg offset normal to the antenna centerline (θ_0 = 90 deg), the guidance system terminal performance deterioration was lessened to a great extent. We observe that the most significant difference between these three cases occurs in mid-flight; the fact that the maximum rms lateral separation is much smaller for θ_0 = 0 deg than for θ_0 = 180 deg can be attributed to an effective change in the seeker dynamics.

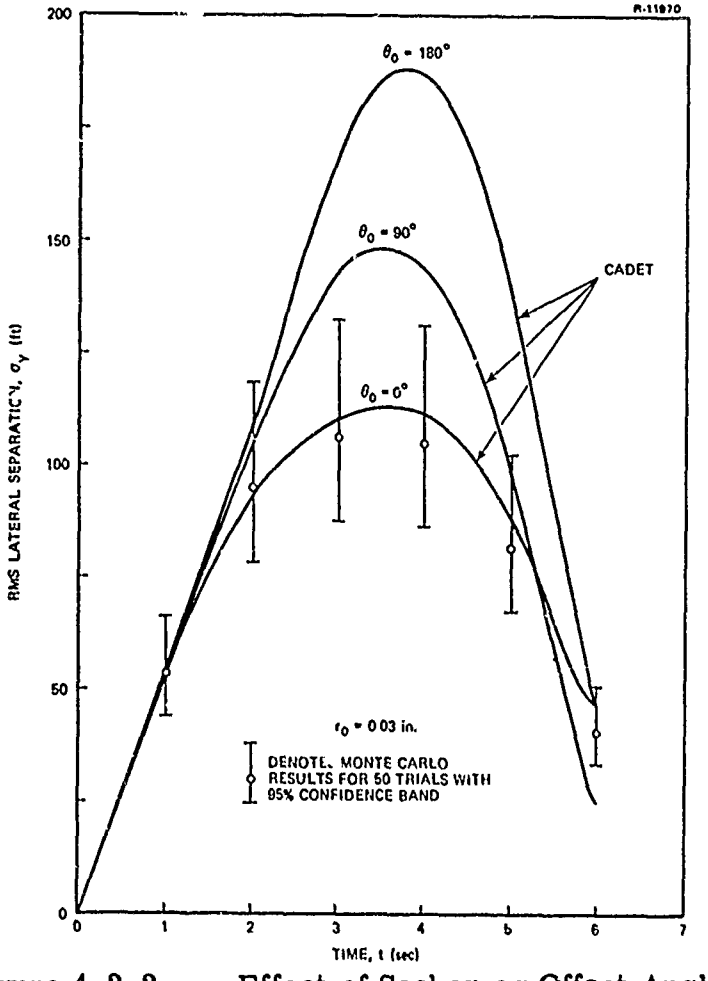

Figure 4.2-2 Effect of Seeker cg Offset Angle with Compensated Seeker

4.3 SEEKER GIMBAL DRY FRICTION

The occurrence of dry or Coulomb friction in the seeker gimbal introduces a disturbance torque of the form

$$T_{\cdot} = k_2 \text{ sign } (\dot{\theta}_h)$$

where $\dot{\theta}_h$ is the seeker angular rate measured relative to the missile airframe. Results from a study of this effect are presented in Fig. 4.3-1.

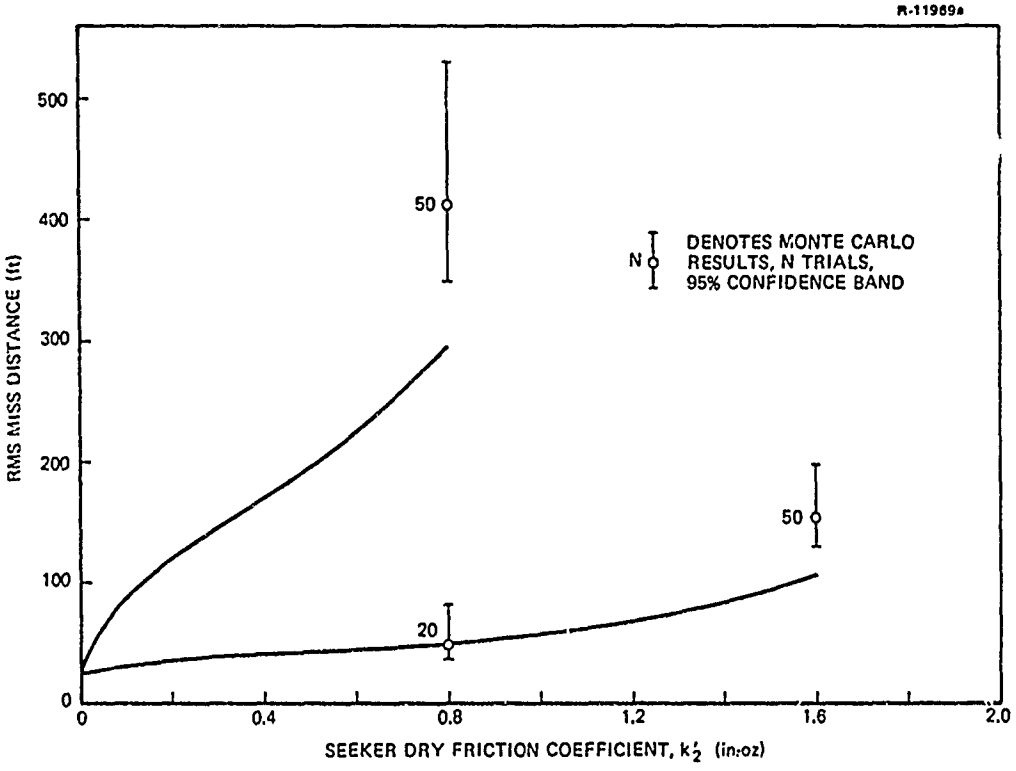

Figure 4.3-1 Effect of Seeker Gimbal Dry Friction on Guidance Accuracy

First, several values of the dry friction coefficient, k_2, were selected and CADET analysis was performed to obtain a prediction of the rms miss distance that would result without seeker dynamic compensation. When proportional plus integral compensation was incorporated in the

seeker track loop, a significant improvement was observed in the performance projections provided by CADET. It can be seen in Fig. 4.3-1 that for a dry friction coefficient of 0.8, the miss distance is reduced by a factor of 6 when compensation is implemented.

Three monte carlo studies were undertaken to check the accuracy of CADET; two for the compensated case and one to verify the large rms miss distance given by CADET for the uncompensated seeker. In every case, the CADET result was near or within the 95% confidence band of the monte carlo estimate, which verifies the ability of CADET to capture the effect of dry friction quite adequately even when the guidance system performance (as measured by rms miss distance) was degraded by an order of magnitude from the nominal case.

It is well known that the dry friction relay-type characteristic can lead to limit cycling in dynamic systems. This phenomenon can be explained, using the standard sinusoidal input describing function theory, by the fact that the effective gain of this discontinuous nonlinearity is extremely large for small signals (Ref. 8). Thus a point of considerable interest is whether or not the missile performance degradation observed in Fig. 4.3-1 is due to limit cycles in the seeker track loop. A single monte carlo simulation was performed for both the compensated and uncompensated seeker, with dry friction coefficients of 1.6 and 0.8 respectively, and limit cycles were clearly observed, as shown for the compensated case in Fig. 4.3-2. It is evident that CADET can provide a reasonably accurate assessment of the missile guidance system performance under such circumstances.

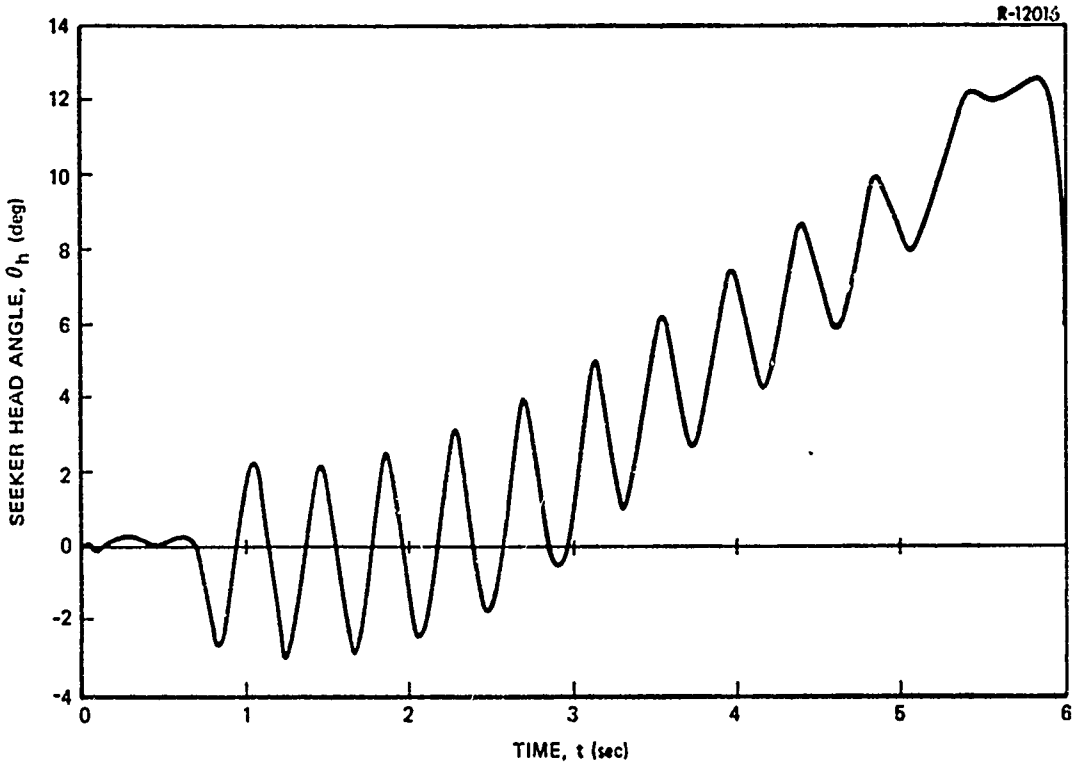

Figure 4.3-2 Existence of Limit Cycles due to Seeker Gimbal Dry Friction with Compensated Seeker

4.4 NONLINEAR SEEKER HEAD RESTORING TORQUES

The classical "hard spring" type of nonlinearity -- usually modeled as a power law characteristic,

$$T_r = k_1 \left| \frac{\theta_h}{\theta_{lim}} \right|^{\kappa} \text{sign}(\theta_h)$$

where κ is an integer greater than one -- provides an example of another class of nonlinear effects, where the output is small for small seeker angle deflections ($\theta_h << \theta_{lim}$) but increases more rapidly than a linear characteristic when θ_h exceeds θ_{lim}. Such a restoring torque might occur as the

result of a seeker head spring restraint system designed to prevent large values of seeker head angle to preclude the seeker head reaching its stops, or might occur naturally due to wiring harnesses or other flexible linkage to the missile body. The case investigated, $\kappa = 11$, corresponds to a negligible spring effect for small θ_h and a very rapid increase in restoring torque as θ_h approaches θ_{lim}. In this study, we confined our attention to the compensated seeker case, and chose θ_{lim} to be 10 deg.

The variation of rms miss distance as a function of the nonlinear spring coefficient, k_1, is shown in Fig. 4.4-1. The CADET analysis indicates that the miss distance increases very abruptly with k_1 for $k_1 < 0.2$; the monte carlo simulations carried out for two cases well verified the performance projections given by CADET.

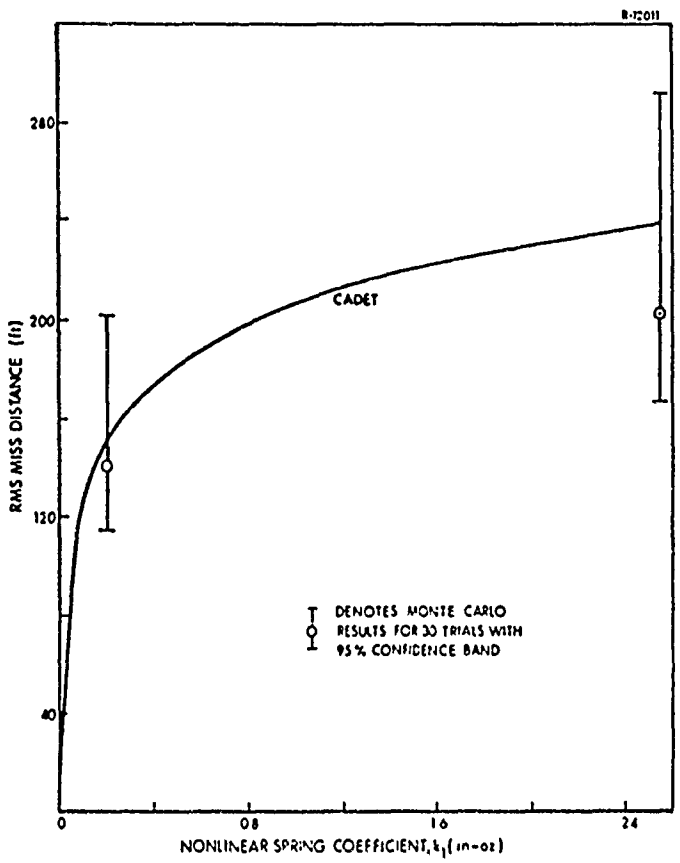

Figure 4.4-1 Effect of Nonlinear Restoring Torques on Guidance System Performance

An interesting aspect of the above comparison is that the monte carlo analysis required a smaller integration step size in simulating the system response than was required in the CADET propagation of the statistics.* The CADET program ran correctly with an integration step size of 0.01 sec, while the monte carlo program required 0.005 sec to avoid overflow due to numerical instability. It is reasonable to conjecture that CADET may be more immune to numerical errors inherent to the integration techniques for solving differential equations on a digital computer, since quasi-linearization tends to "smooth" nonlinearities -- e.g., refer to Fig. 5.1-2; thus in cases where the nonlinearity exhibits large variations in slope, CADET will tend to have an increased computational advantage with respect to the monte carlo method.

4.5 RECEIVER CHARACTERISTIC AND RANGE RATE UNCERTAINTY

The effect of the receiver/signal processing nonlinearity for the case where the boresight error limiter (Fig. 3.6-3) saturates at $\epsilon_{lim} = 0.25$ deg (representative of narrow-beamwidth monopulse radar systems (Ref. 12) or infrared seekers) was considered. The effectiveness of the seeker was reduced by increasing the track loop time constant from 0.12 to 0.32 sec (which increases the boresight error rms level by the same factor, 2.6, and thus increases the effect of limiting). For the above parameter values, Fig. 4.5-1 shows that CADET predicted a deterioration in rms miss distance from 22.9 ft (in the nominal case) to 28.8 ft. The monte carlo method provided a good verification of this result; for 60 trials, the nominal rms miss distance was predicted to be 20.9 ft and the effect of choosing $\epsilon_{lim} = 0.25$ deg and $\tau_1 = 0.32$ sec was to increase

*Both programs used the same integration technique -- the fourth-order Runge-Kutta method.

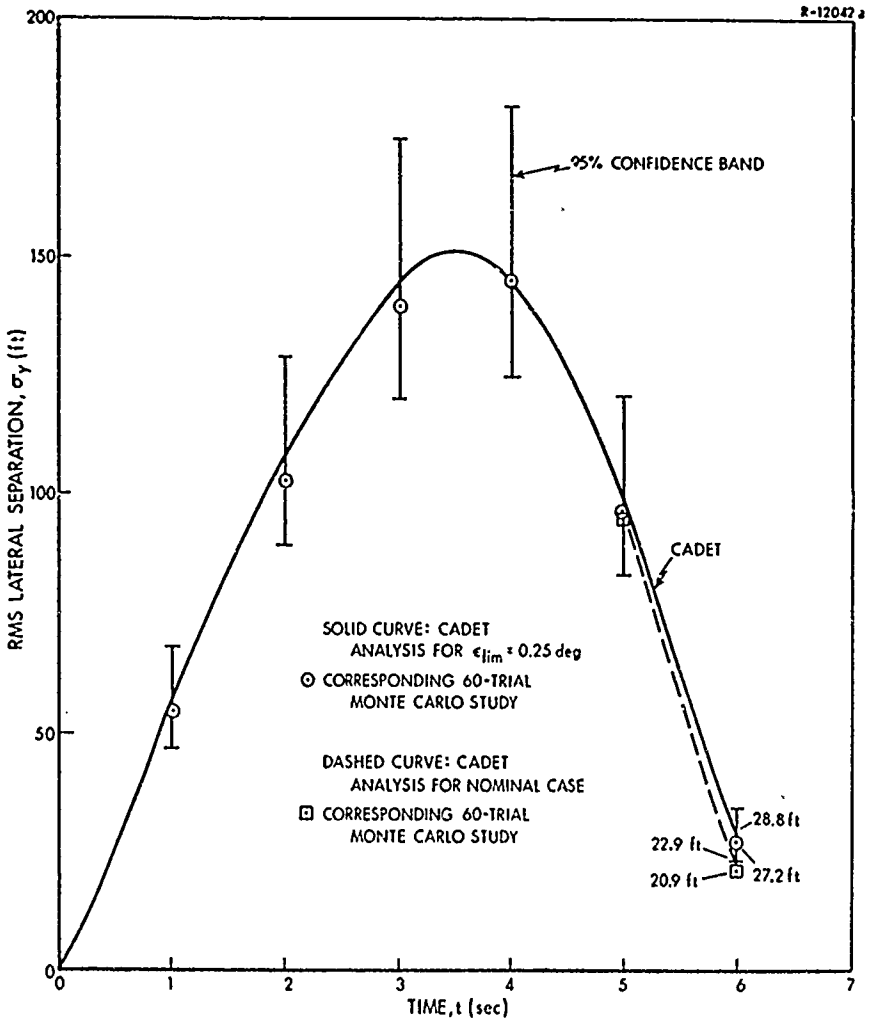

Figure 4.5-1 Effect of Boresight Error Saturation on Guidance Accuracy

this miss to 27.2 ft, where the same sets of initial conditions and noise inputs were used for the two cases.

The effect of range rate uncertainty in the guidance law (refer to Fig. 3.5-1) was assessed for the case of a fixed (bias) uncertainty. It was assumed that the guidance package range rate information was in error by a fixed value of 500 ft/sec. The monte carlo result, shown in Fig. 4.5-2, is that the rms miss distance is decreased slightly by this error; CADET analysis predicts that the effect is virtually insignificant (Fig. 4.5-3). Both methods agree that the rms lateral separation is reduced from the nominal case in mid-flight for e_{vb} = +500 ft/sec; this is to be expected, since the

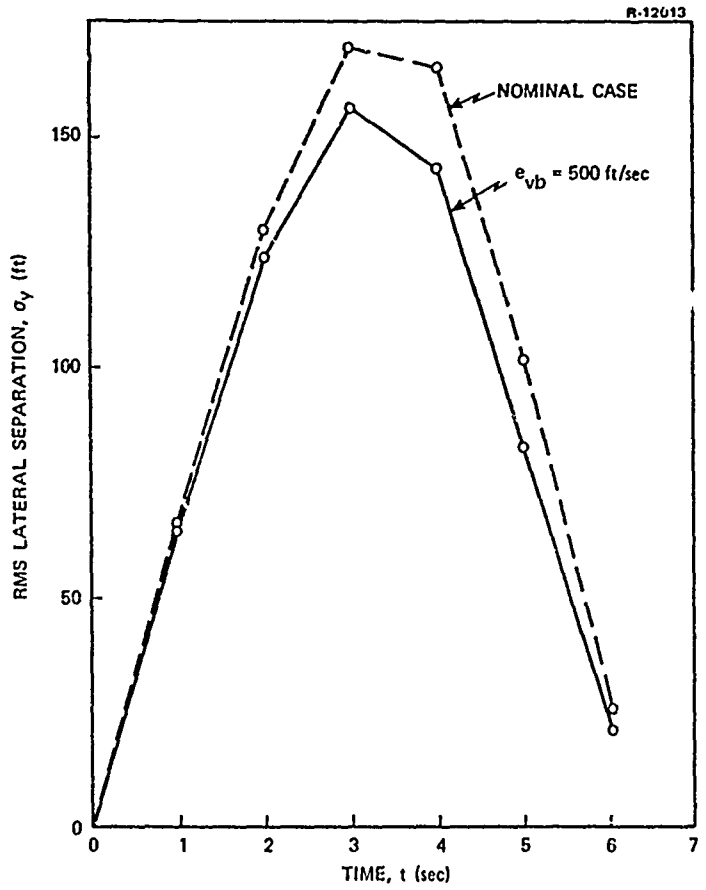

Figure 4.5-2 Effect of Bias Range Rate Uncertainty on Guidance System Performance, 20 Trial Monte Carlo Analysis

error modeled above is equivalent to assuming that the guidance package range rate value is approximately 4500 ft/sec rather than about 4000 ft/sec in the nominal case.* This corresponds to a range rate error of + 12.5%, which is equivalent in effect to the same percentage increase in the navigation ratio, n′. Previous studies (Ref. 2) have shown that the guidance system performance is quite insensitive to moderate changes in n′; however, a higher value of n′ results in a somewhat faster guidance loop which should lead to the reduction in rms 'ateral separation in mid-flight.

*Closing velocity is actually a random variabie, as indicated in Fig. 3.5-1.

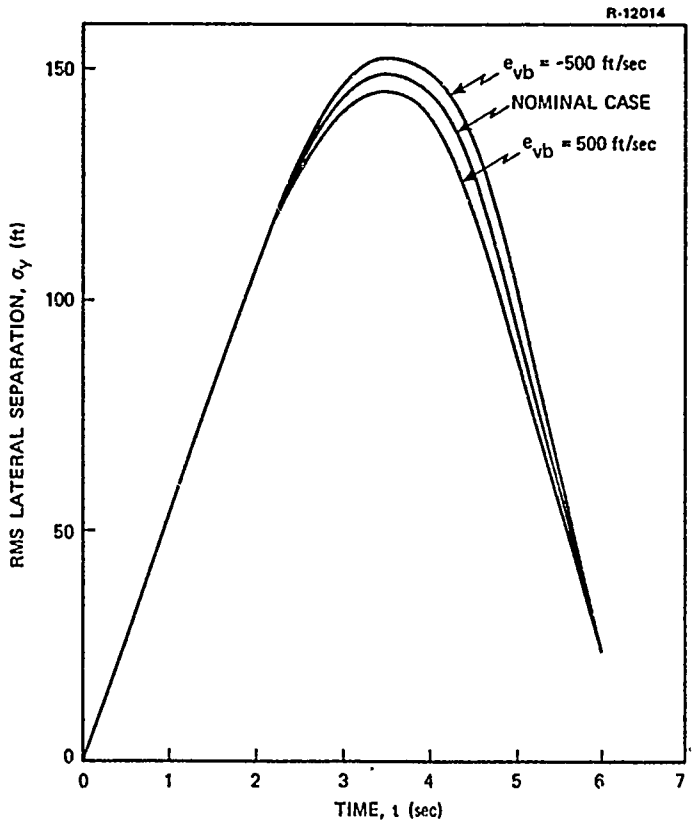

Figure 4.5-3 Effect of Bias Range Rate Uncertainty on Guidance System Performance via CADET

4.6 CADET-MONTE CARLO COMPARISON WITH ALL NONLINEAR EFFECTS

As a final study of the efficacy of CADET in providing an accurate statistical analysis of the performance of a complex, highly nonlinear tactical missile guidance system model, we consider the effect of exercising all of the nonlinearities in combination. Values of the parameters are shown in Table 4.6-1. They were chosen such that each nonlinearity alone had led to a significant deterioration of system performance from nominal in the studies treated in Sections 4.2 to 4.5.

The results of the CADET and monte carlo statistical analysis are shown in Fig. 4.6-1. The CADET value of rms lateral separation is well verified by the 30-trial monte carlo study.

TABLE 4.6-1

PARAMETER VALUES THAT EXERCISE ALL NONLINEARITIES*

Effect	Parameters	Values
Seeker Mass Imbalance	r_0, θ_0	0.03 in, 0 deg
Nonlinear Restoring Torque	k_1, κ; θ_{lim}	0.05 in-oz, 11, 10 deg
Nonlinear Gimbal Friction	k_2	0.8 in-oz
Boresight Error Limiter	ϵ_{lim}	0.25 deg
Seeker Compensation Gain	k_0	20.0

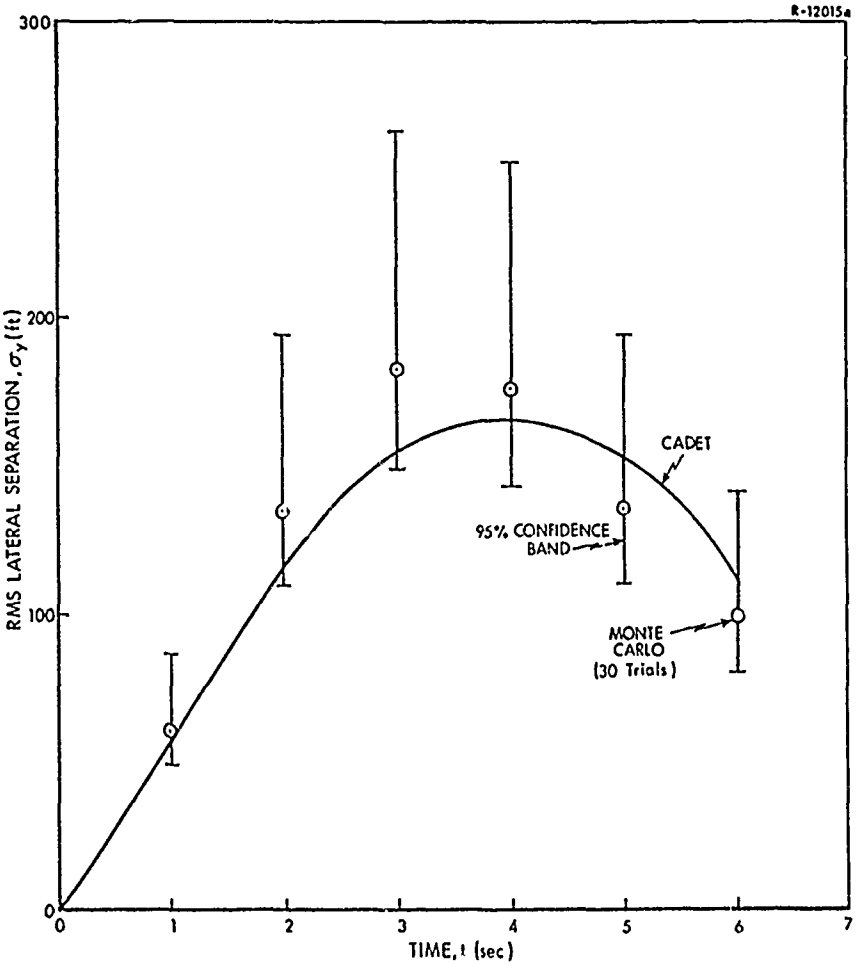

Figure 4.6-1 Guidance System Performance with All Nonlinearities Exercised

*Only deviations from the nominal case, Table 4.1-1, are noted.

4.7 COMPARISON OF CADET AND MONTE CARLO EFFICIENCY

One of the main arguments advanced for the use of CADET in obtaining projections of tactical missile guidance system performance is the significant reduction in computer central processing unit (CPU) time achieved by CADET when compared with the monte carlo method of statistical analysis. In making this evaluation, two issues must be addressed: the number of monte carlo trials that must be performed in order to obtain comparably accurate results, and the practical limitation imposed by computer costs. From the standpoint of accuracy, any such number is somewhat arbitrary, because the error mechanisms of CADET and the monte carlo method are essentially dissimilar, and of necessity the judgement is based on a limited body of experience. Referring to Fig. 4.1-3b, we note that in a situation where the statistics are quite nongaussian the CADET computation of rms lateral separation appears to be at least as accurate as the value estimated with 400 monte carlo trials, in the sense that the 95% confidence band for 400 trials brackets the CADET result. Where the statistics are more nearly gaussian, e.g. as in Fig. 4.1-3a, it would appear that one thousand or more trials may be required in order to achieve comparable accuracy. On the other hand, a pragmatic evaluation of the efficiency of CADET should take into account the fact that most monte carlo studies must be limited in scope by computer budget constraints. A reasonable upper bound is 256 trials since, in the gaussian case, this results in 95% confidence that an accuracy of 10% can be achieved (Section 2.1); for high order systems, even this number of trials may require too much computer time. For the present, we will thus compare the relative efficiency of the monte carlo and CADET approaches on the basis of 256 trials, recognizing that the estimated rms values of the system variables obtained for this number of monte carlo experiments may be less accurate than the CADET results.

In the present study, the savings in computer CPU time is quite significant, even though the system is of considerably higher order (n = 17) and

has more nonlinearities than in previous investigations that compared CADET and the monte carlo technique. Both of these factors tend to reduce the relative efficiency of CADET. Monte carlo simulation requires only the integration of an n-vector differential equation (q times), while CADET involves the propagation of an n-vector and an $n \times n$ symmetric matrix -- a total of $n(n+3)/2$ elements. Thus the computational burden for CADET can increase as fast as $n^2/2$ while the CPU time for monte carlo analysis only varies as n, demonstrating that an increase in the number of states may reduce the advantage of CADET in efficiency. This factor can be mitigated where there is little cross-coupling in the system; in the quasi-linear system model, this corresponds to N_r having few non-zero elements (N_r being sparse). In many practical problems, N_r is sparse and a considerable increase in the computational efficiency of CADET can be realized by the application of techniques which circumvent multiplications involving zero elements, thus streamlining the evaluation of $\dot{P}$ (Eq. (2.2-5)).

The number of nonlinearities may also increase the computation time required by CADET, since the calculation of a random input describing function in CADET generally requires more logical and numerical operations than evaluating the corresponding nonlinear function in the monte carlo program (refer to Appendix B). The present study was exceptional in having nearly as many nonlinearities as states; more typical applications of CADET would focus on a few principal nonlinear effects, leading to a greater reduction in computational burden per performance evaluation in comparison to a monte carlo analysis.

Using the same integration method in performing the monte carlo ensemble of simulations as was used in propagating the system mean vector and covariance matrix via CADET, and assuming that the same integration step size can be used in e' ch procedure, it has been possible to perform 10 CADET sensitivity studies at the same computational expense needed for one accurate monte carlo study. Since we have seen that it is possible

that the monte carlo approach may require a reduced integration step size to avoid failure of the numerical integration technique (Section 4.4), the ratio may be even higher. For the case studied in Section 4.4, the CADET analysis required only 4.4 minutes of CPU time, in contrast to about 92 minutes for a comparable 256 trial monte carlo study with one-half the step size. A more typical application of CADET can exhibit even greater advantages; a simpler but still realistic missile-target intercept problem has been treated in which a ratio of 30 CADET analyses to one monte carlo study was achieved (Ref. 2).

The studies discussed in this chapter have treated the missile-target intercept problem, represented by a nonlinear model of considerable complexity -- with between 9 and 16 nonlinearities. The results presented demonstrate that CADET has been quite successful in capturing the significant sensitivities of rms miss distance to the nonlinear phenomena in question.

5. SENSITIVITY STUDIES AND COMPUTATIONAL ISSUES

5.1 EFFECTS OF PROBABILITY DENSITY FUNCTIONS ON RANDOM INPUT DESCRIBING FUNCTIONS

An important issue that must be investigated in order to assess the potential success of CADET in providing accurate performance projections for tactical missile guidance systems is the effect of the assumption that the state variables are jointly normal on the calculation of random input describing functions (ridf's). The gaussian hypothesis is the only basic approximation made in the application of CADET, so any inaccuracy in the statistical analysis obtained via CADET is due to deviation of the actual joint probability density function (pdf) from normality.

In this section, the sensitivity of CADET to changes in the pdf of the nonlinearity input is investigated by comparing the ridf's corresponding to selected nonlinearities often found in missile guidance system models, computed for a variety of density functions. Three nonlinearities are chosen; these are the limiter, the sinusoidal operator, and a power law nonlinearity. Seven probability density functions with quite different functional forms are considered. Four of these are taken from Table 2.1-1, viz., the exponential, gaussian, triangular, and uniform distributions. Three additional densities are special cases of the sum of two symmetrical triangular functions, generally defined by

$$p(x) \triangleq \begin{cases} \frac{1}{2\Delta}\left(1 - \frac{||x| - x_o|}{\Delta}\right), & ||x| - x_o| \le \Delta \\ 0, & ||x| - x_o| > \Delta \end{cases} \qquad (5.1\text{-}1)$$

which has a zero mean, a variance given by

$$\sigma^2 = x_o^2 + \frac{1}{6}\Delta^2 \tag{5.1-2}$$

and a ratio of fourth moment to variance squared of

$$\lambda \triangleq \frac{\mu_4}{\sigma^4} = \frac{x_o^4 + \Delta^2 x_o^2 + \frac{1}{15}\Delta^4}{x_o^4 + \frac{1}{3}\Delta^2 x_o^2 + \frac{1}{36}\Delta^4} \tag{5.1-3}$$

The three cases of Eq. (5.1-1) chosen for the present study correspond to $\Delta = \frac{1}{2}x_o$, x_o and $2x_o$; the associated pdf's are portrayed in Fig. 5.1-1. Note that two of these densities are bimodal; i.e., they have two peaks.

R-11952

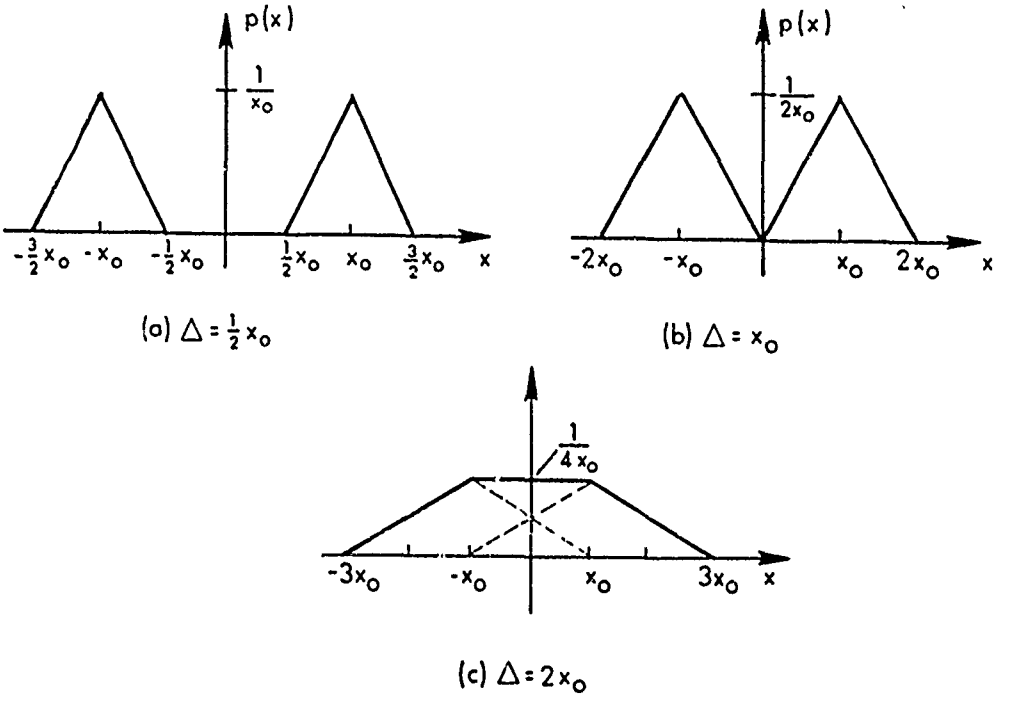

Figure 5.1-1 Three Density Functions Comprised of Two Triangles

which has a zero mean, a variance given by

$$\sigma^2 = x_o^2 + \frac{1}{6}\Delta^2 \tag{5.1-2}$$

and a ratio of fourth moment to variance squared of

$$\lambda \triangleq \frac{\mu_4}{\sigma^4} = \frac{x_o^4 + \Delta^2 x_o^2 + \frac{1}{15}\Delta^4}{x_o^4 + \frac{1}{3}\Delta^2 x_o^2 + \frac{1}{36}\Delta^4} \tag{5.1-3}$$

The three cases of Eq. (5.1-1) chosen for the present study correspond to $\Delta = \frac{1}{2}x_o$, x_o and $2x_o$; the associated pdf's are portrayed in Fig. 5.1-1. Note that two of these densities are bimodal; i.e., they have two peaks.

R-11952

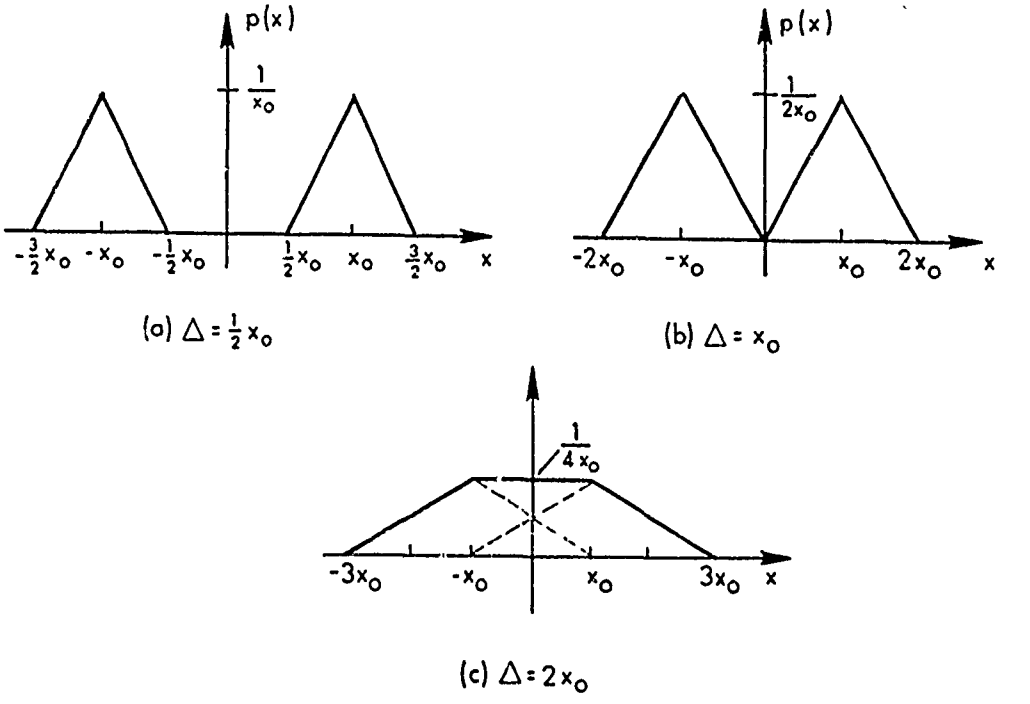

Figure 5.1-1 Three Density Functions Comprised of Two Triangles

in Eq. (5.1-4) have even symmetry, we note that skew densities can be disregarded with no loss in generality. For a skew density $p_s(x)$ we can define its even part by

$$p_{ev}(x) = \frac{1}{2} \left(p_s(x) + p_s(-x)\right)$$

Since the three nonlinearities considered are symmetric (odd) and the mean values of their inputs are zero, only the even part of the pdf contributes to the describing function calculation.

Limiter - The ideal limiter,

$$f(x) = \begin{cases} x & , \quad |x| \leq \delta \\ \delta \ \text{sign}(x) & , \quad |x| > \delta \end{cases} \tag{5.1-5}$$

is probably the most common piece-wise linear function used to model nonlinear phenomena; here it represents several saturation effects in the missile guidance system. In Fig. 5.1-2, we portray the various describing function gains for this nonlinearity, corresponding to the pdf's defined in Eq. (5.1-4), as functions of the ratio of the input rms level, σ, to the saturation point, δ.* As would be expected, all seven quasi-linear gains capture the fact that the effective gain starts to decrease from unity whenever a significant portion of the assumed input pdf lies beyond the saturation point, i.e., whenever there is a significant probability that $|x|$ is greater than δ. As has been pointed out previously, this effect is the key to the success of quasi-linearization techniques in reflecting nonlinear system behavior that is beyond the scope of small-signal (Taylor series) linearization.

*The derivations of these and all subsequent ridf's are given in Appendix B.

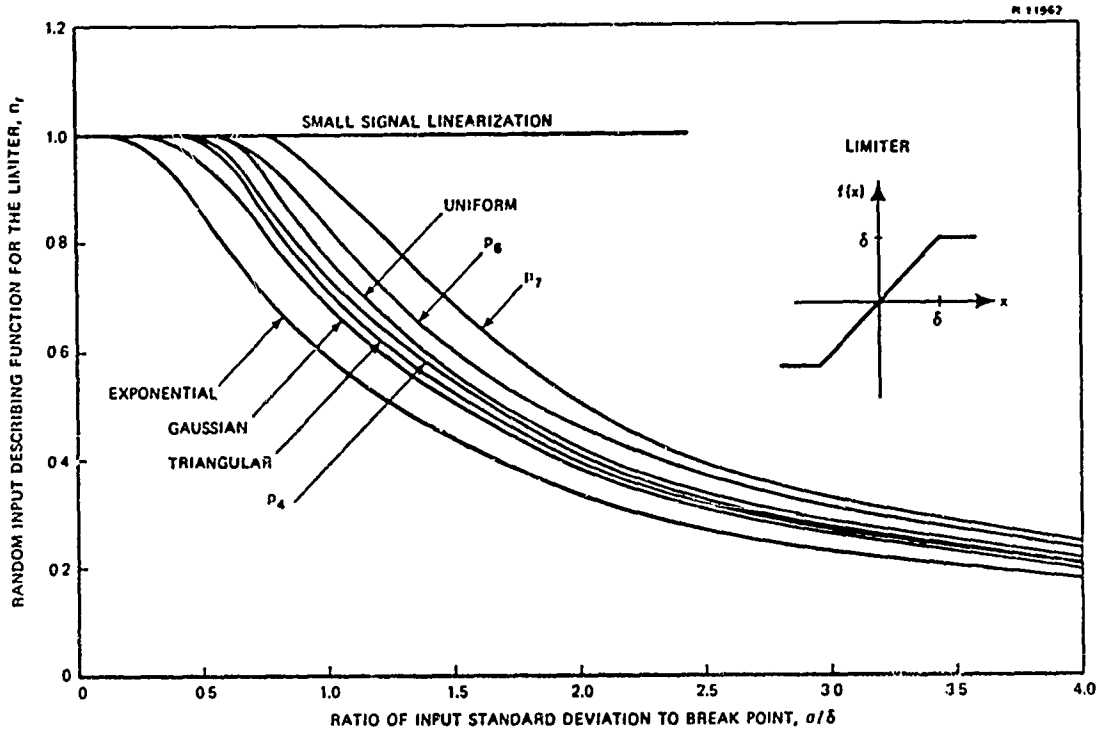

Figure 5.1-2 Random Input Describing Function Sensitivity for the Limiter

It is interesting to observe that the relative position of the curves in Fig. 5.1-2 exhibits a monotonic relation to the value of λ. The greater the difference between λ for a particular pdf and the value for the gaussian case ($\lambda = 3$), the greater the difference between that density function's ridf curve and the curve for a gaussian distribution. This behavior holds in all the cases considered here, and is indicative of the fact that the value of λ is one quantitative measure of how "close" the density function is to being gaussian.

The variation of the ridf's with λ is about at its maximum (on a percentage basis) for the case $\sigma = 2\delta$. This is shown in Fig. 5.1-3; we note that the ridf decreases 13% as λ increases from 3 to 6, and it increases 28% as λ decreases from 3 to 1.16.

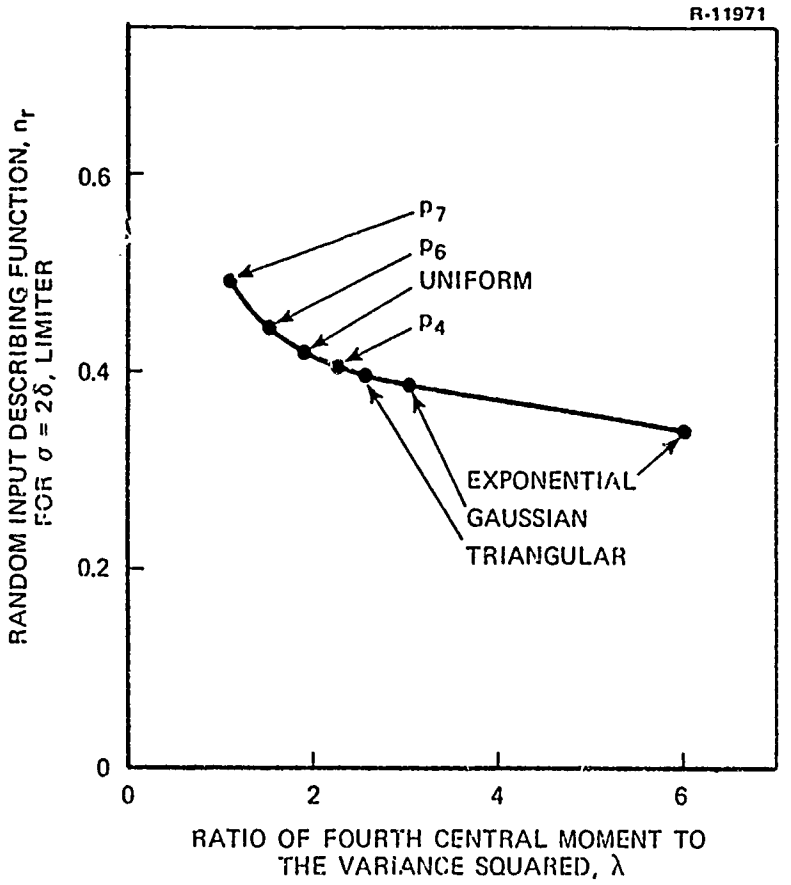

Figure 5.1-3 Random Input Describing Function Sensitivity to λ for the Limiter, $\sigma = 2\delta$

Power Law - A similar study was performed for a power-law characteristic,

$$f(x) = x^2 \text{ sign } (x) \qquad (5.1\text{-}6)$$

This type of nonlinearity is often used to model effects such as the "hard spring" characteristic, as treated in the study of nonlinear restoring torques acting on the seeker head. For the power law, the ridf's calculated for the same density functions considered previously are shown to be of the form

$$n_{r_i} = \mu_i \sigma \qquad (5.1\text{-}7)$$

in Appendix B, where σ is the input rms level and μ_i are coefficients determined by the input pdf's, $p_i(x)$. Thus the describing function gain for f(x) increases linearly with the input rms level, in direct contrast to the small-signal linear gain which is identically equal to zero, as shown in Fig. 5.1-4. It is again observed that there is a monotonic relation between λ_i and the ridf curves, depicted by plotting μ_i versus λ_i in Fig. 5.1-5. In this case, an increase in λ leads to an increase in the describing function gain, which is contrary to the behavior shown for the limiter. This is a result of the fact that the power law output increases more rapidly with increasing input than a linear characteristic, whereas the opposite is true for the limiter. For the power law nonlinearity, the ridf sensitivity is independent of σ, i.e., the ratio of ridf's calculated for $p_i(x)$ and $p_j(x)$ is simply μ_i/μ_j. For f(x) in Eq. (5.1-6), the gain n_r varies from +33% for the exponentially distributed case, to -34% for the pdf $p_7(x)$, compared to the gaussian input ridf, which shows that this nonlinearity is somewhat more sensitive to variations in λ than the limiter.

Sinusoidal Operator - The third nonlinearity considered in these sensitivity studies is the sinusoidal operator,

$$f(x) = \sin x$$

which represents the resolution of the missile and target velocity vectors into orthogonal components in the missile-target intercept model. A potential source of difficulty with this function is that the nonlinearity output periodically changes sign with increasing or decreasing values of its input.* This leads to quasi-linear gains that, for large values of rms input, σ, may even differ in sign for different input pdf's. This problem is not unique to CADET; in many modeling and simulation studies, care must be exercised [illegible] the input to a sinusoidal operator can exceed ± 90 deg ($\pm \frac{\pi}{2}$ rad), [illegible] sense

*This is not a problem in the present study.

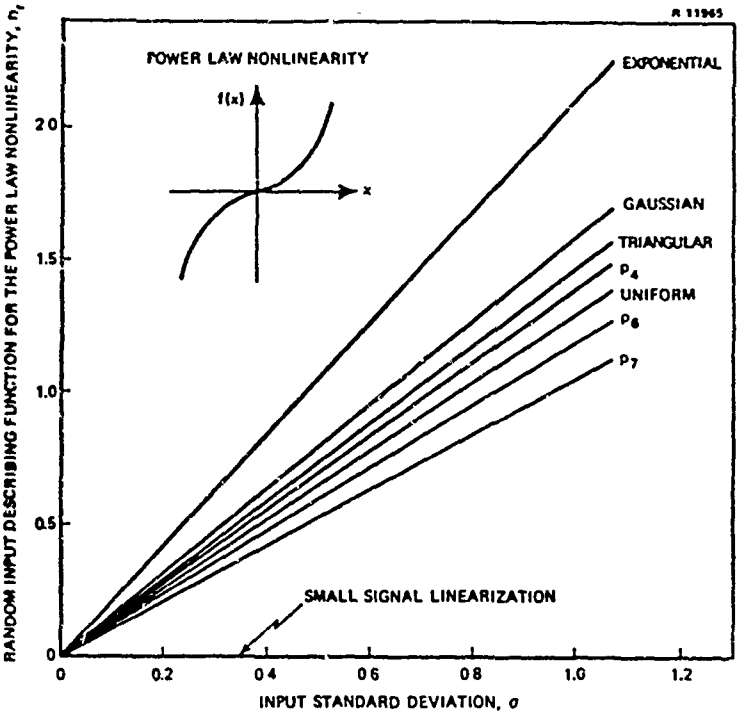

Figure 5.1-4 Random Input Describing Function Sensitivity for the Power Law Nonlinearity

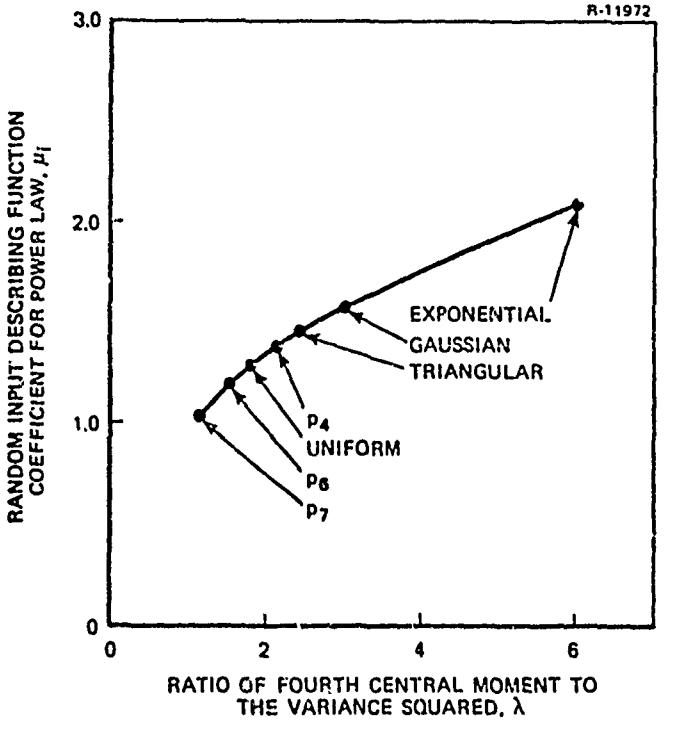

Figure 5.1-5 Random Input Describing Function Sensitivity to λ for the Power Law Nonlinearity

the "gain" can become negative in this situation. Bearing this in mind, we have calculated the random input describing functions for values of σ as large as 3 rad to indicate where such effects become important, as shown in Fig. 5.1-6.

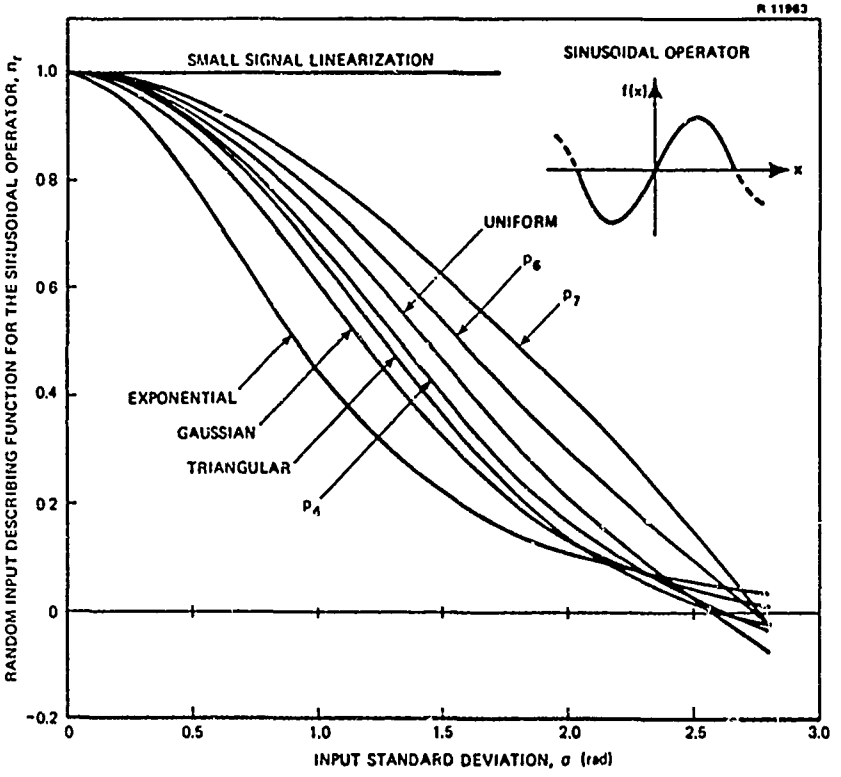

Figure 5.1-6 Random Input Describing Function Sensitivity for the Sinuscidal Operator

The quasi-linear gains for $\sigma < \frac{\pi}{2}$ rad show some similarity to those obtained for the limiter; this is a reasonable mode of behavior, since the sine function shows a definite saturation effect over the range $|x| \leq \frac{\pi}{2}$ rad. As expected, the ridf's are inversely related to λ for $\sigma < \frac{\pi}{2}$ rad, i.e., as λ increases, n_r decreases, as shown in Fig. 5.1-7 for $\sigma = 1.0$ rad. However, as the input rms level approaches 3 rad, the describing functions for all of

the pdf's except $p_1(x)$ and $p_2(x)$ become negative, and the monotonic relationship between λ and n_r appears to be lost.

The preceding studies show that in all three cases the sensitivity of random input describing function calculations to variations in input probability density function is slight for small values of input rms level; as σ approaches zero, the quasi-linear gains approach unity for the limiter and sinusoidal operator, and zero for the power law nonlinearity. These limiting cases are the same values of gain that would be obtained by the traditional small-signal linearization approach -- viz., by replacing f(x) with a linear gain equal to the slope of the function at the origin (Section 2.2). As a general result, it has been shown (Ref. 8) that quasi-linearization subsumes small-signal linearization, i.e., for small signals the two are equivalent. This, in turn, proves that CADET provides nearly exact statistical analyses when the random variables have a small rms value in relation to the system nonlinearities, i.e., when most of each nonlinearity input probability density function lies in the linear region of its nonlinearity. As the rms levels of system variables increase so that the nonlinearities are being exercised significantly, the describing function sensitivity to the input pdf can be appreciable; then it must be ascertained how sensitive the system performance is to variations in gain at each point in the system model where a nonlinearity occurs. No general answer can be given to this question; the verification of CADET for particular applications must be accomplished by direct comparison with monte carlo results, as has been done in Chapter 4 for the missile homing guidance system.

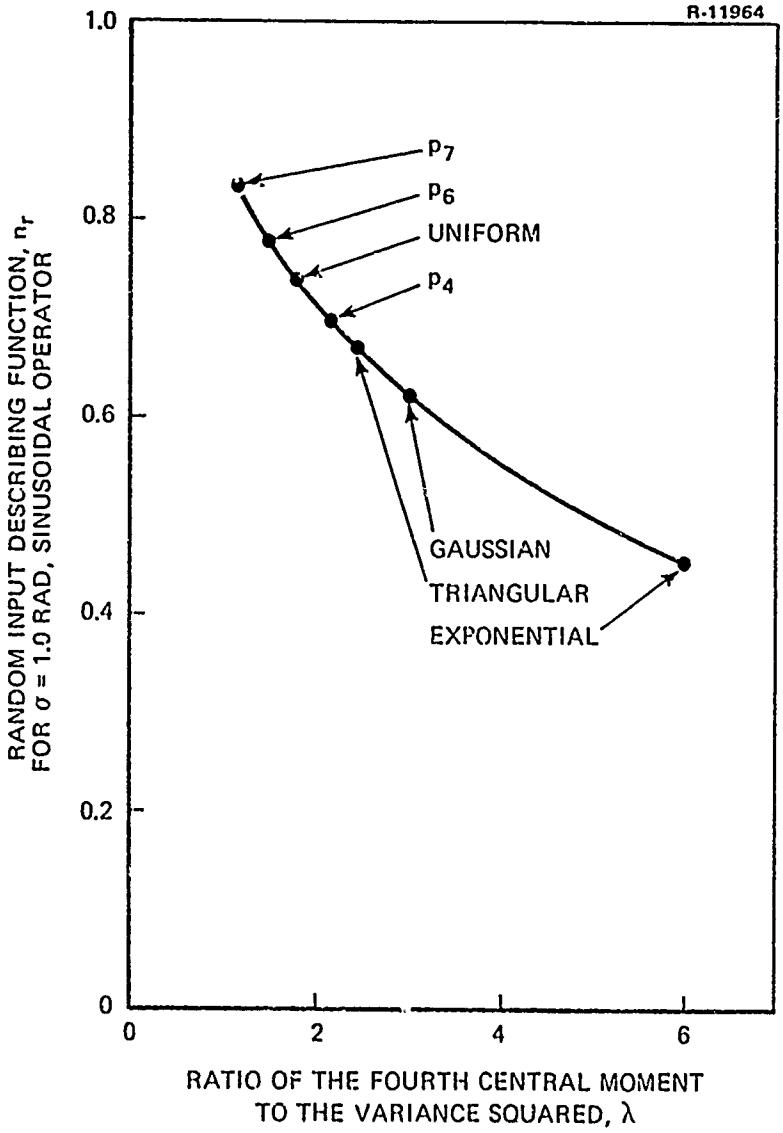

Figure 5.1-7 Random Input Describing Function Sensitivity to λ for the Sinusoidal Operator

5.2 RANDOM INPUT DESCRIBING FUNCTIONS NOT EXISTING IN CLOSED FORM UNDER THE GAUSSIAN ASSUMPTION

For certain nonlinearities, the question of sensitivity has a strong bearing on computational issues. These are cases for which the random input describing functions cannot be obtained in closed form under the assumption that the states are jointly normal. An example of interest in the missile-target intercept problem is the nonlinearity

$$r = \sqrt{x^2 + y^2}$$

which defines the missile-to-target range in terms of the down-range and cross-range components, x and y, respectively. In order to simplify the discussion, we assume that y does not have a mean component, and x has a negligible random component except at the very end of the engagement (refer to Section 4.1). This approximation is valid in the missile-target intercept situations investigated here.

In this case, there are only two ridf's, n_{m_x} and n_{r_y}, needed for a quasi-linear representation of the range. Thus we must evaluate

$$n_{m_x} = \frac{1}{m_x} E\left[\sqrt{m_x^2 + y^2}\right] = \frac{1}{m_x}\int_{-\infty}^{\infty} p(y)\sqrt{m_x^2 + y^2}\, dy$$

$$n_{r_y} = \frac{1}{\sigma_y^2}\int_{-\infty}^{\infty} yp(y)\sqrt{m_x^2 + y^2}\, dy \qquad (5.2\text{-}1)$$

Under the assumption that y is a gaussian random variable, the second of these integrals can be evaluated analytically; however, the first, which is of the form

$$n_{m_x} = \frac{1}{m_x\sqrt{2\pi}\,\sigma_y}\int_{-\infty}^{\infty}\sqrt{m_x^2 + y^2}\;\exp\left(-\frac{y^2}{2\sigma_y^2}\right)\,dy \qquad (5.2\text{-}2)$$

cannot generally be solved in closed form unless $m_x = 0$, viz.,

$$E\left[\sqrt{y^2}\right] = E\left[|y|\right] = \sqrt{\frac{2}{\pi}}\;\sigma_y \qquad (5.2\text{-}3)$$

For the more general case given by Eq. (5.2-2) with $m_x \neq 0$ it is desirable to use some approximate technique to obtain a closed form expression for n_{m_x} that is convenient for use in a CADET analysis.* The two principal approaches that we consider are approximation of the nonlinearity (e.g., by series expansion), and substitution of approximate pdf's.

A Taylor series expansion of a function of a random variable, f(y), about the mean of that variable, here taken to be zero, results in

$$f(y) = f(0) + \left(\frac{df}{dy}\right)_{y=0} y + \frac{1}{2}\left(\frac{d^2f}{dy^2}\right)_{y=0} y^2 + \ldots \qquad (5.2\text{-}4)$$

We desire to determine the expected value of the function, which is given by

$$E[f(y)] = f(0) + \frac{1}{2}\left(\frac{d^2f}{dy^2}\right)_{y=0}\sigma_y^2 + \frac{1}{6}\left(\frac{d^3f}{dy^3}\right)_{y=0} E\left[y^3\right] + \ldots \qquad (5.2\text{-}5)$$

*While n_{m_x} in Eq. (5.2-2) can be calculated by numerical integration, a less time consuming approach is desired for repeated evaluation in a CADET analysis.

where use is made of the fact that E[y] is zero to eliminate the second term in Eq. (5.2-4); all other odd-moment terms ($E[y^3]$ etc.) are also zero for symmetric pdf's. Truncating the series given in Eq. (5.2-5) at the second term, we obtain

$$E[f(y)] \cong f(0) + \frac{1}{2}\left(\frac{d^2f}{dy^2}\right)_{y=0} \sigma_y^2 \qquad (5.2\text{-}6)$$

which is an approximation suggested in Ref. 9. We note that this result is independent of the particular density function of y. If more terms are desired, the higher-order moments can be evaluated using a specified pdf. If y is gaussian, all odd moments are zero and even moments are given by (Ref.9)

$$\mu_{2k} = E\left[y^{2k}\right] = (1)\,(3)\,(5)\,\ldots\,(2k-1)\,\sigma^{2k} \quad , \; k = 1, 2, \ldots$$

which leads to the full expansion

$$E[f(y)] = f(0) + \frac{1}{2}\left(\frac{d^2f}{dy^2}\right)_{y=0} \sigma^2 + \frac{(1)\,(3)}{4!}\left(\frac{d^4f}{dy^4}\right)_{y=0} \sigma^4 + \ldots \qquad (5.2\text{-}7)$$

The use of the first term alone in Eq. (5.2-7) corresponds to small signal linearization; taking two terms as indicated in Eq. (5.2-6) results in a quasi-linear gain that is often useful. In the present case, however, this approach is effective only in situations where m_x is considerably larger in magnitude than σ_y, due to the singularities of the derivatives of $\sqrt{m_x^2 + y^2}$ at the origin ($m_x = 0$). To demonstrate this difficulty, we write the series expansion for the nonlinearity under consideration (Ref. 10),

$$f(y) = \sqrt{m_x^2 + y^2} = |m_x| \left[1 + \frac{1}{2}\left(\frac{y}{m_x}\right)^2 - \frac{1}{8}\left(\frac{y}{m_x}\right)^4 + \cdots\right] \tag{5.2-8}$$

from which we obtain

$$n_{m_x} = \left[1 + \frac{1}{2}\left(\frac{\sigma_y}{m_x}\right)^2 - \frac{3}{8}\left(\frac{\sigma_y}{m_x}\right)^4 + \cdots\right] \text{sign}\,(m_x) \tag{5.2-9}$$

as an approximate describing function to represent the mean component of the range. For m_x considerably larger than σ_y, the first few terms of this expansion yield acceptable accuracy.* Since m_x approaches zero in the missile-target intercept problem, however, this result is generally not suitable.

Another approximation to the nonlinearity leads to a series that is useful for small values of m_x:

$$\sqrt{m_x^2 + y^2} \cong |y| + |m_x| e^{-|y/m_x|} \quad , \; |m_x| < |y| \tag{5.2-10}$$

The right- and left-hand-sides of Eq. (5.2-10) have the same first three terms when their power series expansions are compared. Substituting this approximation into Eq. (5.2-2) leads to an integral that can be evaluated in terms of the complementary error function, denoted as erfc (Ref. 11),

*We note that the expansion indicated in Eq. (5.2-9) never converges formally, i.e., for any value of σ_y/m_x, no matter how small, the series will eventually diverge as more terms are evaluated. This is a standard property of asymptotic expansions which are useful only when truncated after a finite number of terms.

$$n_{m_x} \cong \frac{1}{m_x}\sqrt{\frac{2}{\pi}}\left[\sigma_y + \sqrt{\frac{\pi}{2}}\,|m_x|\,\exp\left(\frac{\sigma_y^2}{2m_x^2}\right)\operatorname{erfc}\left(\frac{\sigma_y}{\sqrt{2}\,m_x^2}\right)\right]$$

which in turn can be represented as an asymptotic expansion (Ref. 6) valid for $\sigma_y \gg |m_x|$:

$$n_{m_x} \cong \sqrt{\frac{2}{\pi}}\,\frac{\sigma_y}{m_x}\left[1 + \left(\frac{m_x}{\sigma_y}\right)^2 - \left(\frac{m_x}{\sigma_y}\right)^4 + 3\left(\frac{m_x}{\sigma_y}\right)^6 - \ldots\right] \qquad (5.2\text{-}11)$$

For $m_x = 0$, the expansion correctly yields the result given in Eq. (5.2-3), and for $|m_x| < \frac{1}{2}\sigma_y$, the result is quite accurate.* However, the series is divergent for larger values of $|m_x|$. This series is of questionable utility in the missile-target intercept problem, since $|m_x| \gg \sigma_y$ at the beginning of the terminal homing phase.

The second method for approximately evaluating the first integral in Eq. (5.2-1) is the substitution of a nongaussian pdf for which the integral can be obtained in closed form. As in previous sensitivity studies (Section 5.1), the best result has been obtained using the triangular pdf. Substituting this distribution into Eq. (5.2-1) leads to an integral that is evaluated in closed form to be

$$n_{m_x} \cong \frac{\text{sign}\,(m_x)}{\nu}\left[\sqrt{1+\nu^2} + \nu^2 \log\left(\frac{1+\sqrt{1+\nu^2}}{\nu}\right) + \frac{4}{\sqrt{6}}\left(\nu^3 - \left(1+\nu^2\right)^{3/2}\right)\right] \qquad (5.2\text{-}12)$$

*Eq. (5.2-11) is also not formally convergent.

where the auxiliary variable ν is given by

$$\nu \triangleq \frac{|m_x|}{\sqrt{6}\sigma_y} \tag{5.2-13}$$

The accuracy of Eq. (5.2-12) is quite good, especially when compared with the poor approximations given by the series expansion in Eqs. (5.2-9) and (5.2-11) when $|m_x|$ is nearly equal to σ_y. The error between Eq. (5.2-12) and the exact result specified in Eq. (5.2-2) is less than 3%, which is adequate for most applications.

In passing, we note a third alternative that might be considered in applications where less accuracy is required; viz.

$$n_{m_x} = \frac{1}{m_x} E\left[\sqrt{m_x^2 + y^2}\right]$$

$$\cong \frac{1}{m_x}\sqrt{E\left[m_x^2 + y^2\right]}$$

$$= \sqrt{1 + \frac{\sigma_y^2}{m_x^2}}\ \text{sign}\,(m_x) \tag{5.2-14}$$

The simplicity of this result -- and the fact that the approximation is better than either series expansion (Eqs. (5.2-9) and (5.2-11)) for $|m_x| \cong \sigma_y$ -- makes it attractive, despite the error of 25% at $m_x = 0$.

All of the approximate solutions for n_{m_x} in Eq. (5.2-2) discussed above are compared in Fig. 5.2-1. Generally, we note that se es

approximations for this nonlinearity are accurate only in applications where $|m_x| \gg \sigma_y$ or $|m_x| \ll \sigma_y$ for the entire CADET simulation; such conditions are never satisfied in studying the expected value of the range in the missile-target intercept problem. The use of an approximate (nongaussian) pdf -- in particular, the triangular density -- yields the best overall accuracy.

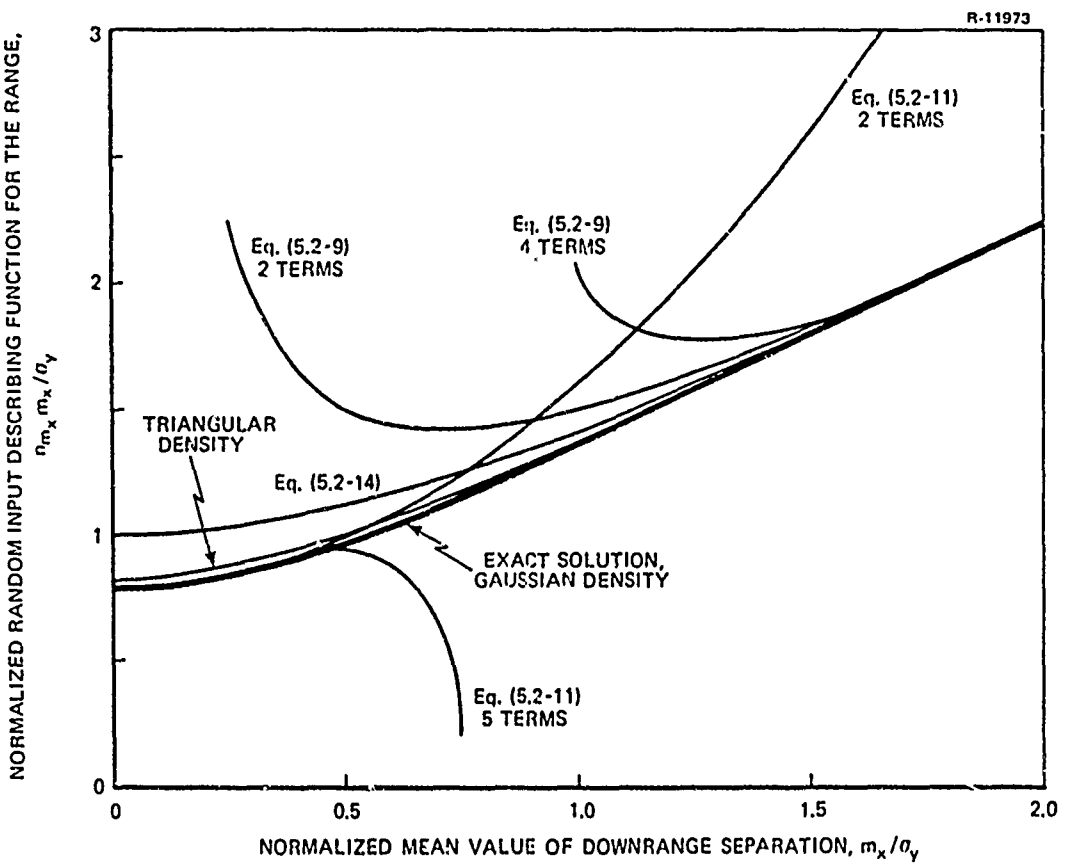

Figure 5.2-1 Comparison of Approximations for the Expected Value of the Range

It should be mentioned that the conclusion that the series expansion techniques are not very accurate for computing the ridf in the case treated above should not be taken as universally true. When series approximations for an ridf can be obtained which are accurate over the entire range of the input statistics, they will generally yield good results.

Ultimately, the issue of sensitivity depends upon how much the CADET analysis results -- e.g., the computed rms miss distance -- are affected by errors or variations in the describing function gains. It is conceivable that the miss distance will not be significantly affected by large changes in a particular ridf, depending upon how the ridf enters into the system model. In the missile guidance system model developed in Appendix A, the only incidence of range dependence is in the seeker noise module. It is intuitively clear that the effect of seeker noise on the statistical performance of the guidance system will not be particularly sensitive to moderate inaccuracies in the quasi-linear representation of range, particularly if these inaccuracies occur only during the last few hundredths of a second of the engagement. This is verified by comparing CADET results obtained for the nominal case (Section 4.1) using the two range ridf approximations labeled "triangular density" and "Eq. (5.2-9), 2 Terms" in Fig. 5.2-1. The difference in the CADET computed rms miss statistics for these cases was negligible; in fact, all state variables had means and standard deviations that differed by less than one percent at terminal time.

On the basis of the insensitivity of the seeker noise module to variations in the ridf representation of range dependent noise sources, we recommend the use of a simpler ridf than that obtained from the triangular density approximation (Eq. (5.2-12)). Rather than using the two-term series expansion considered in the above comparison, however, the application of Eq. (5.2-14) should be an even more attractive alternative, due to the fact that the latter result is more accurate for small values of m_x. In particular, Eq. (5.2-14) does not become infinite as m_x goes to zero.

5.3 HISTOGRAM STUDIES OF NONGAUSSIAN SYSTEM VARIABLES

In considering the impact of the assumption that the state variables are jointly normal on the accuracy of performance projections provided by

CADET, we have performed a histogram study of a case in which there is a significant difference between CADET and monte carlo results. Such a study provides some insight into how nongaussian the state variable pdfs must be in order for CADET results to be inaccurate.

The system under consideration corresponds to the nominal case given in Table 4.1-1, except for a single large initial condition statistic -- an rms initial heading error of 10 deg -- chosen to obtain a significant discrepancy between CADET and monte carlo results; this somewhat unrealistic condition leads to a very large rms miss distance.

The time history of the rms lateral separation, σ_y, over the duration of the engagement is presented in Fig. 5.3-1. The monte carlo confidence limits shown are calculated on the preliminary assumption that y is nearly gaussian, i.e., that $\lambda \cong 3$ (Section 2.1). The CADET and monte carlo results agree well over the first half of the homing phase. However, there is a marked divergence after t = 3 sec, which is evidently due to some inadequacy in the assumption that the states are jointly normal.

To understand the reason for this problem, and to assess how much deviation from normality is required for a discrepancy of this sort to occur, we portray typical monte carlo generated histograms for a number of the system states, obtained from a 100-trial ensemble of simulated missile-target intercept engagements. First, we consider the target aspect angle, θ_a, which is theoretically gaussian over the entire flight. The histograms shown in Fig. 5.3-2 correspond to the midpoint and end of the engagement. We note that they appear to be quite irregular; this is due to the fact that 100 trials are insufficient for obtaining an accurate representation of the probability density function. Thus, for example, the fact that there appears to be a small "valley" slightly to the left of zero at t = 6 sec should not be interpreted to

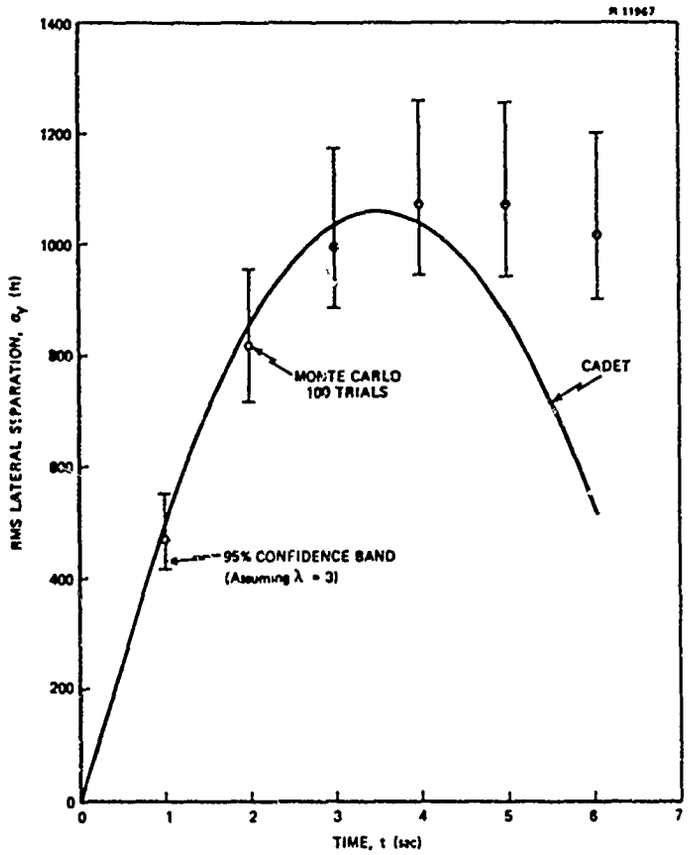

Figure 5.3-1 CADET and Monte Carlo Results for Large Initial rms Heading Error (10 deg.)

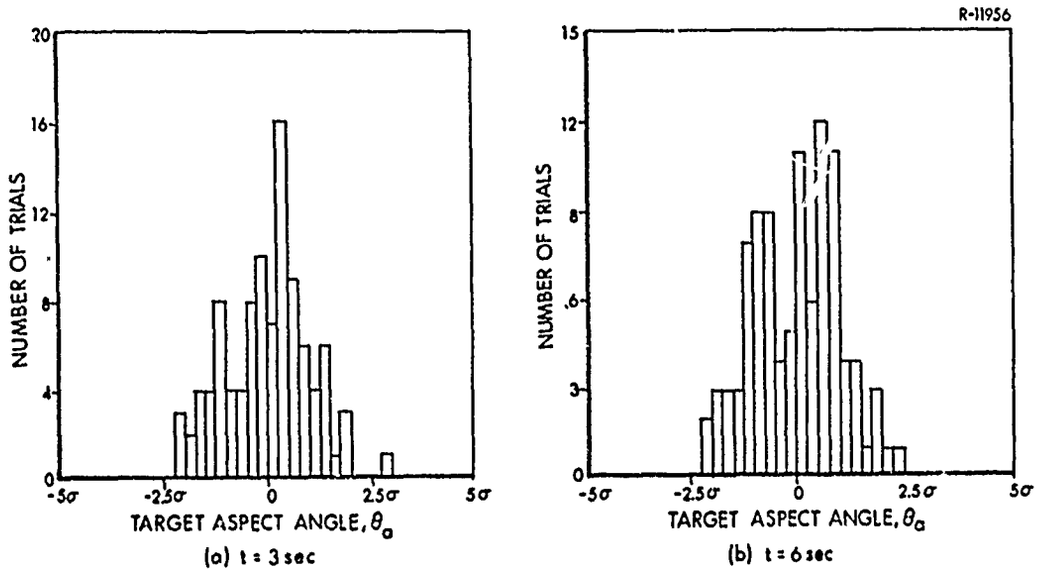

Figure 5.3-2 Typical Histograms for a Random Variable Specified to be Gaussian

mean that θ_a has a bimodal distribution. These histograms provide the basis for a realistic assessment of the departure of other histograms in this study from the normal case.

Next, we consider a system state variable that is distinctly non-gaussian for this trajectory, the missile fin deflection, δ. Because of the large initial rms heading error, there is a high probability that the missile initially attempts to achieve maximum lateral acceleration. Thus the output of the acceleration command limiter, a_c in Fig. 3.5-1, will tend to be bimodal, as will the fin deflection, which is linearly related to a_c. At t = 1 sec a highly bimodal distribution is noted in Fig. 5.3-3. As the terminal homing phase proceeds, δ becomes somewhat less bimodal, but at no time does it appear to be gaussian.

Other variables that exhibit bimodal behavior throughout this engagement are the seeker angle and angle rate, θ_h and $\dot{\theta}_h$; missile body angle and angle rate, θ_m and $\dot{\theta}_m$; and angle of attack, α. We observe in Fig. 5.3-4 that the missile lead angle, θ_ℓ, which is separated from δ by a significant amount of linear dynamics (refer to Fig. 3.7-1) remains nearly gaussian throughout the engagement -- thus providing an example of the "filter hypothesis" that the presence of several stages of low-pass filtering tends to make a signal more nearly gaussian, which forms the basis for the gaussian assumption in CADET.

The cross-range missile-target separation, y, exhibits a behavior that more directly provides an explanation of the failure of CADET to provide accurate lateral separation statistics over the second half of the terminal homing phase. For the first half of the engagement, Fig. 5.3-5 indicates that the pdf's for y are quite nearly gaussian. However, at 4 sec we note

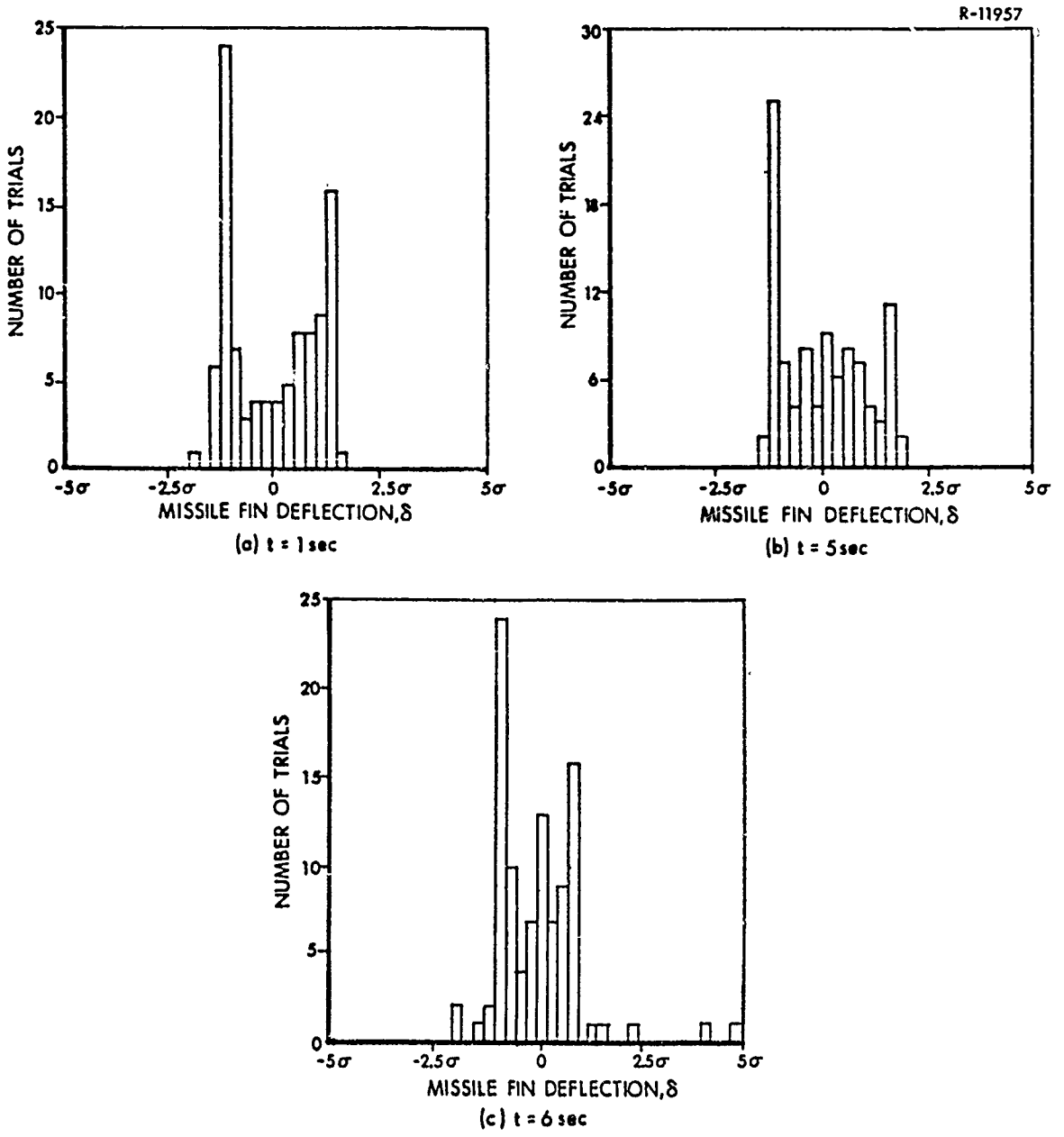

Figure 5.3-3 Histograms for Missile Fin Deflection, δ

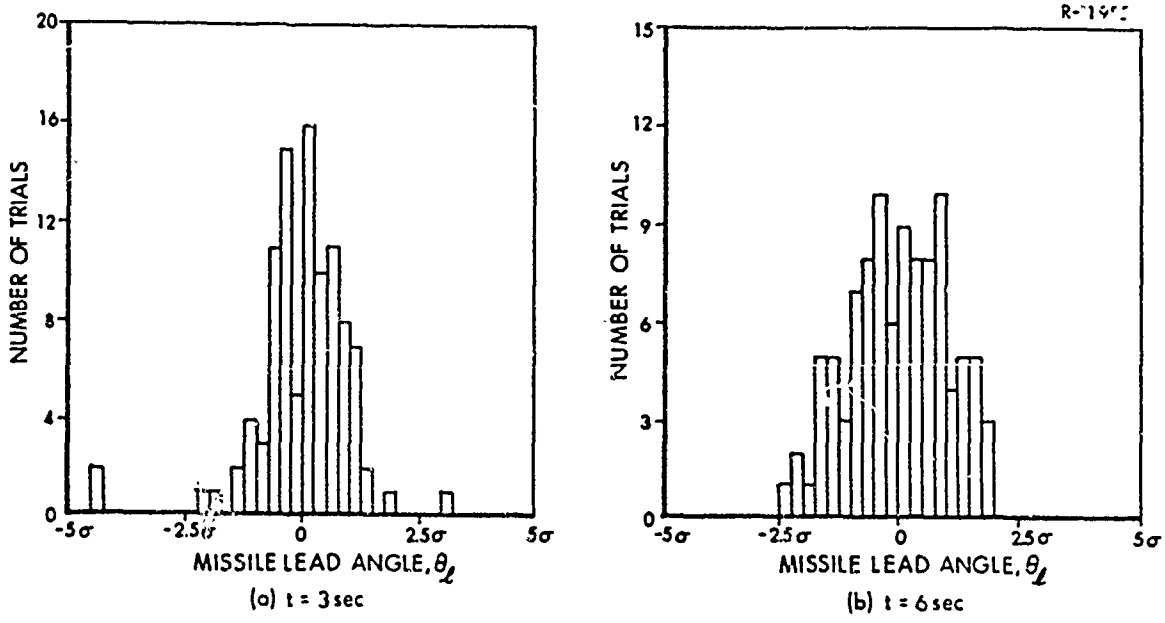

Figure 5.3-4 Histograms for Missile Lead Angle, θ_ℓ

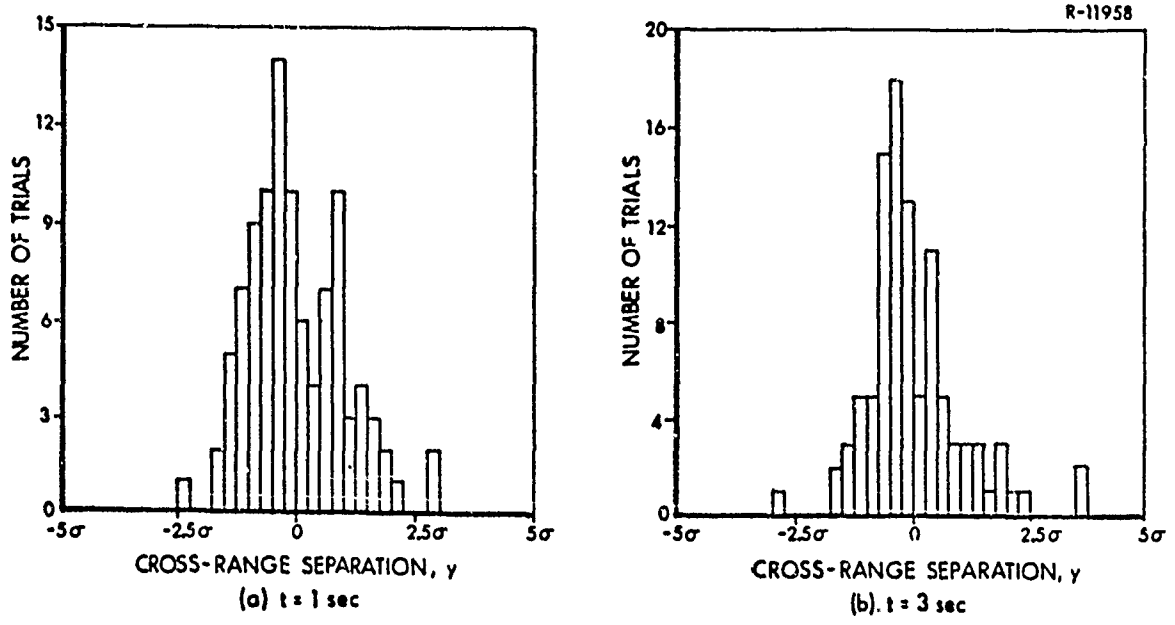

Figure 5.3-5 Histograms for Cross-Range Separation in the First Half of the Homing Phase

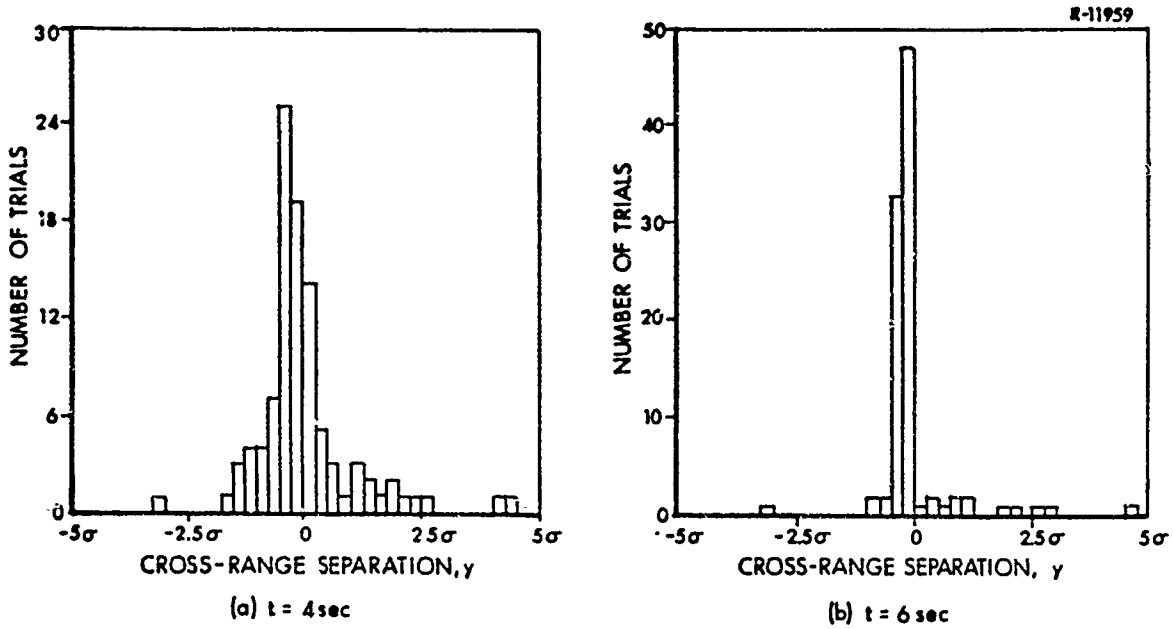

Figure 5.3-6 Histograms for Cross-Range Separation in the Second Half of the Homing Phase

in Fig. 5.3-6a that significant "tails" have developed in the histogram; at 6 sec this effect is more pronounced (Fig. 5.3-6b). A quantitative comparison of the latter histogram with the gaussian density is obtained by computing the ratio of the fourth central moment to the variance squared; this is an estimate of the parameter λ defined in Eq. (5.1-3). The resulting value of 19.5, which is more than six times larger than the value for a gaussian density, indicates a highly nongaussian distribution. Two conclusions can be drawn:

- The monte carlo estimated rms miss distance, $\hat{\sigma}_y(t_f) = 1018$ ft, is statistically considerably less accurate than implied by the confidence band shown in Fig. 5.3-1, under an assumed gaussian distribution for y. For $\lambda = 19.5$, the 95% confidence interval limits on σ_y are

$$\underline{\sigma}_y = 750 \text{ ft}, \qquad \bar{\sigma}_y = 2570 \text{ ft}$$

as given by Eq. (2.1-14).

- The CADET result may also be inaccurate, since the sensitivity studies in Section 5.1 indicate that ridf calculations based on the gaussian assumption ($\lambda = 3$) can be quite different from those based on a pdf with $\lambda = 19.5$.

The latter point indicates the reason why CADET seems to provide an inaccurate guidance system performance projection over the last 3 seconds of flight.

To explain some of the above observed behavior, an analysis of the physical significance of large initial heading error is useful. We consider a simplified example, with the aid of Fig. 5.3-7, wherein a target is proceeding precisely along the original LOS with constant velocity, v_t, and not maneuvering. The missile has been launched with an initial heading error of $\theta_{\ell 0}$ degrees, with constant velocity vector magnitude, v_m. An important limitation is imposed on the missile by assuming that lateral acceleration is constrained by $|a_m| \leq a_{max}$, as a result of acceleration command limiting; this condition makes it impossible for intercept to occur in this simple scenario if $|\theta_{\ell 0}|$ exceeds a certain value. To demonstrate this point, we assume that $a_m = a_{max}$ over the entire flight. Then the missile will follow a circular trajectory with a radius and angular rate given by (Ref. 13)

$$r_c = v_m^2/a_{max}$$
$$\dot{\theta}_c = a_{max}/v_m \qquad (5.3\text{-}1)$$

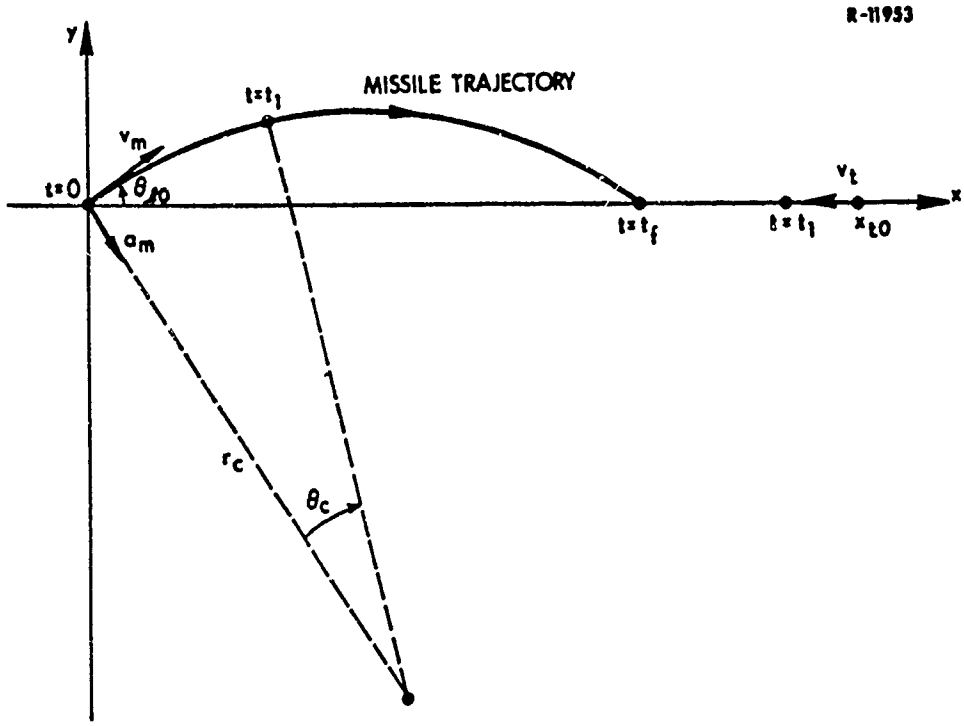

Figure 5.3-7 Intercept with a Circular Missile Trajectory

as shown in Fig. 5.3-7. If an intercept is achieved by applying the maximum acceleration over the entire interval $0 \le t \le t_f$, the equations of motion are

$$x_t(t) = x_{t0} - v_t t$$
$$y_t(t) \equiv 0 \qquad (5.3\text{-}2)$$

$$x_m(t) = r_c \left[\sin \theta_{\ell 0} - \sin (\theta_{\ell 0} - \theta_c)\right] \qquad (5.3\text{-}3)$$

$$y_m(t) = r_c \left[\cos (\theta_{\ell 0} - \theta_c) - \cos \theta_{\ell 0}\right]$$

According to Eq. (5.3-1),

$$\theta_c = \frac{a_{max}\, t}{v_m} \qquad (5.3\text{-}4)$$

In general, in order for intercept to be possible, the point at which the circular arc followed by the missile intersects the x-axis must be in front of the target; i.e., if the earliest time the missile trajectory can intersect the x-axis is t_f, it must be true that

$$x_m(t_f) \leq x_t(t_f) \tag{5.3-5}$$

to permit an intercept. The values of $\theta_{\ell 0}$ and a_{max} determine whether or not Eq. (5.3-5) can be satisfied. From the conditions depicted in Fig. 5.3-7, it is clear that intercept is possible only for $|\theta_{\ell 0}| \leq \bar{\theta}_{\ell 0}$, where $\bar{\theta}_{\ell 0}$ and the corresponding terminal time t_f satisfy

$$x_{t0} - v_t t_f = v_m^2 \left[\sin \bar{\theta}_{\ell 0} - \sin \left(\bar{\theta}_{\ell 0} - \frac{a_{max} t_f}{v_m} \right) \right] / a_{max}$$

$$\cos \bar{\theta}_{\ell 0} = \cos \left(\bar{\theta}_{\ell 0} - \frac{a_{max} t_f}{v_m} \right) \tag{5.3-6}$$

These transcendental equations have the solution

$$\bar{\theta}_{\ell 0} = 14.4^{\circ}$$

$$t_f = 6.048 \text{ sec} \tag{5.3-7}$$

for the parameters used in generating the CADET results given in Fig. 5 3-1. For $\theta_{\ell 0}$ greater than the limit $\bar{\theta}_{\ell 0}$ given in Eq. (5.3-7), the deterministic miss distance (defined in this context to be the absolute value of $y_m(t_f)$) increases very rapidly, as shown in Fig. 5.3-8.

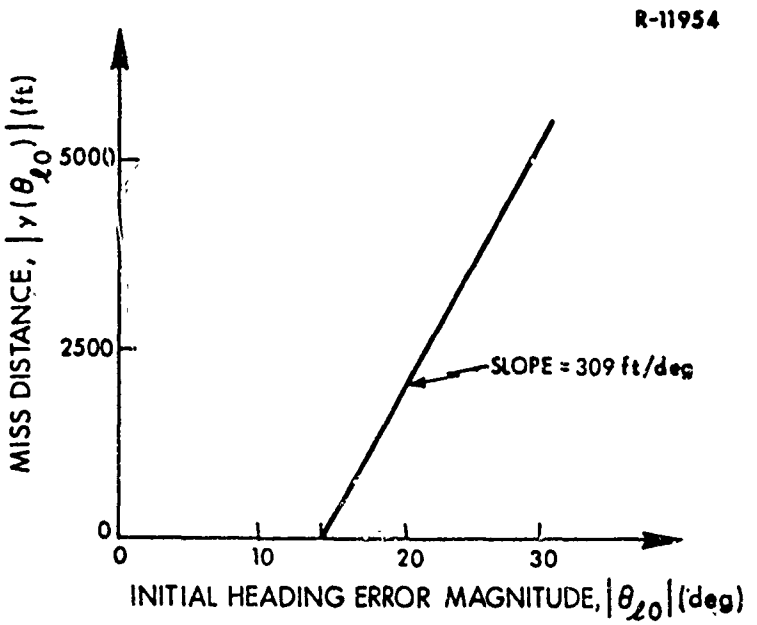

Figure 5.3-8 The Variation of Miss Distance with Initial Heading Error Magnitude

From the above analysis, we can appreciate why the rms heading error chosen for the analysis in Fig. 5.3-1 leads to a large miss distance. Since $\theta_{\ell 0}$ is a gaussian random variable with a standard deviation of 10^{o}, there is a significant probability that $|\theta_{\ell 0}|$ exceeds the maximum value $\theta_{\ell 0}$, viz:

$$\text{Prob}\left[|\theta_{\ell 0}| \geq 14.4 \text{ deg}\right] = 0.15$$

and the impact of initial heading errors greater than 14.4 deg in magnitude is dramatic (Fig. 5.3-8). In fact, we can apply the statistical properties of $\theta_{\ell 0}$ to the characteristic shown in Fig. 5.3-8 to derive the idealized rms miss distance (valid only for the above simplified model of the missile-target intercept problem), defined by

$$\tilde{\sigma}_y^2 \triangleq E[y^2(\theta_{\ell 0})] = \int_{-\infty}^{\infty} y^2(\theta_{\ell 0})\, p(\theta_{\ell 0})\, d\theta_{\ell 0} \qquad (5.3\text{-}9)$$

The resulting value of σ_y is 736 feet. We can also perform a random input describing function analysis of the same effect using Fig. 5.3-8 to demonstate why CADET has given an estimated rms miss distance that is considerably less than the monte carlo result. The characteristic shown in Fig. 5.3-8 is in effect a linear gain with a dead zone, whose random input describing function given by Ref. 8 can be expressed in terms of the complementary error function, erfc,

$$n_r = 309 \text{ erfc} \left(\frac{14.4}{10\sqrt{2}} \right) = 48.6 \text{ ft/deg} \qquad (5.3\text{-}10)$$

Thus the rms miss distance calculated using describing function theory is

$$\tilde{\sigma}_{y,\,ridf} = n_r \sqrt{E\left[\theta_{\ell 0}^{\,2}\right]} = 486 \text{ feet} \qquad (5.3\text{-}11)$$

In the idealized case treated above, quasi-linearization significantly underestimates the rms miss distance. This is reflective of the fact that the ridf calculated in Eq. (5.3-10) is based on the minimization of mean square approximation error, not on variance matching.

This section has analyzed a missile-target engagement situation where CADET and monte carlo results are significantly different, in order to provide insight as to potential sources of error in the CADET results. However, it is typically found that parameter values must be chosen which generate large rms miss distance (more than 100 ft) in order to obtain noticeable deterioration in CADET accuracy. In those cases the missile dynamics are highly nonlinear throughout the trajectory, and generally do not correspond to conditions under which tactical missiles are designed to operate. Furthermore, if the rms miss distance is large, say 500 ft or more, it is not too important that CADET makes a 100 foot error if the missile lethal radius is 50 feet, since a miss distance of 400 ft is still intolerable. For more realistic trajectories

that yield tolerable rms miss distances, CADET results appear to be accurate within $\pm 10\%$, based upon the monte carlo simulations performed in this and other studies.

Finally, we observe that the marked deviation of the density of the terminal cross-range missile-target separation, y, from the gaussian case is a potential source of misinterpretation of the value of σ_y. The cumulative distribution of $|y|$ at the terminal time for 50 monte carlo trials is portrayed in Fig. 5.3-9; the actual rms value of y for this data is $\sigma_y = 1018$ ft. On the same plot we show cumulative distributions corresponding to $|y|$ for a gaussian random variable y having $\sigma_y = 1018$ ft (corresponding to the monte carlo result) and $\sigma_y = 513$ ft (CADET). In terms of guidance system performance, if we assume that it is desired to have $|y|$ less than 50 feet at the terminal time, we see in Fig. 5.3-9 that the actual distribution indicates an effectiveness of 60%, i.e., 60% of the engagements satisfy the condition $|y| < 50$ feet, while the corresponding values of effectiveness for the two gaussian distributions are 8% for CADET and 4% for monte carlo results, based on the miss distance statistics alone. Thus we observe that the rms miss distance is itself of questionable value as a measure of guidance system performance when the nongaussian nature of y leads us to question the accuracy of the CADET and monte carlo results. In one sense, then, the "failure" of CADET in this situation may be linked to the "failure" of rms miss-distance as a single-parameter measure of system performance.

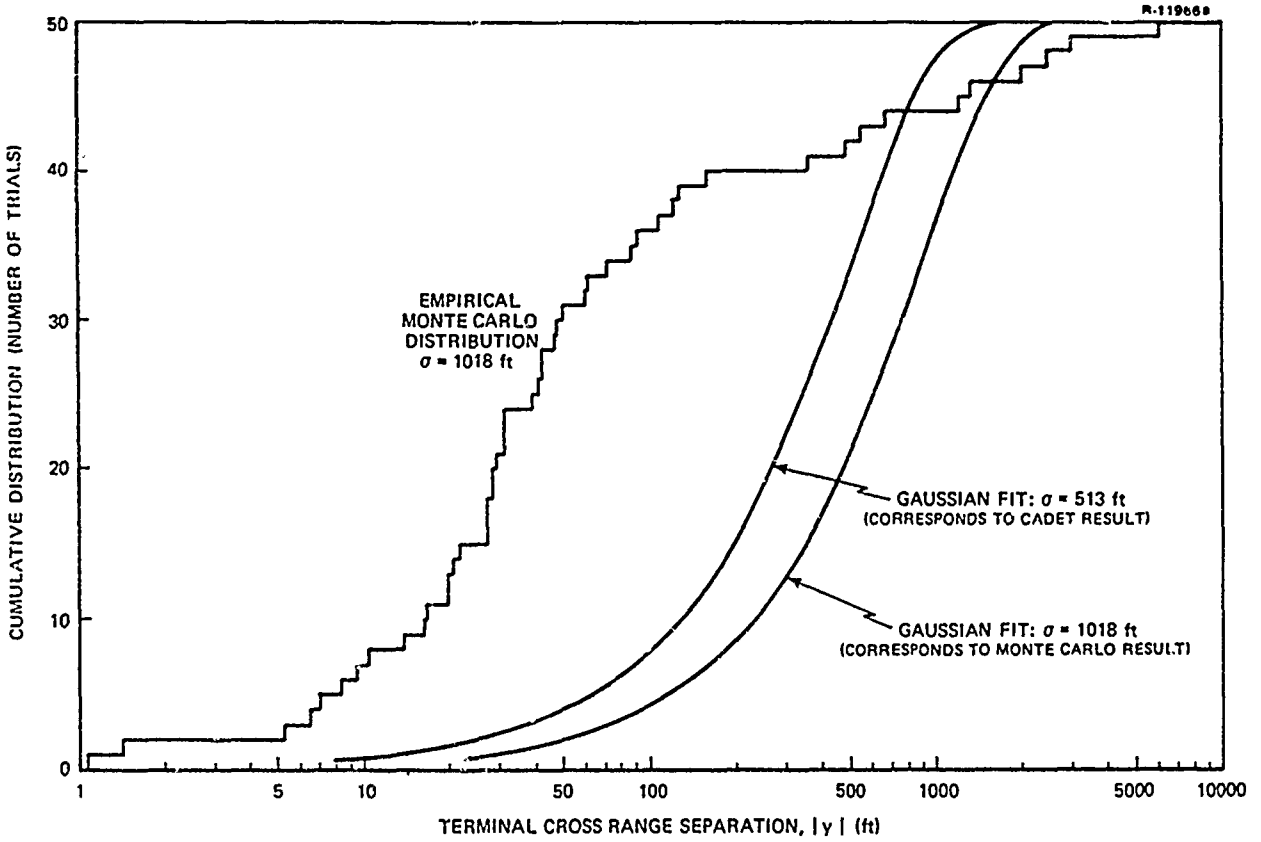

Figure 5.3-9 Empirical Distribution of |y| Compared with Two Gaussian Distributions

6. SUMMARY AND CONCLUSIONS

6.1 SUMMARY

The principal goal of this study is to extend the proven capability of the Covariance Analysis DEscribing Function Technique -- CADET -- to provide accurate performance projections for tactical missile guidance system models that are quite realistic -- i.e., that incorporate a number of significant nonlinear and random effects. The approach used to achieve this objective has entailed

- Verification of CADET performance projections by the use of selected monte carlo performance studies
- Investigation of the sensitivity of CADET analysis to deviation from the assumption that the state variables are jointly normal.

In this investigation, the following quite diverse effects were treated:

Sources of Nonlinearity

- Guidance law
- Acceleration command limiting
- Missile-target intercept geometry (4 nonlinearities)
- Coordinate transformation (2 nonlinearities)
- Range-dependent seeker noise sources (2 nonlinearities)
- Receiver/signal processing characteristic
- Seeker mass imbalance (3 nonlinearities)

- Seeker gimbal Coulomb friction
- Seeker head restoring torques (nonlinear spring effects)

Random Effects

- Tracking sensor noise and measurement errors
- Range rate measurement error
- Target maneuvers
- Deviation of initial conditions from nominal values

The generation of missile performance statistics via CADET, and the subsequent verification of selected points on the parameter sensitivity curves by monte carlo simulation techniques is treated in Chapter 4. The basic system model -- incorporating the first five nonlinear effects listed above, which are fundamental to the missile-target intercept problem -- was studied first, then each of the remaining nonlinearities were investigated singly, and a final CADET-monte carlo comparison was made with all nonlinear phenomena present. Three aspects of the sensitivity problem are considered in Chapter 5: the sensitivity of random input describing function calculations to the probability density function of the nonlinearity input, calculation of approximate random input describing functions when it is inconvenient to use the result for the gaussian case, and a histogram study of a situation where system variables are quite highly nongaussian.

6.2 CONCLUSIONS

The investigation described in this report has indeed shown that CADET is an accurate and efficient tool for conducting statistical analyses of the performance of a tactical missile system, including the effects of a number of significant nonlinear and random phenomena. The conclusions drawn from the study can be summarized as follows:

- CADET has the demonstrated ability to capture the effect of each of the 16 nonlinearities treated in Chapter 4 on guidance system performance. In all cases studied, CADET results are close to or within the 95% confidence limits of the monte carlo analysis. This degree of agreement was generally maintained even in the numerous instances where the nonlinearities were shown to have a marked deleterious effect on rms miss distance.

- Despite the high order of the system (17 state variables) and large number of nonlinearities (16), CADET shows a significant computational advantage over the monte carlo method: Between 10 and 20 CADET performance projections can be obtained for the same amount of computer time required by one accurate monte carlo study.

- It is sometimes necessary to use approximate random input describing functions due to difficulty in deriving closed form solutions. Two approaches are available, based on series expansion techniques and on the substitution of alternative density functions in lieu of the gaussian density. A discussion of some benefits and disadvantages is given in Chapter 5.

- Highly nongaussian system variables not only lead to inaccuracy in the CADET analysis, but also make the monte carlo method less reliable and reduce the meaningfulness of the basic measure of system performance, rms miss distance.

- The value of the parameter λ (the fourth central moment of a density function divided by the variance squared) is a useful measure of the departure of the density of a random variable from the gaussian case. It would thus be valuable to estimate this parameter for each nonlinearity input in the monte carlo analysis to help in appraising the accuracy of the monte carlo method and CADET.

In light of these and related findings, it is felt that confidence in the applicability of CADET to perform statistical analyses of complex nonlinear missile guidance systems with a number of random disturbances has been significantly enhanced.

APPENDIX A

MISSILE-TARGET INTERCEPT MODEL

A.1 INTRODUCTION

This appendix presents the derivation of the mathematical model of the general missile-target intercept problem used for verifying the capability of CADET to provide an efficient, accurate statistical analysis of guidance system performance. The essential guidelines used in deriving the model are realism, completeness, and the desire to include enough significant nonlinear and random effects to establish confidence in the capability of CADET to treat complex nonlinear missile systems with random inputs.

The overall interconnection of the subsystems which comprise the missile-target intercept model is indicated in Fig. A.1-1. The principal variables are shown as outputs of the appropriate blocks, and random disturbances are denoted w_i. Detailed models underlying each input-output relationship are given in subsequent sections of the appendix. While the basic structure of the guidance system remains essentially unchanged from an earlier study described in Ref. 2, there are numerous extensions and refinements incorporated in the present investigation.

The final model is a state vector differential equation having the formulation

$$\dot{\underline{x}} = \underline{f}(\underline{x}) + G\underline{w}(t) \qquad \text{(A.1-1)}$$

where $\underline{w}(t)$ is a vector of gaussian white noise inputs which represents various random effects, the matrix G determines which state or states are driven by

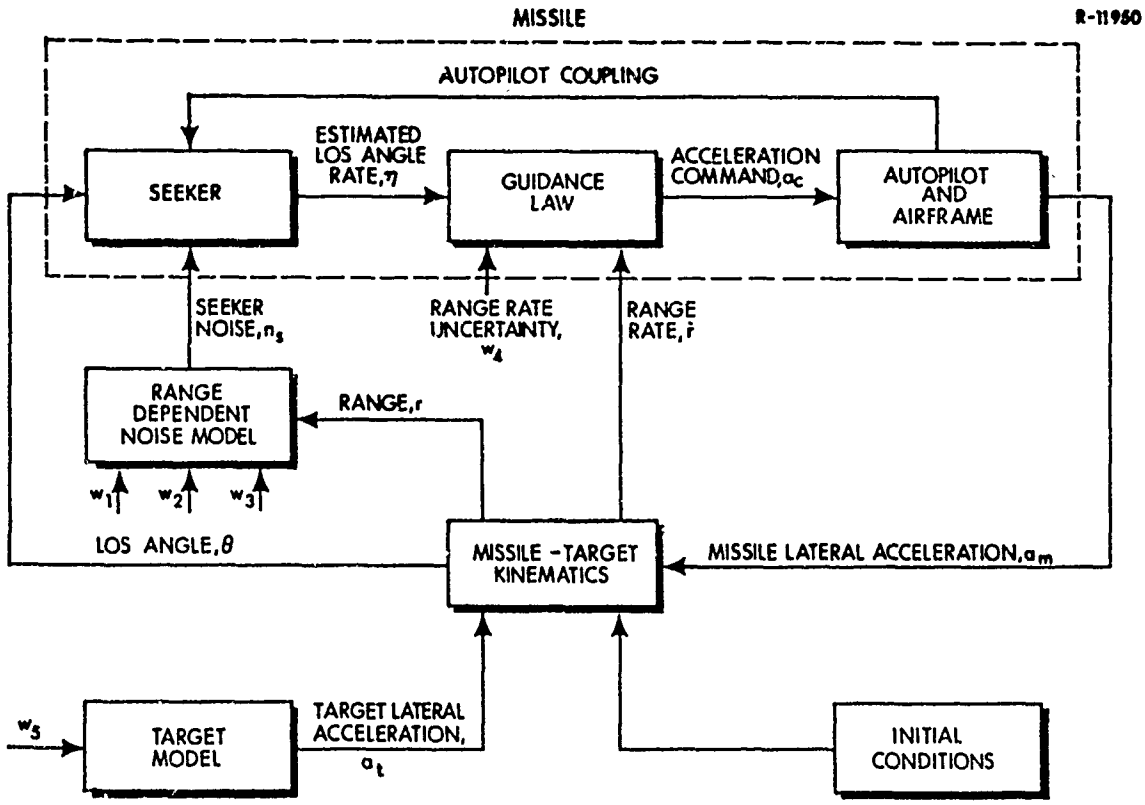

Figure A. 1-1 Basic System Block Diagram

each noise input, and $\underline{f}(\underline{x})$ embodies the linear and nonlinear dynamic relations within the system.

A. 2 THE MISSILE-TARGET KINEMATICS MODEL

The missile target engagement treated in this study is restricted to the terminal homing phase in a planar intercept configuration. Both the target and the missile are assumed to have a constant magnitude velocity vector which may be rotated by the application of a lateral (normal) acceleration.

An initial coordinate system is defined by the positions of the missile and target at the initiation of the terminal homing phase (taken to occur at t = 0); the missile is at the origin and the line-of-sight (LOS) to the target defines the x-axis at t = 0 (Fig. A. 2-1). The origin moves with the missile, without rotation, so that x and y, respectively, provide the instantaneous down range and cross range missile-target separation. Expressing the separation in polar coordinates, the relations

$$r = \sqrt{x^2 + y^2}$$
$$\theta = \tan^{-1}(y/x) \qquad \text{(A. 2-1)}$$

define the instantaneous range and LOS angle of the target. The angles θ_ℓ missile lead angle) and θ_a (target aspect angle) specify the orientation of the missile and target velocity vectors; by convention, θ_ℓ and θ_a are positive in the directions defined in Figure A. 2-1.

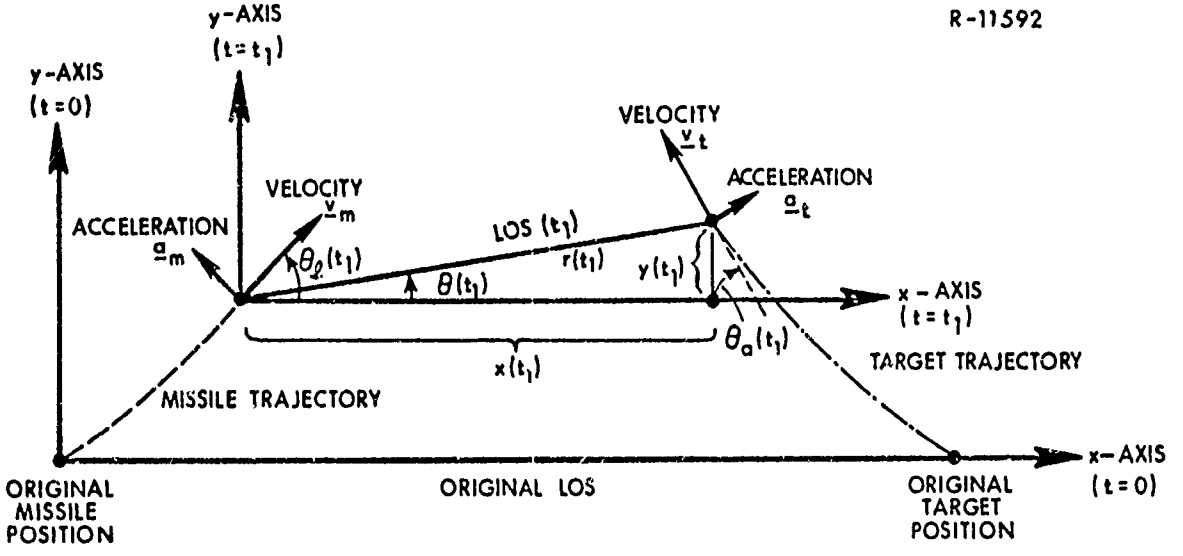

Figure A. 2-1 Target-Missile Planar Intercept Geometry

In terms of the variables defined in Fig. A.2-1, the differential equations

$$\dot{\theta}_\ell \triangleq \dot{x}_8 = \frac{1}{v_m}\, a_m$$

$$\dot{\theta}_a \triangleq \dot{x}_9 = \frac{1}{v_t}\, a_t \qquad \text{(A.2-2)}$$

$$\dot{y} \triangleq \dot{x}_{10} = v_t \sin(x_9) - v_m \sin(x_8)$$

$$\dot{x} \triangleq \dot{x}_{11} = -v_t \cos(x_9) - v_m \cos(x_8)$$

express the dynamics of the missile-target separation under the above assumptions, and identify the state variables (elements of $\underline{x}$ in Eq. (A.1-1)) x_8 to x_{11}. The LOS angle θ and range r are obtained by nonlinear operations on x and y, given in Eq. (A.2-1) and shown in Fig. A.2-2.

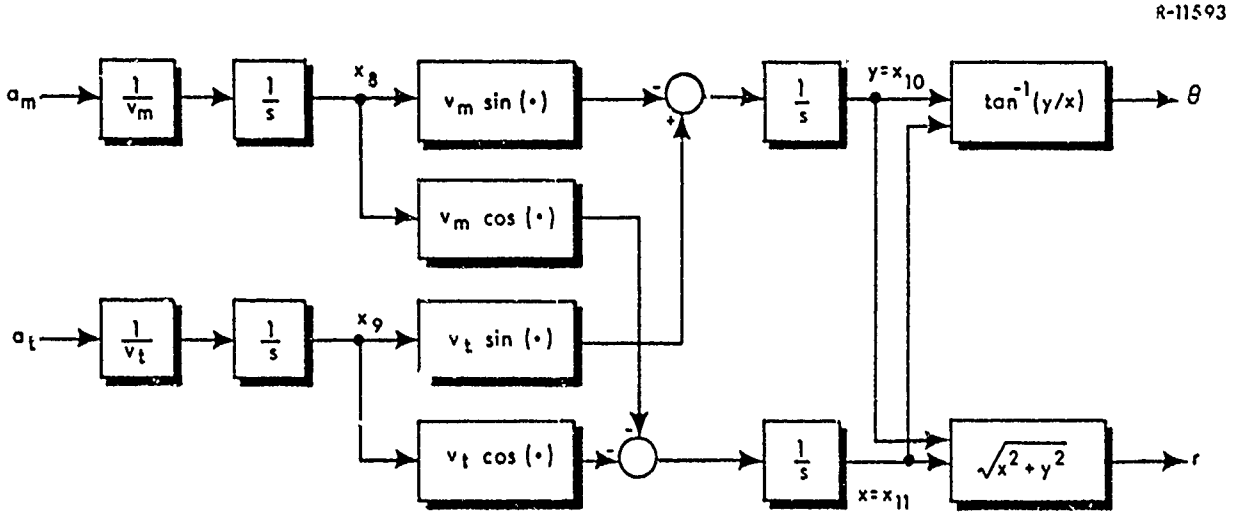

Figure A.2-2 State Vector Formulation of Missile-Target Kinematics

A.3 THE TARGET MODEL

The model representing the target behavior remains unchanged from prior studies (Ref. 2). As mentioned previously, the target velocity vector is assumed to have a constant magnitude, and a direction described by θ_a in Fig. A.2-1. The target maneuver model used in this study represents target lateral acceleration as a band-limited gaussian process derived from a gaussian white noise input by one stage of low-pass filtering. In differential equation formulation, we have

$$\dot{x}_{13} = - \omega_t x_{13} + w_5 \qquad \text{(A.3-1)}$$

where the state variable is the target lateral acceleration, a_t; the equivalent low-pass filter representation is depicted in Fig. A.3-1.

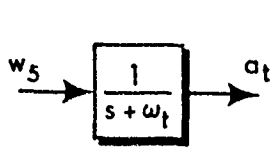

Figure A.3-1 Target Maneuver Model

The target maneuver rms level σ_{13} is determined by the spectral density of w_5 and the initial condition on σ_{13};

$$E[w_5(t)\, w_5(\tau)] = q_5\, \delta(t-\tau)$$
$$E[x_{13}(0)^2] = \frac{q_5}{2\omega_t} \qquad \text{(A.3-2)}$$

gives us an rms level that is constant throughout the engagement,

$$\sigma_{13} \equiv \sqrt{q_5/2\omega_t} \qquad \text{(A.3-3)}$$

It is interesting to note that the autocorrelation function and the corresponding power spectral density for a poisson square wave -- i.e. a square wave that switches between $\pm \sigma_{13}$ ft/sec^2 with random poisson distributed switching times having an average of $\omega_t/2$ zero-crossings per second -- are identical to those of the above gaussian process, although the associated probability density functions are quite different. The poisson model is often used to represent target evasive or "jinking" maneuvers. The poisson square wave can only take on values of $\pm \sigma_{13}$, so at any given time its probability density function consists of impulses with a weighting of 0.5 at plus and minus σ_{13}, whereas the above markov process is assumed to have a gaussian amplitude distribution. Therefore, the response of an amplitude dependent nonlinear operator could be quite different when driven by each of these two signal forms. However, if the random square wave is passed through a narrow band filter or integrator, it would experience broadening due to the filter's finite bandwidth. In the case of an integrator, the resulting wave shape would be a series of linear segments of constant slope. By application of the central limit theorem, as discussed in Ref. 9, the output distribution approaches the gaussian density function as the number of stages of filtering increases. Thus, although the poisson square wave may in some respects be a more realistic target maneuver model, we take advantage of the statistical similarity of these processes to justify representing this random effect by a band-limited gaussian process to facilitate the subsequent CADET analysis.

A.4 THE AUTOPILOT-AIRFRAME MODEL

In accordance with the assumption that the missile and target trajectories are confined to a plane, we describe the missile airframe orientation by the variables depicted in Figure A.4-1. This figure establishes the sign convention of each quantity; each variable is positive as shown. Note that we are particularizing the airframe model at this point by discussing the tail-controlled tactical missile. This is done to provide a concrete model for study, and not necessarily to exclude other configurations.

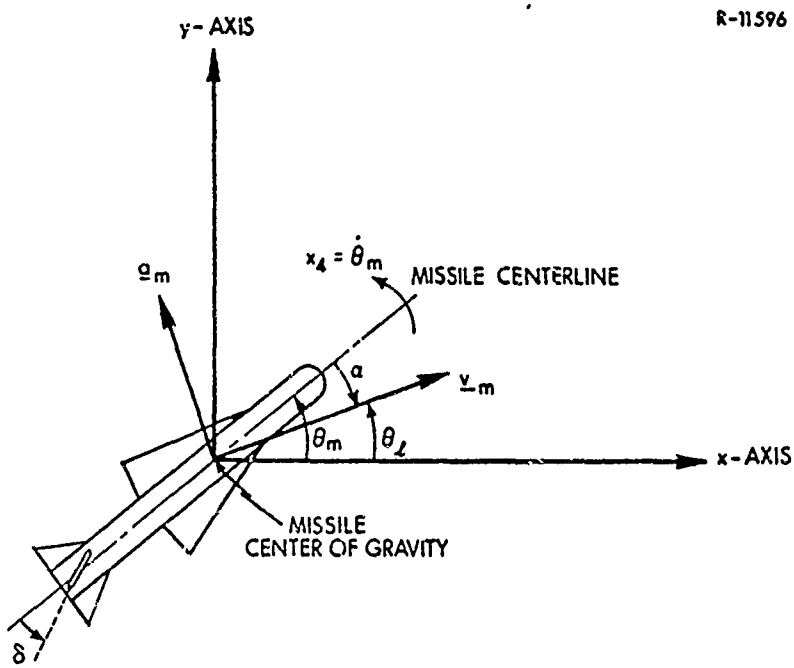

A. 4-1 Geometric Definition of Intercept Plane System Variables

The airframe variables under consideration are

$x_4 = \dot{\theta}_m$ = body angular rate

$x_5 = \alpha$ = angle of attack

$x_6 = \delta$ = control surface deflection

a_m = missile lateral acceleration (normal to the missile velocity vector)

We neglect gravity effects, tacitly assuming that the intercept plane is horizontal or that the missile has perfect gravity compensation. In a general situation, the differential equations expressing the airframe dynamics are nonlinear and time-varying due to the dependence of the airframe parameters on altitude, angle of attack, and mach number. However, in this

study we express the state variable differential equations in linear form*,

$$\dot{x}_4 = M_q x_4 + M_\alpha x_5 + M_\delta x_6$$

$$\dot{x}_5 = x_4 - L_\alpha x_5 - L_\delta x_6$$

$$\dot{x}_6 = - \mu x_6 + \mu u(t)$$

where u(t) represents a commanded fin deflection, $1/\mu$ is the control fin actuator time-constant, and the constants M_q, M_α, M_δ, L_α and L_δ represent the airframe stability derivatives. The latter are obtained from the nonlinear airframe parameters by making the following assumptions:

- Missile velocity is constant (drag effects are negligible over the period of time considered).
- Altitude remains nearly constant.
- The center of pressure, mass and inertia of the missile are constant.
- Lift force is linearly related to changes in angle of attack about some trim condition and to control fin deflection.
- Control fin actuator dynamics are linear.
- Fin effectiveness is independent of angle of attack.

Practical experience has shown that the resulting autopilot response characteristics closely approximate those of the nonlinear airframe near the given nominal conditions. The output of the airframe model is the missile lateral acceleration, which is given by

* A highly nonlinear airframe including drag effects has been studied via CADET in Ref. 3.

$$a_m = v_m[x_4 - \dot{x}_5] = v_m[L_\alpha x_5 + L_\delta x_6] \qquad \text{(A.4-2)}$$

where v_m is the magnitude of the missile velocity vector.

For typical values of the stability derivatives in Eq. (A.4-1), the missile airframe will exhibit an underdamped or even an unstable response to a commanded fin deflection. Acceptable control is achieved by introducing feedback compensation in the fin deflection command,

$$\begin{aligned} u(t) &= -[k_c a_c - k_a (a_m/v_m) - k_b \dot{\theta}_m] \\ &= -[k_c a_c - k_a (L_\alpha x_5 + L_\delta x_6) - k_b x_4] \end{aligned} \qquad \text{(A.4-3)}$$

where a_c is the commanded acceleration provided by the guidance law model (Section A.5). The parameter k_c is chosen to give unity steady state gain from a_c to a_m, and k_b and k_a are chosen to give the desired transient response. A complete block diagram of the compensated missile dynamic equations is shown in Fig. A.4-2.

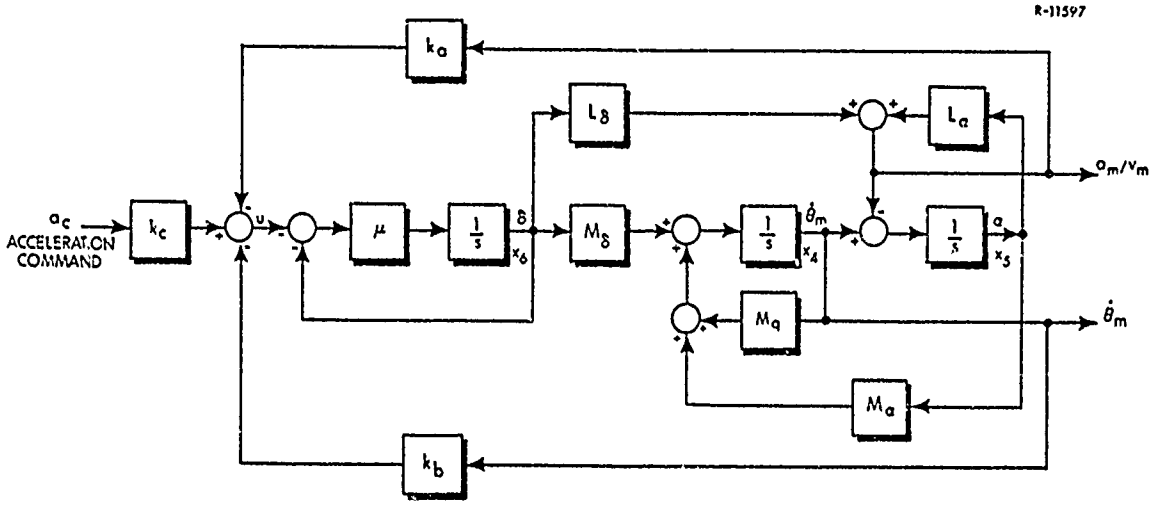

Figure A.4-2 Compensated Missile Airframe Dynamics

For ready assessment of the compensated missile airframe dynamics, it is convenient to use a transfer function formulation of the model. Given two outputs, a_m and $\dot{\theta}_m$, we desire to obtain $g_1(s)$ and $g_2(s)$ to provide the input-output relations indicated in Fig. A. 4-3. Utilization of standard block diagram

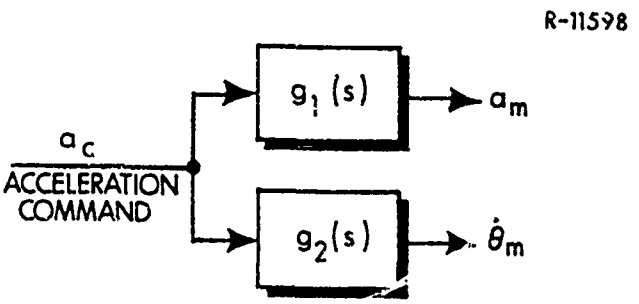

Figure A. 4-3 Transfer Function Formulation of the Compensated Missile Airframe Dynamics

reduction techniques shows that the dynamics indicated in Fig. A. 4-2 are equivalent to the transfer function formulation depicted in Fig. A. 4-3, where

$$g_1(s) = \frac{e_3 s^2 + e_2 s + e_1}{s^3 + c_3 s^2 + c_2 s + c_1} \qquad \text{(A. 4-5)}$$

$$g_2(s) = \frac{d_2 s + d_1}{s^3 + c_3 s^2 + c_2 s + c_1} \qquad \text{(A. 4-6)}$$

with

$$c_1 = \mu[\gamma + (k_a + k_b)\ \beta]$$

$$c_2 = \gamma + \mu[\zeta + L_\delta M_q k_a - M_\delta k_b]$$

$$c_3 = \zeta + \mu(1 - L_\delta k_a) \qquad \text{(A. 4-7)}$$

$$d_1 = \mu \beta k_c$$

$$d_2 = -\mu M_\delta k_c \qquad \text{(A.4-8)}$$

$$e_1 = \mu v_m \beta k_c$$

$$e_2 = \mu v_m L_\delta M_q k_c$$

$$e_3 = -\mu v_m L_\delta k_c \qquad \text{(A.4-9)}$$

$$\beta = L_\delta M_\alpha - L_\alpha M_\delta$$

$$\gamma = -M_\alpha - L_\alpha M_q \qquad \text{(A.4-10)}$$

$$\zeta = L_\alpha - M_q$$

The aerodynamic coefficients used in this study are chosen to correspond to an intercept at 35,000 ft., with a missile velocity magnitude $v_m = 3000$ ft/sec, the data being taken from Ref. 14, Vol. II, Appendix H. The compensating gains k_a, k_b and k_c Eq. (A.4-3) are set to achieve a dynamic performance that is typical of a missile in the terminal homing phase. These parameters and the corresponding transfer function coefficients are given in Table A.4-1.

The dominant time constant of the compensated airframe is $\tau_d = 1/s_1 = 0.316$ sec. The fact that e_1, e_2 and e_3 do not all have the same algebraic sign demonstrates that $g_1(s)$ has a right half plane zero, which is characteristic of the tail-controlled missile configuration depicted in Fig. A.4-1.

TABLE A.4-1

COMPENSATED MISSILE AIRFRAME DATA IN THE TERMINAL HOMING PHASE

Parameter	Symbol	Value
Actuator Lag Time Constant	$1/\mu$	0.0533 sec
Aerodynamic Coefficients	M_q	$-0.462\ \text{sec}^{-1}$
	M_α	$-5.81\ \text{sec}^{-2}$
	M_δ	$-72.0\ \text{sec}^{-2}$
	L_α	$0.379\ \text{sec}^{-1}$
	L_δ	$0.070\ \text{sec}^{-1}$
Compensating Gains	k_a	1.02 sec
	k_b	0.188 sec
	k_c	$0.476 \times 10^{-3}\ \text{sec}^2/\text{ft}$
Transfer Function Coefficients	c_1	$720.0\ \text{sec}^{-3}$
	c_2	$275.3\ \text{sec}^{-2}$
	c_3	$18.3\ \text{sec}^{-1}$
	d_1	$0.240\ \text{sec}^{-2}\ \text{ft}^{-1}$
	d_2	$0.642\ \text{sec}^{-1}\ \text{ft}^{-1}$
	e_1	$720.0\ \text{sec}^{-3}$
	e_2	$-0.865\ \text{sec}^{-2}$
	e_3	$-1.87\ \text{sec}^{-1}$
Transfer Function Poles	s_1	$-3.16\ \text{sec}^{-1}$
	s_2	$-7.56 + 13.0j\ \text{sec}^{-1}$
	s_3	$-7.56 - 13.0j\ \text{sec}^{-1}$

A.5 THE GUIDANCE SUBSYSTEM MODEL

The guidance signal from the seeker (discussed in the following section) is passed through a single-stage low-pass noise filter, the output of which is thus a filtered estimate of LOS angle rate, $x_7 \cong \dot{\theta}$. The classical proportional guidance law is then implemented, which calls for a commanded acceleration whose component normal to the line-of-sight (LOS) is proportional to the closing velocity times the estimated LOS angle rate, $x_7 = \hat{\dot{\theta}}$; that is, we desire to cause a_m to satisfy

$$a_m \cos(\theta_\ell - \theta) = n' v_c \hat{\dot{\theta}} \qquad \text{(A.5-1)}$$

where the parameter n' is designated the navigation ratio. The closing velocity is obtained by projecting the missile and target velocity vectors onto the instantaneous line of sight; as shown in Fig. A.2-1,

$$v_c = v_m \cos(\theta_\ell - \theta) + v_t \cos(\theta_a + \theta) \qquad \text{(A.5-2)}$$

In order to achieve a response that obeys Eq. (A.5-1), the ideal acceleration command a_c' should be chosen to satisfy

$$a_c' = \frac{n' v_c \hat{\dot{\theta}}}{\cos(\theta_\ell - \theta)} \qquad \text{(A.5-3)}$$

where the incorporation of the factor $1/\cos(\theta_\ell - \theta)$ is known as <u>secant compensation</u>.

In mechanizing the guidance law, the value of the closing velocity is never known exactly. If a radar homing seeker is used, then a reasonable estimate of v_c can be obtained by doppler measurements or by differencing range measurements. An infrared seeker system generally does not yield a good estimate of range, in which case v_c may be taken to be a prespecified

constant. Any uncertainty in the closing velocity is modelled by introducing a variable e_v into Eq. (A.5-3) which represents either a band limited noise, obtained by a single-stage low-pass filter with white noise input, or a bias, denoted simply e_{vb}. Thus

$$a_c' = n' \hat{\dot{\theta}} \left[v_m + v_t \frac{\cos(x_9 + \theta)}{\cos(x_8 - \theta)} + e_v \right] \tag{A.5-4}$$

provides the final ideal acceleration command used in this study, where $x_{12} \triangleq e_v$ is modelled by one of the differential equations

$$\begin{aligned} &\text{Random Uncertainty:} \quad \dot{x}_{12} = -\omega_4 x_{12} + w_4, \; E[x_{12}(0)] = 0 \\ &\text{Bias Uncertainty:} \quad \dot{x}_{12} = 0, \; x_{12}(0) = e_{vb} \end{aligned} \tag{A.5-5}$$

and w_4 is a white noise. Thus we can study either the effect of the noisy estimation of v_c or of a constant error in the assumed value of v_c.

Finally, the guidance law must account for an important nonlinear constraint on missile operation -- namely, acceleration command limiting. The actual acceleration command a_c that determines the input to the fin deflection actuator in Fig. A.4-2 must not exceed the structural capacity of the airframe and must not be so large as to cause the missile to stall. Thus the ideal acceleration command a_c' must be limited in order to prevent excessive lateral acceleration command levels; the limiting procedure is represented by the saturation nonlinearity

$$a_c = \begin{cases} a_c', & |a_c'| \leq a_{max} \\ a_{max} \, \text{sign}(a_c'), & |a_c'| > a_{max} \end{cases} \tag{A.5-6}$$

The guidance law features described above are all incorporated in the system model, as illustrated by the block diagram in Fig. A.5-1.

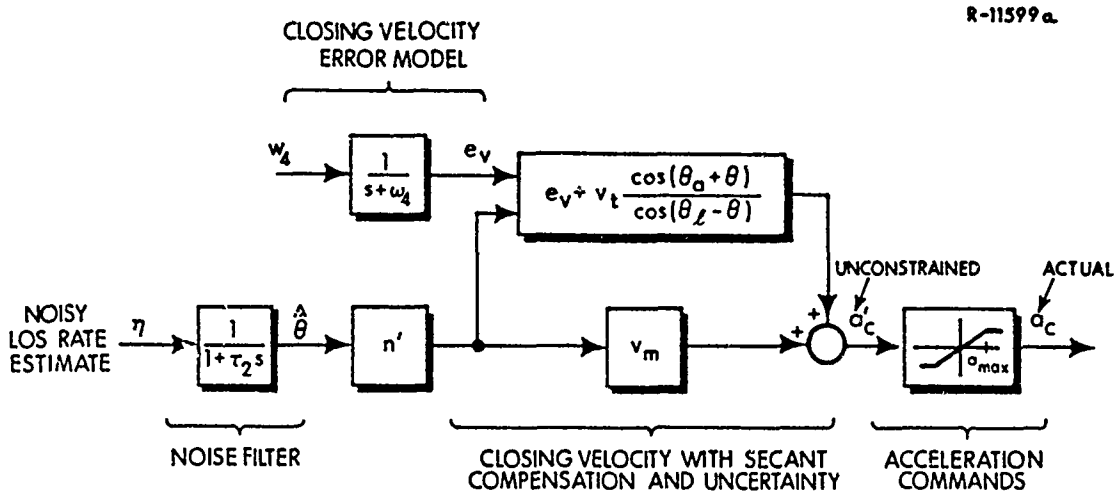

Figure A.5-1 Guidance Law Model

A.6 THE SEEKER SUBSYSTEM MODEL

There are several effects inherent to the seeker which can have a marked influence on overall missile performance. These include

- Boresight error distortion
  - Noise
  - Aberration
  - Receiver and signal processing characteristics
- Disturbance torque inputs
  - Seeker mass imbalance
  - Seeker gimbal friction
  - Spring restoring forces on the seeker head

Boresight Error Distortion - A fundamental variable in the seeker subsystem is the true boresight error, ϵ_{true} defined by the angle between the antennal centerline and the instantaneous line-of-sight (LOS); referring to Fig. A.6-1,

$$\epsilon_{true} = \theta - \theta_h - \theta_m = \theta - \phi \qquad \text{(A.6-1)}$$

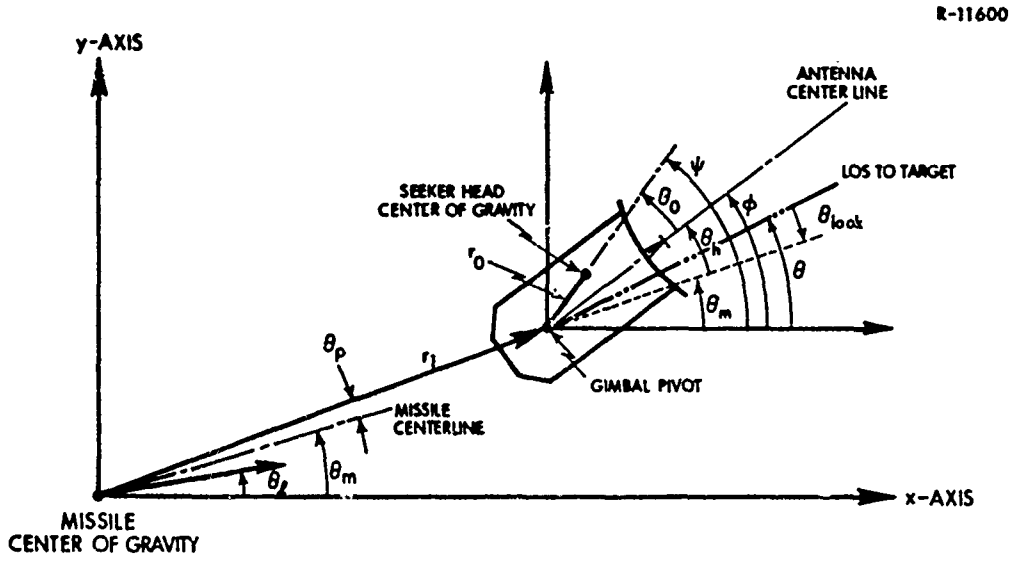

Figure A.6-1 Seeker System Configuration

The estimated or measured value of the boresight error will differ from ϵ_{true} due to several factors; among the more important of these are aberration, noise, and nonlinear receiver characteristics.

The effect of aberration is very highly dependent upon the geometry of the seeker-detector cover, the frequency and polarization of the incident energy and other factors; furthermore, it is variable due to manufacturing tolerances, possible erosion during flight and changes in environmental parameters. This phenomenon can be represented by a nonlinear and possibly time-varying operation on the look angle, $\theta_{look} = \theta - \theta_m$, so that an effective boresight error, ϵ_{eff}, is obtained in the form

$$\epsilon_{eff} = \theta_{look} + \theta_{ab} - \theta_h$$

where

$$\theta_{ab} = f_{ab}(\theta_{look})$$

as depicted in Fig. A.6-2.

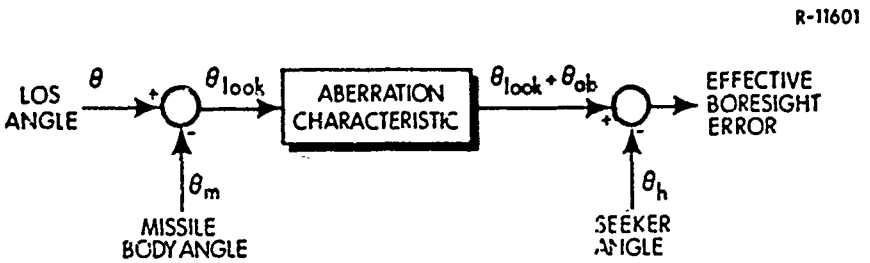

Figure A.6-2 Boresight Aberration Model

The effect of a linear aberration characteristic ($\theta_{ab} = k_r\, \theta_{look}$) was studied in Ref. 2. The case in which a radar homing system with nonlinear aberration is considered (where the aberration of incident energy is caused by the protective radome) was successfully analyzed via CADET in Ref. 3. In the latter study, the radome aberration characteristic was modelled as a piece-wise linear relation with odd symmetry and five distinct linear segments, as depicted in Fig. A.6-3. To avoid duplication, this effect is not considered further in this study.

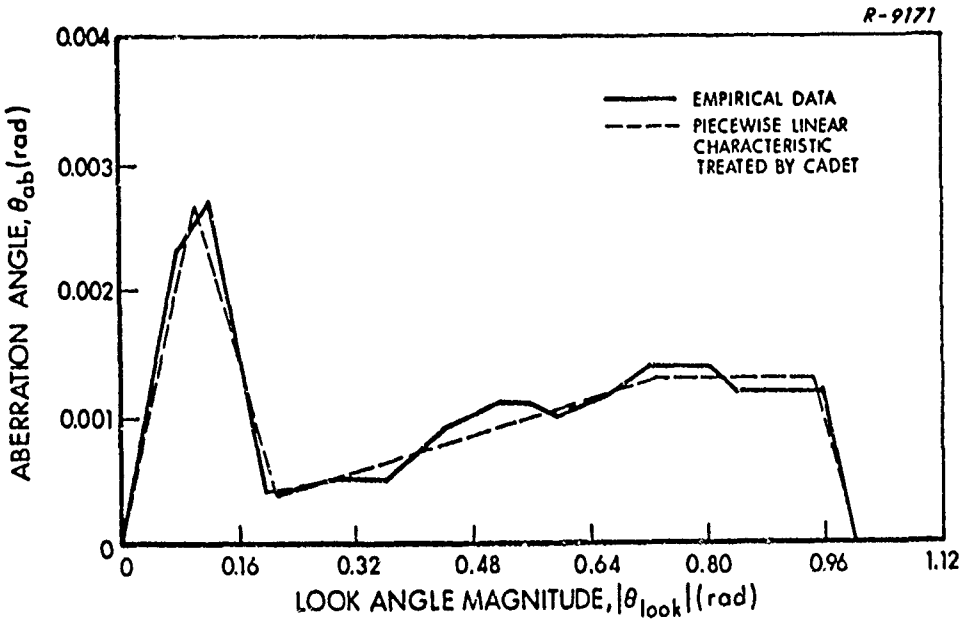

Figure A.6-3 Nonlinear Angular Aberration Characteristic Investigated in Ref. 3

In considering the degrading effects of noise, we include three fundamental categories of effects. Inverse range proportional noise, which has an effective rms level of the form

$$\sigma_a = \frac{\sigma_{14}}{r}$$

is representative of a noise source that increases in effect as range approaches zero. Such a phenomenon is target angular scintillation (caused by the apparent motion of the target due to the change in position of the target centroid of radiation). This can be modelled as a wide-band noise state, x_{14}, with constant rms level, σ_{14}, multiplied by a gain 1/r. Range proportional noise includes any noise source that remains constant in rms level in such a way that the effective signal-to-noise ratio decreases as the missile approaches the target, i.e., as range approaches zero. This type of random disturbance is represented by an equivalent noise with an rms level of the form

$$\sigma_b = r\sigma_{15}$$

which in turn can be modelled by a wide-band noise state x_{15} with a constant rms level of σ_{15} passing through a gain, r. Noise sources that exhibit this property are the distant stand-off jammer and receiver noise (generally due to thermal effects). Range independent noise represents noise sources that have a constant effect on the signal-to-noise ratio; target amplitude scintillation (due to time-varying effective target cross section, for example) and seeker servo noise are typical examples of such noise sources that can be modelled by a noise state x_{16} of constant variance σ_{16}^2. The complete noise model is shown in Fig. A.6-4 where w_1, w_2, and w_3 are gaussian white noise processes.

All three types of noise considered above have been treated in previous studies (Refs. 2, 3). It should be noted, however, that the earlier implementations of this model were linear time-varying; i.e., r(t) was assumed to be known

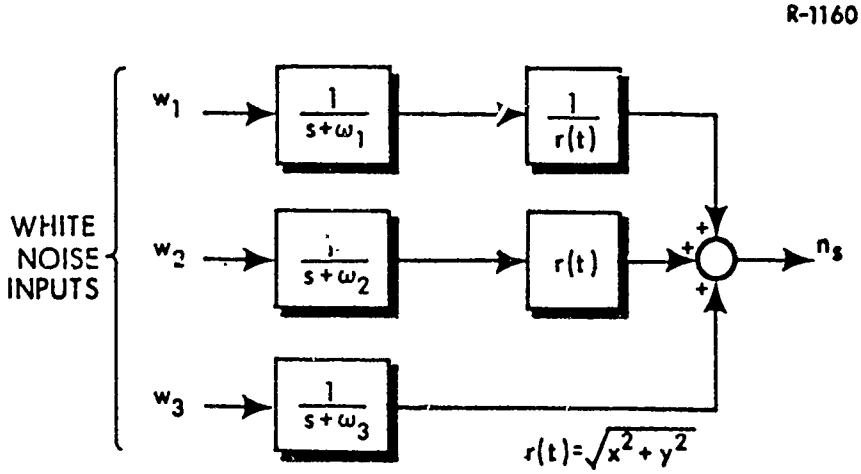

Figure A.6-4 General Seeker Noise Model

exactly in the noise model. Here we rigorously implement the nonlinear relation indicated in Fig. A.6-4,

$$n_s = x_{16} + x_{15}\sqrt{x_{10}^2 + x_{11}^2} + x_{14}\Big/\sqrt{x_{10}^2 + x_{11}^2} \qquad \text{(A.6-2)}$$

The receiver characteristic is a potentially complicated effect, highly dependent upon the specific antenna design, type of detector, and signal processing scheme. In order to avoid a very specialized model based on a particular tactical missile, we confine our attention to one phenomenon: the attenuation of the received signal which occurs when boresight error ϵ becomes large, i.e., when ϵ approaches ϵ_{max} in Fig. A.6-5a. The detector alone will have an output which is very nearly proportional to its input for small values of ϵ; however, as the boresight error approaches ϵ_{max}, we note in Fig. A.6-5b that the signal strength decreases to a null. If the antenna pattern has appreciable sidelobe sensitivity, there may also be some response for values of ϵ greater than ϵ_{max}. The upper limit on the boresight error, $\bar{\epsilon}$, such that the detector characteristic

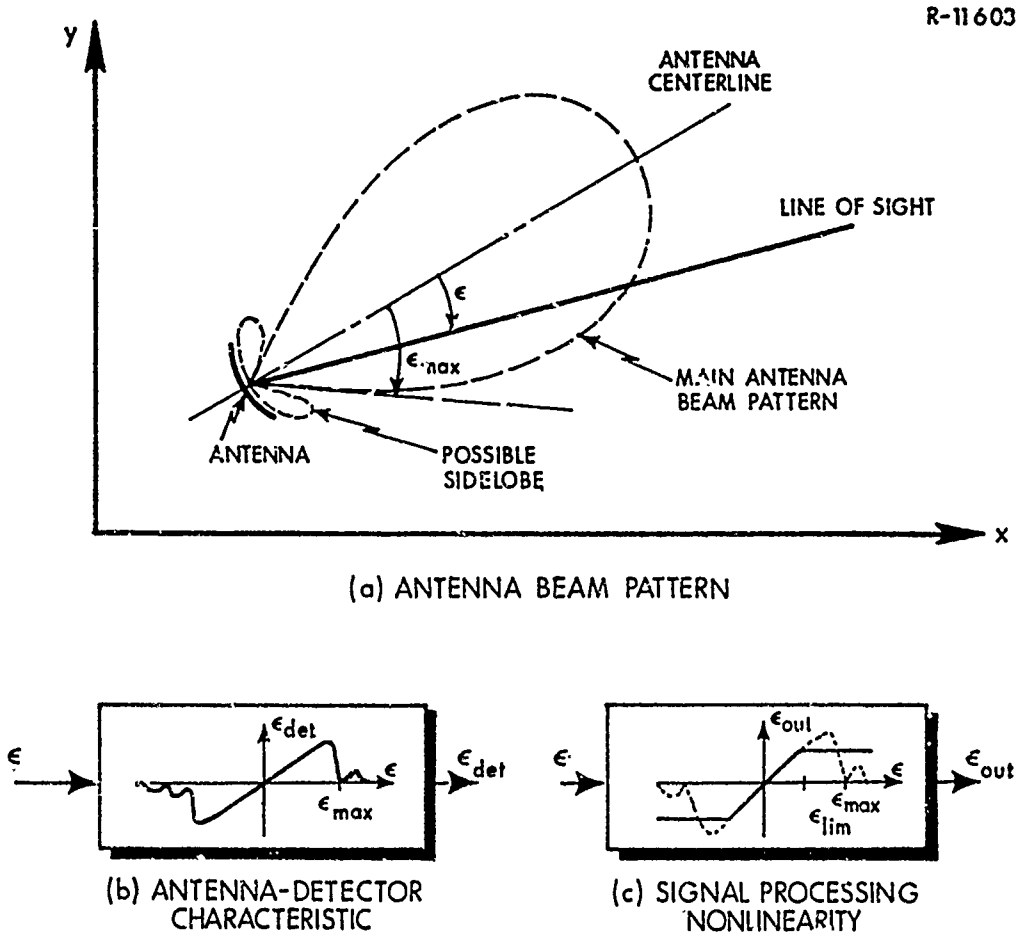

Figure A.6-5 Receiver Boresight Error Distortion Effects

is nearly linear for $|\epsilon|$ less than $\bar{\epsilon}$ is quite variable, depending on the type of target tracking system under consideration. For monopulse radar or infrared detectors, $\bar{\epsilon}$ could be as small as a fraction of a degree.

The undesirable detector null and possible sidelobe response can be circumvented in the signal processing scheme. In the case considered here, some value $\epsilon_{lim} < \bar{\epsilon}$ is chosen; a nonlinearity is then introduced such that whenever the boresight error magnitude exceeds ϵ_{lim}, the output of the signal processor is held at $\pm\epsilon_{lim}$. This provides a simple model, depicted in Fig. A.6-5c, which will capture the effect of a narrow antenna beamwidth and a reasonable signal processing nonlinearity.

The combined effects of noise and receiver/signal processing characteristics are illustrated in the general boresight error model (without aberration) shown in Fig. A.6-6. We mention in passing that a more exact noise model might divide noise sources into external and internal effects, i.e., noise sources entering the boresight error model just before, as well as after, the receiver characteristic. However, this categorization is somewhat artifically detailed when compared with a realistic situation where noise levels are only approximately known. While the aberration and signal processing nonlinearities may have a significant impact on the closed loop dynamics of the overall missile-target intercept model, the actual noise input point is not particularly critical. In fact, injecting all noise sources after the receiver in Fig. A.6-6 results in a worst-case model of the effect of the signal processing nonlinearity, since it neglects the attenuation of external noise sources.

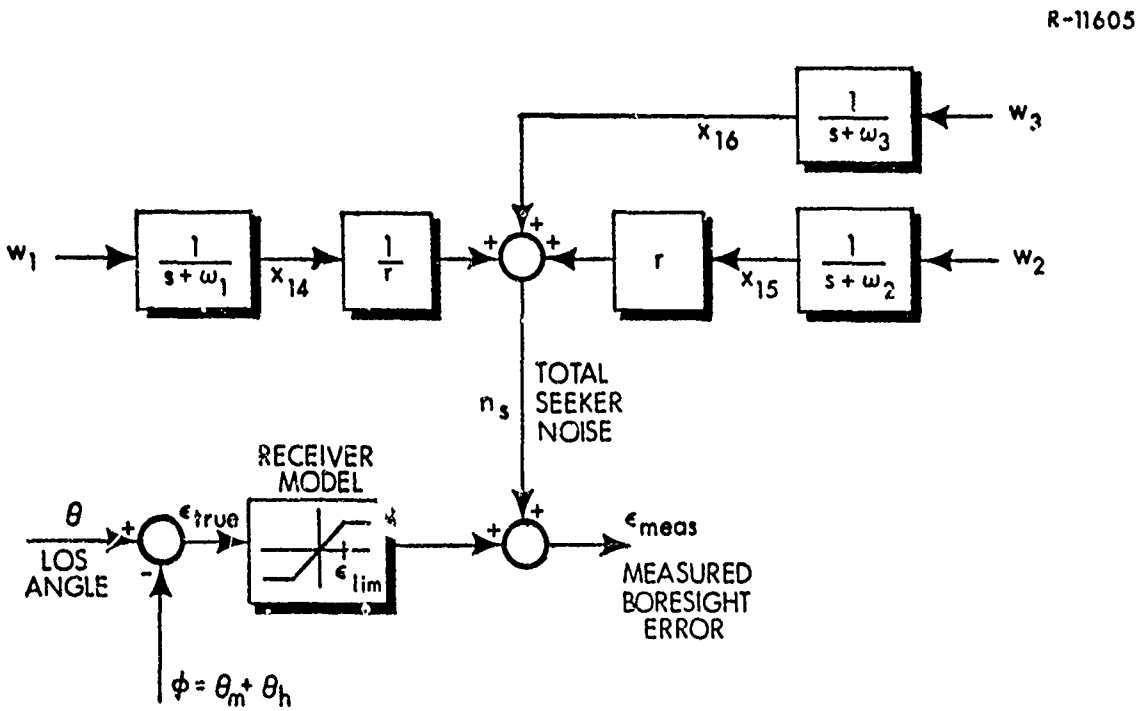

Figure A.6-6 Final Boresight Error Measurement Model

Disturbance and Control Torques - The seeker model is completed by developing a suitable tracking and stabilization control system including several important sources of disturbance torque inputs. In terms of the inertially-referenced angles ϕ and ψ shown in Fig. A.6-1, we will derive a relation of the form

$$I_p \ddot{\phi} = I_p \ddot{\psi} = T_c - T_d \qquad \text{(A.6-3)}$$

where I_p is the moment of inertia of the seeker head about the gimbal pivot, T_c is the external control torque (derived from an electric servo motor, for example), and T_d is the total disturbance torque. The latter has three components,

$$T_d = T_m + T_f + T_r \qquad \text{(A.6-4)}$$

where T_m is an effective torque due to mass imbalance, and we consider two external torque components, T_f due to nonlinear friction in the gimbal and T_r due to nonlinear restoring torques. Since the seeker head center of gravity (cg) is generally displaced from the pivot point, as shown in Fig. A.6-1 and specified by the parameters r_0 and θ_0, the moment of inertia I_p is related to the corresponding moment inertia referred to the cg by

$$I_p = I_0 + mr_0^2 \qquad \text{(A.6-5)}$$

where m is the mass of the seeker head.

The external torques due to spring and friction effects are modelled by the relations

$$\text{Restoring Torque:} \quad T_r = f_1(\theta_h)$$

$$\text{Friction Torque:} \quad T_f = f_2(\dot{\theta}_h) \qquad \text{(A.6-6)}$$

where θ_h is the angle between the seeker and missile center lines. Often restoring torques are linear for small angle deflections, becoming nonlinear only as θ_h increases in magnitude, as illustrated in Fig. A.6-7a. This behavior corresponds to the symmetric "hard spring" case (Ref. 15) where the elastic limit of a spring is exceeded and Hooke's law for linear spring behavior becomes invalid; often the nonlinear term is taken to be a power law relation,

$$f_1(\theta_h) = k_1 \left| \frac{\theta_h}{\theta_{lim}} \right|^{\kappa} \text{sign}\,(\theta_h)$$

where κ is an integer greater than one, so that T_r exhibits a distinct departure from linearity as $|\theta_h|$ exceeds θ_{lim} which is typical of a symmetric nonlinear spring characteristic. A common type of nonlinear friction is the dry or Coulomb effect (Ref. 15), where

$$f_2(\dot{\theta}_h) = k_2 \text{ sign } (\dot{\theta}_h)$$

i.e., the friction term of the disturbance torque has constant magnitude with the algebraic sign of the gimbal angle rate. Illustrations of these disturbance torque terms are depicted in Fig. A.6-7.

R-11604

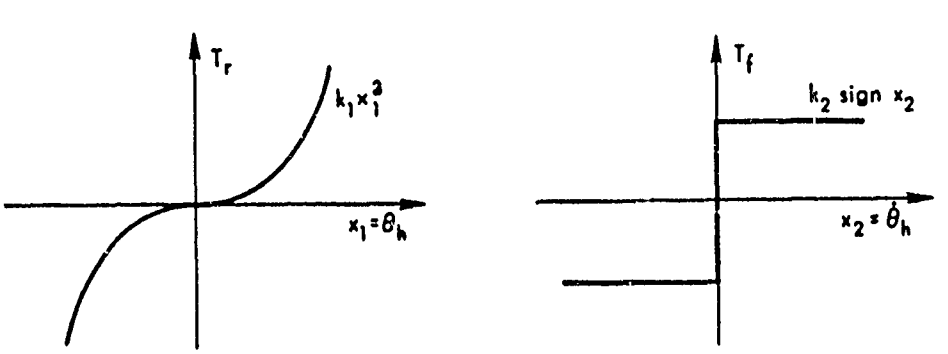

(a) Nonlinear Restoring Torque (b) Nonlinear Friction Effect

Figure A.6-7 External Disturbance Torque Models

The effective disturbance torque component due to seeker mass imbalance can readily be determined by application of the basic principles of mechanics (Ref. 13). The equations of motion of the seeker head can be derived directly by applying the Euler equation

$$\frac{d}{dt}\left(\frac{\partial U}{\partial \dot{\psi}}\right) - \frac{\partial U}{\partial \psi} = T_c - T_r - T_f \qquad \text{(A.6-7)}$$

where U is the seeker head kinetic energy, and the right side represents all external torque sources. The kinetic energy of the seeker head has two terms:

$$U = \frac{1}{2} mv^2 + \frac{1}{2} I_0 (\dot{\psi})^2 \qquad \text{(A.6-8)}$$

where v is the magnitude of the velocity of the seeker head center of gravity and $\dot{\psi}$ is the angular velocity of the seeker head rotation about the cg. The velocity magnitude is obtained by resolving the missile velocity vector $\underline{v}_m$ (describing the motion of the missile cg) into x and y components, then adding to this the relative motion of the seeker cg with respect to the missile cg. Referring to Fig. A.6-1, the seeker head cg has the relative coordinates

$$x = r_1 \cos(\theta_m + \theta_p) + r_0 \cos\psi$$

$$y = r_1 \sin(\theta_m + \theta_p) + r_0 \sin\psi$$

Generally θ_p (the fixed angle between the missile centerline and the seeker gimbal pivot) is quite small, so it will be neglected here. The total velocity components of the seeker head cg are then

$$v_x = v_m \cos\theta_\ell + \frac{dx}{dt} = v_m \cos\theta_\ell - r_1 \dot{\theta}_m \sin\theta_m - r_0 \dot{\psi} \sin\psi$$

$$v_y = v_m \sin\theta_\ell + \frac{dy}{dt} = v_m \sin\theta_\ell + r_1 \dot{\theta}_m \cos\theta_m + r_0 \dot{\psi} \cos\psi$$

Using standard trigonometric identities, the squared velocity magnitude is then determined to be

$$v^2 = v_m^2 + (r_1 \dot{\theta}_m)^2 + (r_0 \dot{\psi})^2 + 2 r_0 r_1 \dot{\theta}_m \dot{\psi} \cos(\psi - \theta_m)$$

$$+ 2 r_0 v_m \dot{\psi} \sin(\theta_\ell - \psi) + 2 r_1 v_m \dot{\theta}_m \sin(\theta_\ell - \theta_m) \qquad \text{(A.6-9)}$$

The equation of motion can then be derived directly from Eqs. (A.6-7) to (A.6-9); combining these relations, we obtain the final differential equation of motion,

$$T_c - T_f - T_r - I_p \ddot{\psi} = m r_0 r_1 [\ddot{\theta}_m \cos(\psi - \theta_m) + (\dot{\theta}_m)^2 \sin(\psi - \theta_m)]$$

$$+ m r_0 v_m \dot{\theta}_\ell \cos(\theta_\ell - \psi) \qquad \text{(A.6-10)}$$

Comparing Eq. (A.6-10) with Eqs. (A.6-3) and (A.6-4), we identify the seeker mass imbalance disturbance torque, T_m in Eq. (A.6-4), to be given by the terms on the right side of Eq. (A.6-10). Combining the latter with the friction and spring disturbance torque components, we obtain

$$T_d = f_1(\theta_h) + f_2(\dot{\theta}_h) + m r_0 [r_1 \ddot{\theta}_m \cos(\psi - \theta_m)$$

$$+ r_1 (\dot{\theta}_m)^2 \sin(\psi - \theta_m) + v_m \dot{\theta}_\ell \cos(\psi - \theta_\ell)] \qquad \text{(A.6-11)}$$

The control torque T_c in Eq. (A.6-3) is chosen to make the seeker track the target, i.e., to maintain the measured boresight error at a small value. The nominal seeker is designed under the assumption that there is no

friction and that spring effects are negligible; thus, it is necessary to include rate feedback in the torque command (a feedback term proportional to $\dot{\phi}$ which is measured by a rate gyro) to provide suitable damping. Thus we write the nominal control torque as

$$T_{cn} = k_s \left[\frac{\epsilon}{\tau_1} - k_g(\dot{\theta}_m + \dot{\theta}_h)\right]$$

where τ_1 is the track loop time constant, k_g is the rate gyro gain, and k_s is the torque servo gain. The implementation of this control law is depicted in Fig. A.6-8.

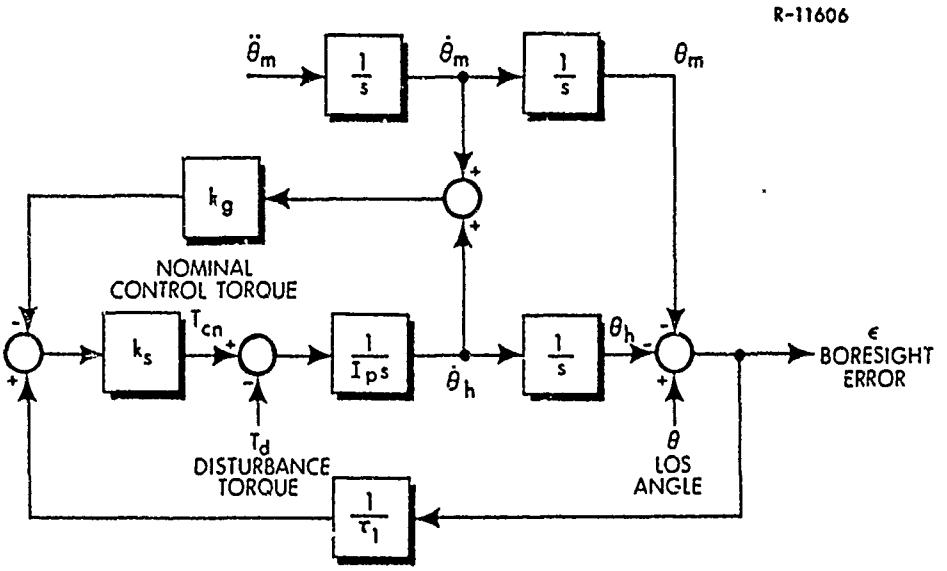

Figure A.6-8 Nominal Seeker Track Loop
(Neglecting All Nonlinear Effects)

While the implementation of the seeker control function depicted in Fig. A.6-8 will provide an adequate response under ideal conditions, it can be shown (see Section A.7) that the dynamic response of the seeker is quite sensitive to steady state disturbance torque inputs. Since we have already indicated that disturbance torques are to be considered in our study, compensation of the seeker must be included to achieve satisfactory performance. A simple and effective

compensation procedure is to insert proportional plus integral cascade compensation before the torque summing junction in Fig. A.6-8. That is, we specify the compensated control torque by

$$T_{cc} = \frac{s + k_0}{s} T_{cn} \qquad \text{(A.6-13)}$$

This relation corresponds to the differential equation

$$\dot{T}_{cc} = k_0 T_{cn} + \dot{T}_{cn} \qquad \text{(A.6-14)}$$

The complete seeker simulation model, representing the synthesis of the dynamic equations derived in this section, is shown in Fig. A.6-9. We demonstrate in Section A.7 that the indicated output, η, is a noisy estimate of LOS rate ($\dot{\theta}$).

A.7 TRANSFER FUNCTION REPRESENTATION OF THE EQUIVALENT LINEAR SEEKER

For a subsystem of the complexity of the seeker as modelled in Fig. A.6-9, it is often helpful to derive the transfer function formulation of the linear system obtained by neglecting all nonlinearities. Several assertions made in simplifying the seeker model are based on this representation, and the procedure used for the purpose of designing the compensation network (choice of k_0) can best be treated in this way.

We define four inputs (refer to Fig. A.7-1),

$$\begin{aligned} u_1 &= \theta \\ u_2 &= \ddot{\theta}_m \\ u_3 &= n_s(t) \\ u_4 &= T_m \end{aligned} \qquad \text{(A.7-1)}$$

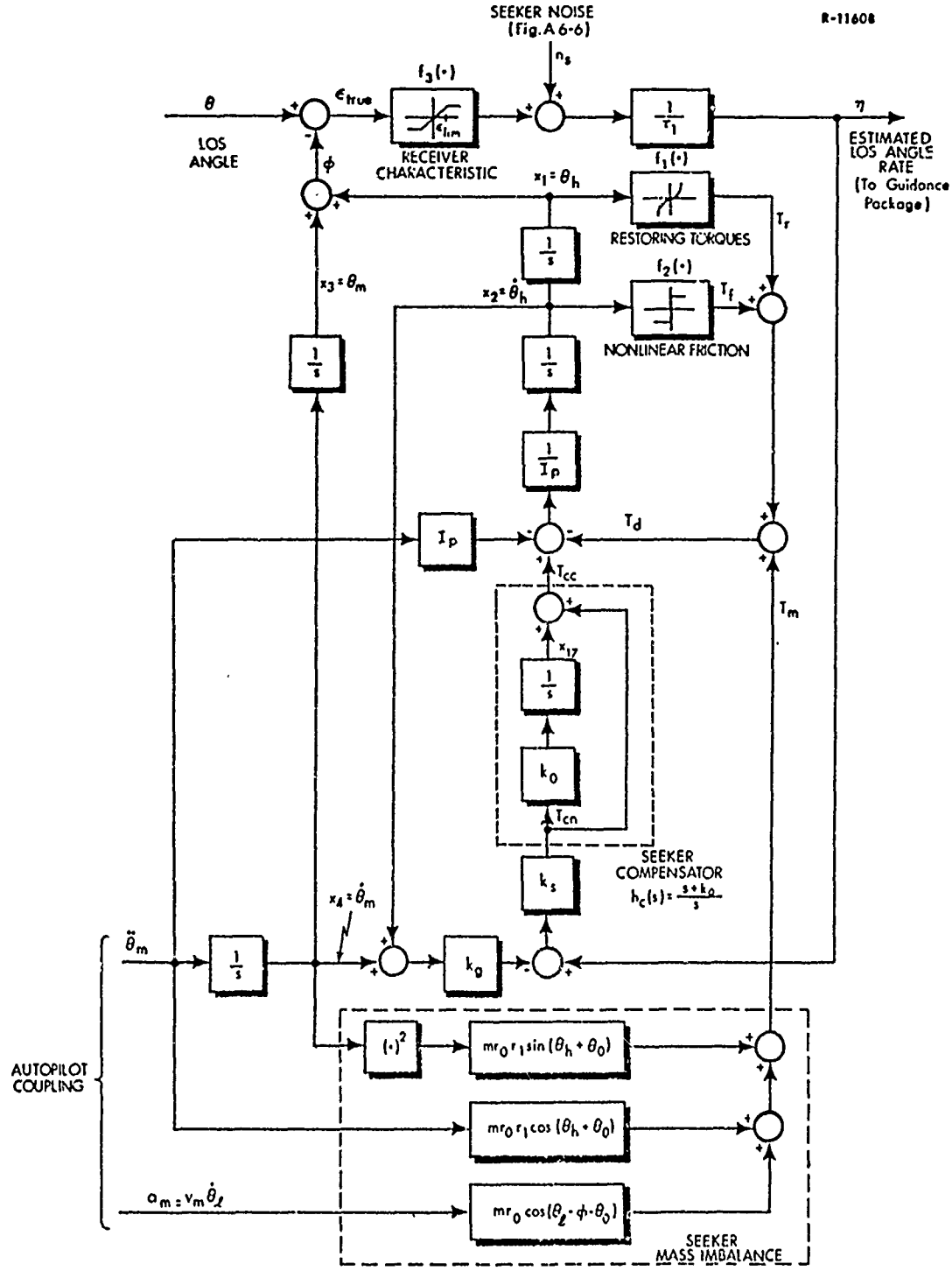

Figure A.6-9 Complete Seeker Model

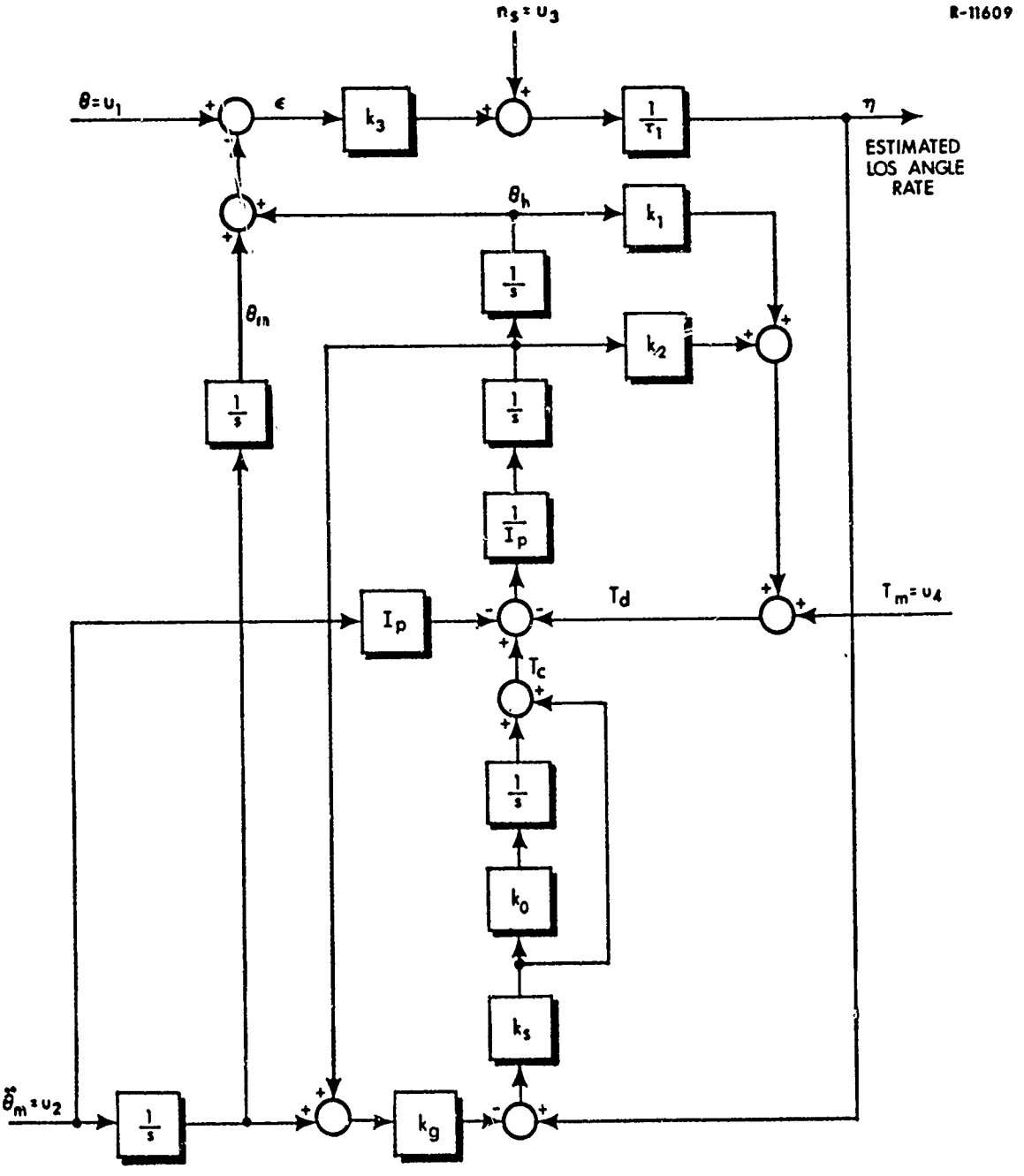

Figure A.7-1 Linear Seeker Model

The transfer functions $d_1(s)$ to $d_4(s)$ can be found for the equivalent block diagram representation depicted in Fig. A.7-2 using standard state vector formulation techniques,

$$\left.\begin{aligned} \dot{\underline{x}} &= F\underline{x} + G\underline{u} \\ \eta &= H\underline{x} + E\underline{u} \end{aligned}\right\} \quad D(s) = E + H(sI - F)^{-1}G \qquad (A.7\text{-}2)$$

where

$$u = \begin{bmatrix} u_1 \\ u_2 \\ u_3 \\ u_4 \end{bmatrix}, \quad D(s) = [d_1(s),\ d_2(s),\ d_3(s),\ d_4(s)] \qquad (A.7\text{-}3)$$

and $d_i(s)$, the elements of D, correspond to the scalar transfer function indicated in Fig. A.7-2. The final results of this analysis are summarized in Eqs. (A.7-4) and (A.7-5).

R-11610

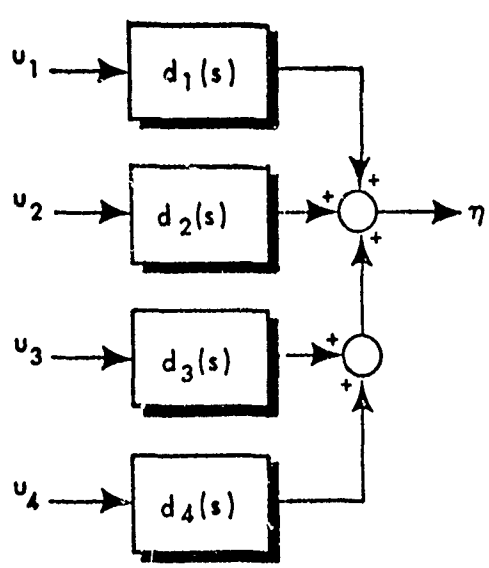

Figure A.7-2 Linear Seeker Model in Transfer Function Form

$$d_1(s) = \frac{k_3}{\tau_1} \quad \frac{s[s^2 + q_3 s + p_1]}{s^3 + q_3 s^2 + q_2 s + q_1}$$

$$d_2(s) = \frac{-k_3}{I_p \tau_1} \quad \frac{k_2 s + k_1}{s[s^3 + q_3 s^2 + q_2 s + q_1]}$$

$$d_3(s) = \frac{1}{k_3} \quad d_1(s) \qquad \text{(A.7-4)}$$

$$d_4(s) = \frac{k_3}{I_p \tau_1} \quad \frac{s}{s^3 + q_3 s^2 + q_2 s + q_1}$$

$$p_1 = \frac{k_1 + k_s k_g k_0}{I_p}$$

$$q_1 = \frac{k_s k_0 k_3}{I_p \tau_1}$$

$$q_2 = p_1 + \frac{k_s k_3}{I_p \tau_1} \qquad \text{(A.7-5)}$$

$$q_3 = \frac{k_2 + k_s k_g}{I_p}$$

The nominal seeker is defined by a choice of parameters that leads to acceptable dynamic behavior in the absence of disturbance torques; the data and

transfer functions are given in Table A.7-1. A second case is the nominal compensated seeker, which has been designed to exhibit a significantly better performance in the presence of disturbance torques; the design by root locus techniques is indicated subsequently and the transfer functions are summarized in Table A.7-2.

In both the nominal and the nominal compensated seeker, we note that $d_2(s) \equiv 0$. This demonstrates that with no linear friction or spring restoring torques, the seeker has perfect stabilization, i.e., the measured boresight error is unaffected by rotation of the missile body.

For frequencies considerably less than 10 rad/sec, we have $d_{n1} \cong d_{c1} \cong s$, which is the transfer function of a differentiator. Hence, the assertion that η is an estimate of the LOS angular rate ($\dot{\theta}$) holds at low frequencies.

The seeker compensation removes steady state disturbance torque sensitivity, as is shown by the zero of $d_{c4}(s)$ at $s = 0$. To demonstrate this point in more detail, we assume a step disturbance torque input,

$$u_4(t) = T_0, \quad t \geq 0, \tag{A.7-6}$$

yielding a response which is represented in Laplace transform notation by

$$\eta(s) = d_4(s) \frac{T_0}{s}$$

or, by substitution,

$$\eta_n(s) = \frac{1000}{12} \quad \frac{T_0}{s(s+10)(s+50)}$$

$$\eta_c(s) = \frac{1000}{12} \quad \frac{T_0}{s^3 + 60\,s^2 + 1700\,s + 10{,}000} \tag{A.7-7}$$

TABLE A.7-1

THE NOMINAL SEEKER

Parameters	Transfer Functions
$k_0 = k_1 = k_2 = 0$	$d_{n1}(s) = \frac{100}{12} \frac{s\,(s+60)}{(s+10)(s+50)}$
$k_3 = 1$	
$k_g = 1$	$d_{n2}(s) \equiv 0$
$k_s = 6 \frac{\text{in-oz-sec}}{\text{rad}}$	$d_{n3}(s) = d_{n1}(s)$
$I_p = 0.1$ in-oz-sec^2	$d_{n4}(s) = \frac{1000}{12} \frac{1}{(s+10)(s+50)}$
$\tau_1 = 0.12$ sec	

TABLE A.7-2

THE NOMINAL COMPENSATED SEEKER

Parameters	Transfer Functions
$k_1 = k_2 = 0$	$d_{c1}(s) = \frac{100}{12} \frac{s\,[s^2 + 60s + 1200]}{s^3 + 60s^2 + 1700s + 10,000}$
$k_3 = k_g = 1$	
$k_0 = 20$ sec^{-1}	$d_{c2}(s) \equiv 0$
$k_s = 6 \frac{\text{in-oz-sec}}{\text{rad}}$	$d_{c3}(s) = d_{c1}(s)$
$I_p = 0.1$ in-oz-sec^2	
$\tau_1 = 0.12$ sec	$d_{c4}(s) = \frac{1000}{12} \frac{s}{s^3 + 60s^2 + 1700\,s + 10,000}$
POLES: $s = -7.71$, $s = -26.1 \pm 24.8j$	

To obtain the effect of the disturbance torque after transients disappear, we evaluate the steady state value of η by the final value theorem of Laplace transform theory: if f(s) is the Laplace transform of f(t) and if a finite steady state value of f(t) exists, then

$$f_{ss} \triangleq \lim_{t \to \infty} f(t) = \lim_{s \to 0} [\, s\, f(s)]$$

The application of this result to Eq. (A.7-7) yields

$$\eta_{nss} = \frac{T_\theta}{6}$$

$$\eta_{css} = 0 \qquad \text{(A.7-8)}$$

which establishes that the proportional plus integral compensation technique (insertion of the transfer function

$$h_c(s) = \frac{s + k_0}{s}$$

in Eq. (A.6-13)) is effective in eliminating the response to constant disturbance torque inputs.

To complete the seeker compensation design, we note that for the nominal values of the seeker variables given in Table A.7-1 (except $k_0 \neq 0$), the denominator of the transfer functions $d_i(s)$ is given by

$$s^3 + q_3 s^2 + q_2 s + q_1 = s^3 + 60s^2 + (500 + 60\, k_0)\, s + 500\, k_0$$

$$= (s^3 + 60s^2 + 500s) + 60\, k_0\, (s + 8.333)$$

In choosing k_0, it is desired to achieve a dominant pole at $s \cong -10$ and to have the remaining subsidiary poles as far from the origin of the s-plane as possible subject to the condition that they must be suitably damped. A root locus analysis is effective in finding a suitable value of k_0 satisfying these conditions. In Fig. A.7-3, we see that as $k_0 \to \infty$, the dominant pole approaches -8.33; however, for $k_0 > 20$, we have subsidiary poles with unsatisfactory damping, i.e., $\zeta < 0.707$. The condition $\zeta = 0.707$ is specified in order to ensure a transient step response with no overshoot; thus our final compensated seeker design is achieved by choosing $k_0 = 20$, as indicated in Table A.7-2.

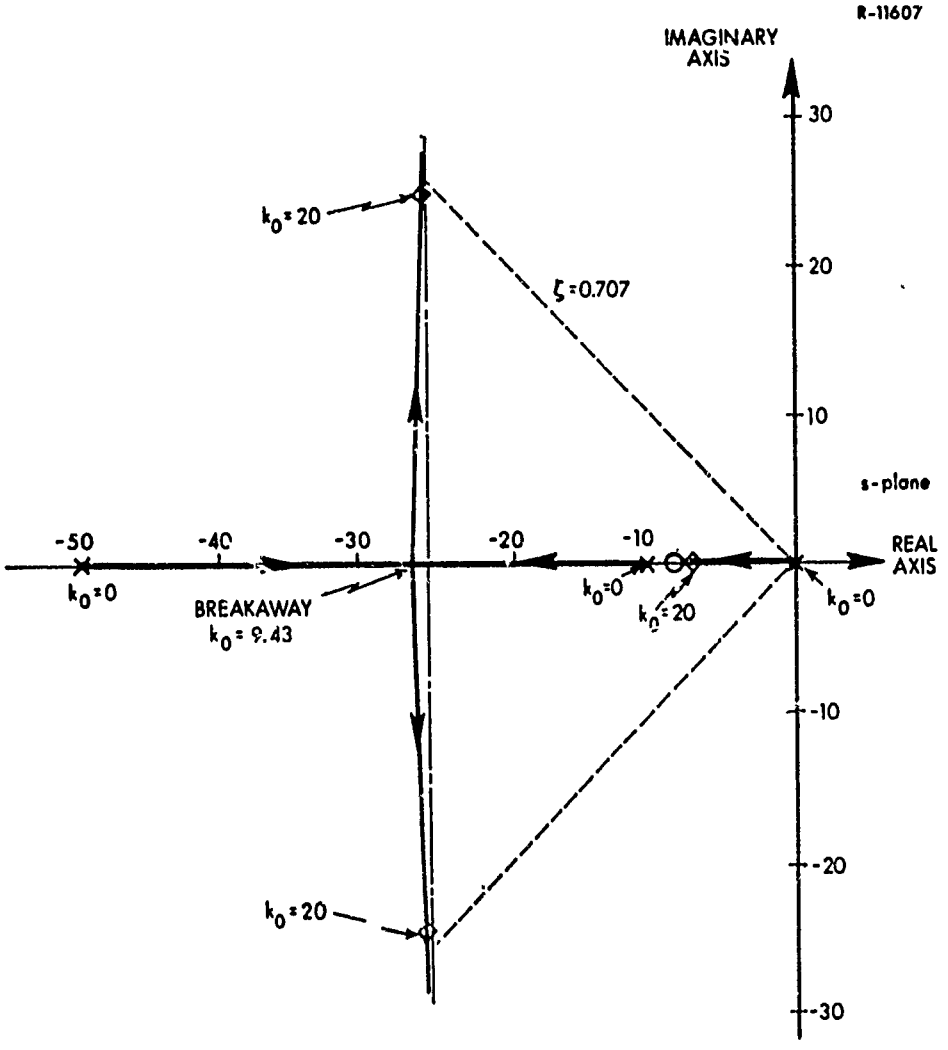

Figure A.7-3 Root Locus Compensator Design

A.3 SYSTEM MODEL SUMMARY

In Fig. A.8-1 the complete missile-target intercept model is portrayed with all of the subsystems described in the previous sections appropriately interconnected. All of the state variables are depicted except x_5, x_6, and x_{17} (angle of attack, control fin deflection and the seeker compensation state, respectively) which are encompassed in the linear dynamics represented by the transfer functions $g_1(s)$, $g_2(s)$, and $(1+k_0/s)$. For convenient reference, we list the nonlinearities incorporated in the system model and indicate their form:

- Seeker head restoring torque

$$f_1(x_1) = k_1 \left| \frac{x_1}{\theta_{lim}} \right|^K \text{sign}(x_1)$$

- Seeker gimbal friction

$$f_2(x_2) = k_2 \text{ sign}(x_2)$$

- Receiver/signal processing characteristic

$$f_3(\epsilon) = \begin{cases} \epsilon, & |\epsilon| \le \epsilon_{lim} \\ \epsilon_{lim} \text{ sign}(\epsilon), & |\epsilon| > \epsilon_{lim} \end{cases}$$

- Range dependent noises (2 nonlinearities)

$$\eta_s = x_{16} + x_{15}\sqrt{x^2+y^2} + x_{14}/\sqrt{x^2+y^2}$$

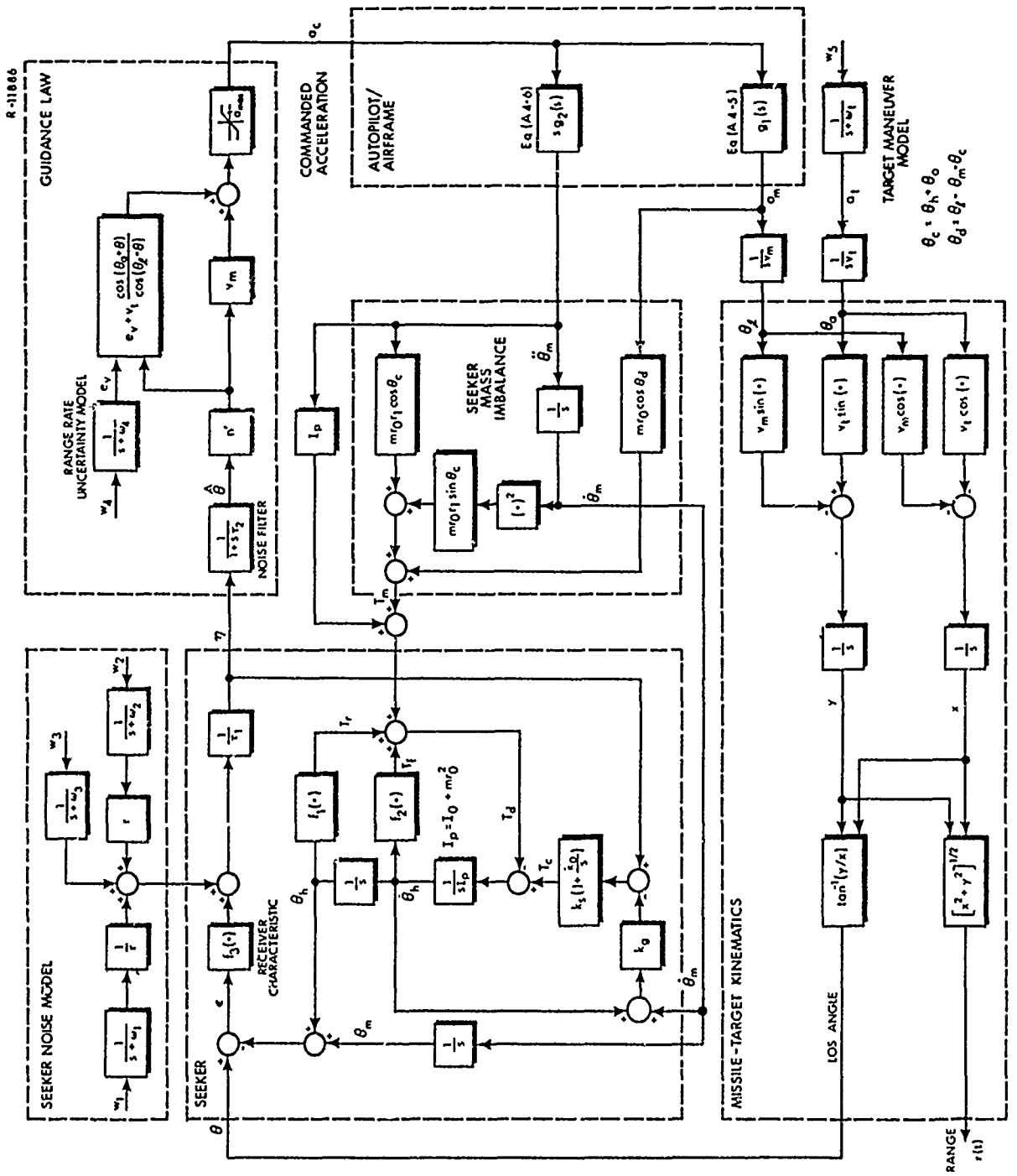

Figure A.8-1 Overall Missile-Target Intercept Model

- Seeker mass imbalance torque (3 nonlinearities)

$$T_m = mr_0 [r_1 \ddot{\theta}_m \cos(\theta_h + \theta_0) + r_1 (\dot{\theta}_m)^2 \sin(\theta_h + \theta_0)$$

$$+ v_m \dot{\theta}_\ell \cos(\theta_\ell - \theta_m - \theta_h - \theta_0)]$$

- LOS angle calculation

$$\theta = \tan^{-1}(y/x)$$

- Range calculation

$$r = \sqrt{x^2 + y^2}$$

- Velocity resolution (4 nonlinearities)

$$\dot{x} = -v_m \cos(\theta_\ell) - v_t \cos(\theta_a)$$

$$\dot{y} = -v_m \sin(\theta_\ell) + v_t \sin(\theta_a)$$

- Acceleration command limiting

$$a_c = \begin{cases} a_c' , & |a_c'| \le a_{max} \\ a_{max} \text{ sign } (a_c'), & |a_c'| > a_{max} \end{cases}$$

- Proportional guidance law with secant compensation

$$a_c' = n' x_7 \left[v_m + v_t \frac{\cos(\theta_a + \theta)}{\cos(\theta_\ell - \theta)} + x_{12} \right]$$

In addition, the state variables are defined as indicated in Table A. 8-1.

TABLE A.8-1

SYSTEM STATE VARIABLES

State Variable	Physical Notation	Description
x_1	θ_h	Seeker head angle with respect to missile centerline
x_2	$\dot{\theta}_h$	Seeker head angular rate
x_3	θ_m	Missile body angle with respect to original LOS
x_4	$\dot{\theta}_m$	Missile body angular rate
x_5	α	Angle of attack (incremental)
x_6	δ	Missile control fin deflection
x_7	$\hat{\dot{\theta}}$	Estimated LOS angular rate (output of guidance law filter
x_8	θ_ℓ	Missile lead angle (angle of missile velocity vector with respect to original LOS)
x_9	θ_a	Target aspect angle (angle of target velocity vector with respect to original LOS)
x_{10}	y	Cross-range separation (component of range normal to original LOS)
x_{11}	x	Down-range separation (component of range along original LOS)
x_{12}	e_v	Closing velocity error state
x_{13}	a_t	Target lateral acceleration
x_{14} to x_{16}	None	Seeker noise states
x_{17}	None	Seeker compensation state

APPENDIX B

RANDOM INPUT DESCRIBING FUNCTIONS FOR THE MISSILE-TARGET INTERCEPT PROBLEM

B.1 RANDOM INPUT DESCRIBING FUNCTIONS USED IN THE CADET ANALYSIS

The random input describing functions (ridf's) derived in this section are based on the assumption that all system variables are jointly normal. To summarize the quasi-linearization procedure, treated more fully in Section 2.2 and Appendix C, we consider a general function of two variables*, $\varphi(v_1, v_2)$, which is to be represented approximately by

$$\varphi(v_1, v_2) \cong E[\varphi] + n_{r_1}(v_1 - m_1) + n_{r_2}(v_2 - m_2) \qquad \text{(B.1-1)}$$

Thus is it necessary to evaluate

$$E[\varphi] = \frac{1}{2\pi\sqrt{p_{11}p_{22} - p_{12}^2}} \int_{-\infty}^{\infty}\int_{-\infty}^{\infty} \omega(v_1, v_2) \exp\left[-\frac{1}{2(1-\rho^2)}\left\{\left(\frac{v_1-m_1}{\sigma_1}\right)^2 - 2\rho\left(\frac{v_1-m_1}{\sigma_1}\right)\left(\frac{v_2-m_2}{\sigma_2}\right) + \left(\frac{v_2-m_2}{\sigma_2}\right)^2\right\}\right] dv_1 dv_2$$

$$= n_{m_1} m_1 + n_{m_2} m_2$$

$$n_{r_1} = \frac{\partial E[\varphi]}{\partial m_1} \qquad \text{(B.1-2)}$$

$$n_{r_2} = \frac{\partial E[\varphi]}{\partial m_2}$$

The nonlinearities considered are generally ordered according to Appendix A.

---

*In this appendix, variables are generally designated v, or v_1, v_2 etc. as required, to avoid the need to refer to the system model. The statistics are $m = E[v]$, $p = E[(v-m)^2]$, $\sigma = \sqrt{p}$ for one variable; $m_i = E[v_i]$, $p_{ij} = E[(v_i - m_i)(v_j - m_j)]$, $\sigma_i = \sqrt{p_{ii}}$ for two or more variables. With two variables, the correlation coefficient is useful; $\rho = p_{12}/\sqrt{p_{11}p_{22}}$.

Missile-Target Kinematics — The nonlinearities used to project the missile and target velocity vectors into down- and cross-range components are of the form sin (v) and cos (v), where v is a gaussian random variable. The ridf's required for these functions have been derived previously to be (Refs. 3, 8)

$$\sin(v) \rightarrow \begin{cases} n_m = \frac{1}{m} \sin(m)\, e^{-\frac{1}{2}p} \\ n_r = \cos(m)\, e^{-\frac{1}{2}p} \end{cases} \qquad \text{(B.1-3)}$$

$$\cos(v) \rightarrow \begin{cases} n_m = \frac{1}{m} \cos(m)\, e^{-\frac{1}{2}p} \\ n_r = -\sin(m)\, e^{-\frac{1}{2}p} \end{cases}$$

Guidance Law — Referring to Eq. (A.5-4), the unconstrained acceleration command is a highly nonlinear function of six system variables of the form

$$\varphi' = a_1\varphi_1 + a_2\varphi_2 + a_3 v_1 \qquad \text{(B.1-4)}$$

One component of φ' is a product of states,

$$\varphi_1(v_i) = v_1 v_6 \qquad \text{(B.1-5)}$$

and a second constituent is given by

$$\varphi_2(v_i) = v_1 \frac{\cos(v_2 + \theta)}{\cos(v_3 - \theta)} \qquad \text{(B.1-6)}$$

when θ is given by

$$\theta = \tan^{-1}\left(\frac{v_4}{v_5}\right) \tag{B.1-7}$$

Substituting Eq. (B.1-7) into Eq. (B.1-6) yields

$$\varphi_2(v_i) = v_1 \frac{v_5 \cos(v_2) - v_4 \sin(v_2)}{v_5 \cos(v_3) + v_4 \sin(v_3)} \tag{B.1-8}$$

For the product of variables, φ_1, we have the following results (Ref. 3):

$$\begin{aligned} E\left[\varphi_1(v_1, v_6)\right] &= n_{m_1} m_1 + n_{m_6} m_6 \\ &= m_1 m_6 + p_{16} \end{aligned} \tag{B.1-9}$$

$$n_{r_1}^{(1)} = m_6$$

$$n_{r_6}^{(1)} = m_1$$

We point out that in treating nonlinear functions of more than one variable, it is generally impossible to identify the individual elements of the describing function for the mean part, e.g., in this case we do not obtain n_{m_1} and n_{m_2} explicitly; however, the quantity $E[\varphi_1]$ is all that is required for propagation of the mean via CADET (refer to Eq. (C.2-5)). It should also be observed that the representation in Eq. (B.1-7) is not useful if both of the means, m_1 and m_6, and the covariance are zero -- i.e., the describing function approximation to the nonlinearity is zero for this case. Since this point is considered in detail in Ref. 3, we do not treat the subject here.

The second term, $\varphi_2(v_i)$ in Eq. (B.1-4), is impossible to quasi-linearize exactly in closed form under the gaussian assumption; thus we use a generalization of the series approach discussed in Section 5.2 (Ref. 9).

$$E\left[\varphi_2(v_i)\right] = \sum_{i=1}^{5} n_{m_i} m_i$$

$$\cong \varphi_2(m_1, m_2, \ldots, m_5) + \frac{1}{2}\sum_{i=1}^{5}\sum_{j=1}^{5} \frac{\partial^2 \varphi_2}{\partial m_i \partial m_j} p_{ij} \qquad \text{(B.1-10)}$$

$$n^{(2)}_{r_i} \cong \frac{\partial \varphi_2(m_1, m_2, \ldots, m_5)}{\partial m_i}, \qquad i = 1, 2, \ldots, 5 \qquad \text{(B.1-10)}$$

Listing the partial derivatives called for in Eq. (B.1-10) requires the introduction of some auxiliary notation:

$$\begin{aligned} \psi_1 &= m_5 \cos m_2 - m_4 \sin m_2 \\ \psi_2 &= m_5 \cos m_3 + m_4 \sin m_3 \\ \psi_3 &= -m_5 \sin m_2 - m_4 \cos m_2 \\ \psi_4 &= -m_5 \sin m_3 + m_4 \cos m_3 \end{aligned} \qquad \text{(B.1-11)}$$

In terms of these expressions, the quantities required to evaluate Eq. (B.1-10) can be shown to be

$$\varphi_2(m_1, m_2, \ldots, m_5) = m_1 \frac{\psi_1}{\psi_2}$$

$$\frac{\partial \varphi_2}{\partial m_1} = \frac{\psi_1}{\psi_2} \cong n^{(2)}_{r_1} \qquad \text{(B.1-12)}$$

$$\frac{\partial \varphi_2}{\partial m_2} = \frac{\psi_3}{\psi_2} m_1 \cong n_{r_2}^{(2)}$$

$$\frac{\partial \omega_2}{\partial m_3} = -\frac{\psi_1 \psi_4}{\psi_2^2} m_1 \cong n_{r_3}^{(2)}$$

$$\frac{\partial \varphi_2}{\partial m_4} = -\frac{m_1 m_5}{\psi_2^2} \sin (m_2 + m_3) \cong n_{r_4}^{(2)}$$

$$\frac{\partial \varphi_2}{\partial m_5} = \frac{m_1 m_4}{\psi_2^2} \sin (m_2 + m_3) \cong n_{r_5}^{(2)}$$

(B. 1-12)(cont.)

$$\frac{\partial^2 \varphi_2}{\partial m_1^2} = 0$$

$$\frac{\partial^2 \varphi_2}{\partial m_1 \partial m_2} = \frac{\psi_3}{\psi_2}$$

$$\frac{\partial^2 \varphi_2}{\partial m_1 \partial m_3} = -\frac{\psi_1 \psi_4}{\psi_2^2}$$

$$\frac{\partial^2 \varphi_2}{\partial m_1 \partial m_4} = -\frac{m_5}{\psi_2^2} \sin (m_2 + m_3)$$

$$\frac{\partial^2 \varphi_2}{\partial m_1 \partial m_5} = \frac{m_4}{\psi_2^2} \sin (m_2 + m_3)$$

$$\frac{\partial^2 \varphi_2}{\partial m_2^2} = -\frac{\psi_1}{\psi_2} m_1$$

$$\frac{\partial^2 \varphi_2}{\partial m_2 \partial m_3} = -\frac{\psi_3 \psi_4}{\psi_2^2} m_1$$

$$\frac{\partial^2 \varphi_2}{\partial m_2 \partial m_4} = -\frac{m_1 m_5}{\psi_2^2} \cos (m_2 + m_3)$$

$$\frac{\partial^2 \varphi_2}{\partial m_2 \partial m_5} = \frac{m_1 m_4}{\psi_2^2} \cos (m_2 + m_3)$$

$$\frac{\partial^2 \varphi_2}{\partial m_3^2} = \frac{\psi_1 m_1}{\psi_2^3} \left(\psi_2^2 + 2\psi_4^2 \right) \qquad \text{(B. 1-12)(cont.)}$$

$$\frac{\partial^2 \varphi_2}{\partial m_3 \partial m_4} = \frac{m_1 m_5}{\psi_2^3} \left(\psi_4 \sin (m_2 + m_3) - \psi_1 \right)$$

$$\frac{\partial^2 \varphi_2}{\partial m_3 \partial m_5} = -\frac{m_1 m_4}{\psi_2^3} \left(\psi_4 \sin (m_2 + m_3) - \psi_1 \right)$$

$$\frac{\partial^2 \varphi_2}{\partial m_4^2} = 2 \frac{m_1 m_5}{\psi_2^3} \sin (m_3) \sin (m_2 + m_3)$$

$$\frac{\partial^2 \varphi_2}{\partial m_4 \partial m_5} = -\frac{m_1}{\psi_2^3} \left(\psi_2 - 2m_5 \cos (m_3) \right) \sin (m_2 + m_3)$$

$$\frac{\partial^2 \varphi_2}{\partial m_5^2} = -\frac{2m_1 m_4}{\psi_2^3} \cos(m_3) \sin(m_2 + m_3) \qquad \text{(B.1-12)(cont.)}$$

Returning to Eq. (B.1-4), we have

$$E[\varphi'] \triangleq m'_\varphi = a_1 E[\varphi_1] + a_2 E[\varphi_2] + a_3 m_1 \qquad \text{(B.1-13)}$$

where $E[\varphi_1]$ and $E[\varphi_2]$ are given in Eqs. (B.1-9) and (B.1-10); the random component of φ can be expressed in terms of the quasi-linear gains in the same equations to be

$$r'_\varphi = \begin{bmatrix} r_1 & r_2 \ldots r_6 \end{bmatrix} \begin{bmatrix} a_1 n_{r_1}^{(1)} + a_2 n_{r_1}^{(2)} + a_3 \\ a_2 n_{r_2}^{(2)} \\ a_2 n_{r_3}^{(2)} \\ a_2 n_{r_4}^{(2)} \\ a_2 n_{r_5}^{(2)} \\ a_1 n_{r_6}^{(1)} + 0 + 0 \end{bmatrix}$$

$$\triangleq \underline{r}^T \underline{b}_\varphi \qquad \text{(B.1-14)}$$

Since r'_φ is a quasi-linear combination of the random components of the six variables v_i, the variance is approximately

$$p'_\varphi = E\left[r_\varphi^2\right] \cong E\left[\underline{b}_\varphi^T \underline{r}\,\underline{r}^T \underline{b}_\varphi\right] = \underline{b}_\varphi^T \begin{bmatrix} p_{11} & p_{12} & \cdot & \cdot & \cdot & p_{16} \\ p_{12} & p_{22} & \cdot & \cdot & \cdot & p_{26} \\ \cdot & \cdot & & & & \cdot \\ \cdot & \cdot & & & & \cdot \\ \cdot & \cdot & & & & \cdot \\ p_{16} & p_{26} & \cdot & \cdot & \cdot & p_{66} \end{bmatrix} \underline{b}_\varphi \qquad \text{(B.1-15)}$$

Thus we can obtain the approximate mean and variance of the unconstrained acceleration command in terms of the quasi-linear gains summarized above. With these statistics, we treat the acceleration command limiter in the regular manner; i.e., we assume its input φ' is a gaussian random variable with statistics m'_φ and p'_φ. The ridf's for the limiter are given by (Refs. 2 and 8)

$$E[\varphi] = n_{m_\varphi} m_\varphi = \sqrt{p'_\varphi}\left(G\left(\frac{\varphi_{lim}+m'_\varphi}{\sqrt{p'_\varphi}}\right) - G\left(\frac{\varphi_{lim}-m'_\varphi}{\sqrt{p'_\varphi}}\right)\right) - m'_\varphi$$

$$n_{r_\varphi} = PI\left(\frac{\varphi_{lim}+m'_\varphi}{\sqrt{p'_\varphi}}\right) + PI\left(\frac{\varphi_{lim}-m'_\varphi}{\sqrt{p'_\varphi}}\right) - 1 \qquad \text{(B.1-16)}$$

where the auxiliary functions G and PI are defined in terms of the normal density function, PF, as follows:

$$PF(\psi) = \frac{1}{\sqrt{2\pi}} \exp\left(-\frac{\psi^2}{2}\right)$$

$$PI(\psi) = \int_{-\infty}^{\psi} PF(\zeta)\, d\zeta \qquad \text{(B.1-17)}$$

$$G(\psi) = \psi\, PI(\psi) + PF(\psi)$$

The describing functions outlined above complete the quasi-linear representation of the guidance law; in summary, $E[\varphi]$ is used directly in propagating the mean vector of the system, and the random component of the actual acceleration command is

$$r_\varphi = n_{r_\varphi} r'_\varphi = n_{r_\varphi} \underline{b}_\varphi^T \underline{r} \qquad \text{(B.1-18)}$$

and $n_{r_\varphi} \underline{b}_\varphi$ is the overall describing function matrix (in this case, a row vector) specified in Eqs. (B.1-9), (B.1-10) and (B.1-14).

The approach outlined above in Eqs. (B.1-4) to (B.1-17) considers a nonlinearity of the form

$$\varphi = \varphi\left(\varphi'(v_1, v_2, \ldots, v_6)\right)$$

i.e., a nonlinear function of a nonlinearity. Because it is essentially impossible to quasi-linearize this relation as a whole, we have first quasi-linearized φ' to obtain the statistics m'_φ and p'_φ necessary to calculate the ridf for $\varphi(\varphi')$, Eq. (B.1-16), then "cascaded the ridfs" for the random part in arriving at Eq. (B.1-18). While this is not a completely rigorous procedure, we rely on our a priori knowledge that in the guidance law, φ' is approximately v_1 times the closing velocity which, while not a constant, is nearly so (i.e., the closing velocity has a mean that is much larger than its random part until the last few hundredths of a second of an engagement in realistic situations), and v_1 is generally nearly gaussian. Thus it is reasonable to assume that φ' is nearly gaussian. In this situation, the above technique adequately represents the guidance law nonlinear effects, as shown in Chapter 4.

Range Dependent Noise Sources – Since the range, $r = \sqrt{x^2 + y^2}$, enters into the seeker noise model, we find that the ridf's cannot be

calculated under the gaussian assumption, due to the inability to evaluate certain integrals in closed form (cf. Section 5.2). The first nonlinearity we treat is the range proportional seeker noise term,

$$\varphi_3 = v_1 \sqrt{m_x^2 + y^2} \triangleq v_1 \sqrt{m_x^2 + v_2^2} \qquad \text{(B.1-19)}$$

where we assume that x has no random component, as before (Section 5.2). The expected value of φ_3, given by

$$E[\varphi_3] = \frac{1}{2\pi\sigma_1\sigma_2\sqrt{1-\rho^2}} \int_{-\infty}^{\infty}\int_{-\infty}^{\infty} v_1 \sqrt{m_x^2 + v_2^2}\, \exp\left[-\frac{1}{2(1-\rho^2)}\left\{\left(\frac{v_1-m_1}{\sigma_1}\right)^2 - 2\rho\left(\frac{v_1-m_1}{\sigma_1}\right)\left(\frac{v_2-m_2}{\sigma_2}\right) + \left(\frac{v_2-m_2}{\sigma_2}\right)^2\right\}\right] dv_1 dv_2 \qquad \text{(B.1-20)}$$

can be integrated with respect to v_1 to yield

$$e[\varphi_3] = \frac{1}{\sqrt{2\pi}} \int_{-\infty}^{\infty} (m_1 + \rho\sigma_1 u) \sqrt{(\sigma_2 u + m_2)^2 + m_x^2}\; e^{-\frac{1}{2}u^2}\, du \qquad \text{(B.1-21)}$$

with the substitution $u = (v_2 - m_2)/\sigma_2$. To determine the ridf's for the random components, we take the indicated partial derivatives with respect to m_i; these are simplified significantly by the further assumption that the cross-range separation, $y = v_2$, has a zero mean:

$$E[\varphi_3]_{m_2=0} = \frac{m_1}{\sqrt{2\pi}} \int_{-\infty}^{\infty} \sqrt{(\sigma_2 u)^2 + m_x^2}\; e^{-\frac{u^2}{2}}\, du$$

$$n_{r_1} = \left(\frac{\partial E[\varphi_3]}{\partial m_1}\right)_{m_2=0} = \frac{1}{\sqrt{2\pi}} \int_{-\infty}^{\infty} \sqrt{(\sigma_2 u)^2 + m_x^2}\; e^{-\frac{u^2}{2}}\, du \qquad \text{(B.1-22)}$$

$$n_{r_2} = \left(\frac{\partial E[\varphi_3]}{\partial m_2}\right)_{m_2=0} = \frac{\rho\sigma_1\sigma_2}{\sqrt{2\pi}} \int_{-\infty}^{\infty} \frac{u^2 e^{-\frac{u^2}{2}}}{\sqrt{(\sigma_2 u)^2 + m_x^2}}\, du$$

where we have eliminated terms of the form

$$\int_{-\infty}^{\infty} u \sqrt{(\sigma_2 u)^2 + m_x^2}\; e^{-\frac{1}{2}u^2}\, du = 0$$

We note that none of the above integrals can be evaluated in closed form. The study of approximate methods presented in Section 5.2 demonstrates that accurate results are obtained by replacing the gaussian pdf's in Eq. (B.1-22) with a triangular density with the same mean and standard deviation,

$$\frac{1}{\sqrt{2\pi}} e^{-\frac{u^2}{2}} \rightarrow \begin{cases} \dfrac{\sqrt{6} - |u|}{6} & , \quad |u| \le \sqrt{6} \\ 0 & , \quad |u| > \sqrt{6} \end{cases} \qquad \text{(B.1-23)}$$

Furthermore, we recognize that n_{r_1} is the expected value of the range, as treated in Section 5.2, so we immediately have (from Eq. (5.2-12))

$$E[\varphi_3] \cong \frac{m_1}{\nu} \operatorname{sign}(m_x) \left[\sqrt{1+\nu^2} + \nu^2 \log\left(\frac{1+\sqrt{1+\nu^2}}{\nu} \right) + \frac{4}{\sqrt{6}} \left(\nu^3 - (1+\nu^2)^{3/2} \right) \right] \qquad \text{(B.1-24)}$$

$$n_{r_1} \cong E[\varphi_3]/m_1$$

where

$$\nu \triangleq \frac{|m_x|}{\sqrt{6}\,\sigma_2} \qquad \text{(B.1-25)}$$

Evaluating the last integral in Eq. (B.1-22) in the same manner, we obtain

$$n_{r_2} \cong \sqrt{\frac{2}{3}}\, p_{12} \left[(1+4\nu^2)\sqrt{1+\nu^2} - 4\nu^3 - 3\nu^2 \log\left(\frac{1+\sqrt{1+\nu^2}}{\nu} \right) \right] \qquad \text{(B.1-26)}$$

The inverse range proportional noise,

$$\varphi_4 = \frac{v_3}{\sqrt{m_x^2 + y^2}} = \frac{v_3}{\sqrt{m_x^2 + v_2^2}}$$

can be treated in the same manner as φ_3 above, yielding

$$E[\varphi_4] \cong \sqrt{\frac{2}{3}} \frac{m_3}{\sigma_2} \left[\log\left(\frac{1+\sqrt{1+\nu^2}}{\nu} \right) + \nu - \sqrt{1+\nu^2} \right]$$

$$n_{r_3} \cong E[\varphi_4]/m_3 \qquad \text{(B.1-27)}$$

$$n_{r_2} \cong -\sqrt{\frac{2}{3}} \frac{p_{23}}{\sigma_2^3} \left[\log\left(\frac{1+\sqrt{1+\nu^2}}{\nu} \right) + 2\left(\nu - \sqrt{1+\nu^2} \right) \right]$$

Receiver/Signal Processing Characteristic — The boresight error limiter has the same form as the acceleration command limiter; consequently the evaluation of quasi-linear gains is accomplished with Eq. (B.1-16) substituting the boresight error statistics, m_ϵ and p_ϵ for m'_φ and p'_φ. The boresight error is a linear combination of the LOS angle, missile body angle and seeker angle, and the LOS angle is related to the system variables x and y by the inverse tangent relation, Eq. (A.2-1). Thus to determine m_ϵ and p_ϵ, consider

$$\epsilon = \tan^{-1}\left(\frac{v_1}{v_2}\right) - v_3 - v_4$$

$$\triangleq \omega_5(v_1, v_2) - v_3 - v_4 \qquad \text{(B.1-28)}$$

The nonlinearity φ_5 is quasi-linearized below so that the mean and random components of the boresight error are

$$\begin{aligned} m_\epsilon &= E[\varphi_5] - m_3 - m_4 \\ r_\epsilon &= n_{r_1}^{(5)} r_1 + n_{r_2}^{(5)} r_2 - r_3 - r_4 \\ &\triangleq \underline{b}_5 \underline{r} \end{aligned} \tag{B.1-29}$$

The boresight error variance is thus approximately

$$p_\epsilon \cong \underline{b}_5^T \begin{bmatrix} p_{11} & p_{12} & \cdot\cdot & p_{14} \\ p_{12} & p_{22} & \cdot\cdot & p_{24} \\ \cdot & \cdot & & \cdot \\ \cdot & \cdot & & \cdot \\ p_{14} & p_{24} & \cdot\cdot & p_{44} \end{bmatrix} \underline{b}_5 \tag{B.1-30}$$

Using m_ϵ and p_ϵ from Eqs. (B.1-27) and (B.1-28), the boresight error limiter ridf's can be evaluated directly, from Eq. (B.1-16).

Inverse Tangent LOS Angle Calculation — The nonlinearity $\varphi_5 = \tan^{-1}(v_1/v_2)$ cannot be quasi-linearized in closed form under the gaussian assumption; thus we again make use of the series expansion approach given in Eq. (B.1-10). The required partial derivatives are

$$\begin{aligned} \frac{\partial \varphi_5}{\partial m_1} &= \frac{m_2}{m_1^2 + m_2^2} \cong n_{r_1}^{(5)} \\ \frac{\partial \varphi_5}{\partial m_2} &= \frac{-m_1}{m_1^2 + m_2^2} \cong n_{r_2}^{(5)} \end{aligned} \tag{B.1-31}$$

$$\frac{\partial^2 \varphi_5}{\partial m_1^2} = \frac{-2m_1 m_2}{\left(m_1^2 + m_2^2\right)^2}$$

$$\frac{\partial^2 \varphi_5}{\partial m_1 \partial m_2} = \frac{m_1^2 - m_2^2}{\left(m_1^2 + m_2^2\right)^2} \qquad \text{(B.1-31) (cont.)}$$

$$\frac{\partial^2 \varphi_5}{\partial m_2^2} = \frac{2m_1 m_2}{\left(m_1^2 + m_2^2\right)^2}$$

The expected value of φ_5 is obtained approximately by substituting Eq. (B.1-31) into the series expansion,

$$E[\varphi_5] \cong \tan^{-1}\left(\frac{m_1}{m_2}\right) + \frac{1}{\left(m_1^2 + m_2^2\right)^2}\left[m_1 m_2 \left(p_{22} - p_{11}\right) + \left(m_1^2 - m_2^2\right) p_{12}\right] \qquad \text{(B.1-32)}$$

The quantities $E[\varphi_5]$, $n_{r1}^{(5)}$ and $n_{r2}^{(5)}$ constitute the quasi-linear approximation to the inverse tangent function.

Seeker Head Restoring Torque — The nonlinear representation of the "hard spring" effect studied in Section 4.4 is of the form

$$\varphi_6 = |v|^k \operatorname{sign}(v) \qquad \text{(B.1-33)}$$

where k is an integer. The ridf is directly available (Ref. 8), in general form for k odd, and also for k = 2, as follows:

$$\underline{k = 1} \qquad n_r = 1, \quad n_m = 1 \qquad \text{(B.1-34)}$$

$$\underline{k = 2} \qquad n_r = 4\sigma\, PF\left(\frac{m}{\sigma}\right) + 2m\left(2PI\left(\frac{m}{\sigma}\right) - 1\right)$$

$$n_m = 2\sigma\, PF\left(\frac{m}{\sigma}\right) + m\left(1+\left(\frac{\sigma}{m}\right)^2\right)\left(2PI\left(\frac{m}{\sigma}\right) - 1\right)$$

$$\underline{k = 3} \qquad n_r = 3\sigma^2 + 3m^2$$

$$n_m = 3\sigma^2 + m^2 \qquad \text{(B.1-34) (cont.)}$$

$$\underline{k = 5} \qquad n_r = 15\sigma^4 + 30\sigma^2 m^2 + 5m^4$$

$$n_m = 15\sigma^4 + 10\sigma^2 m^2 + m^4$$

The general form for k odd, say $k = 2g+1$, is

$$n_r = \sum_{j=0}^{g} \frac{(2g+1)!\ (1)(3)(5)\cdots(2g-2j+1)}{(2j)!\ (2g-2j+1)!}\ p^{g-j}\ m^{2j}$$

$$n_m = m^{2g} + \sum_{j=0}^{g-1} \frac{(2g+1)!\,(1)(3)(5)\cdots(2g-2j-1)}{(2j+1)!\ (2g-2j)!}\ p^{g-j}\ m^{2j} \qquad \text{(B.1-35)}$$

we note above that for k odd, the nonlinearity in Eq. (B.1-33) is simply $\varphi_6 = v^{2g+1}$ which leads to quite straightforward polynomial ridf's, while for k even the factor sign (v) leads to terms involving the probability function, PF, and probability integral, PI, given in Eq. (B.1-17).

Seeker Gimbal Dry Friction -- The dry or coulomb friction effect is modeled by a nonlinearity of the form

$$\varphi_7(v) = \text{sign}\,(v) \qquad \text{(B.1-36)}$$

which is often used to represent the ideal relay. The ridf's for this effect are available in Ref. 8,

$$n_r = \frac{2}{\sigma} PF\left(\frac{m}{\sigma}\right)$$
$$n_m = \frac{1}{m}\left(2 PI\left(\frac{m}{\sigma}\right) - 1\right) \qquad \text{(B.1-37)}$$

Seeker Mass Imbalance — The effective disturbance torque due to an offset of the seeker center of gravity from the gimbal has three terms, with two distinct forms:

$$\varphi_8 = v_1 \cos(v_2)$$
$$\varphi_9 = v_1^2 \sin(v_2) \qquad \text{(B.1-38)}$$

In the nonlinearities φ_8 and φ_9, the variables v_1 and v_2 are generally not state variables, but linear combinations thereof, viz.,

$$\underline{v} = \begin{bmatrix} v_1 \\ v_2 \end{bmatrix} = \begin{bmatrix} \underline{h}_1^T \underline{x} \\ \underline{h}_2^T \underline{x} \end{bmatrix} \pm \begin{bmatrix} 0 \\ \theta_0 \end{bmatrix} \qquad \text{(B.1-39)}$$

where we have indicated that the angle v_2 generally contains a constant parameter, θ_0, which is the angular coordinate of the seeker center of gravity with respect to the antenna centerline (Fig. A.6-1). Then the statistics of v_1 and v_2 can be obtained from the state variable statistics, $\underline{m} = E[\underline{x}]$ and $P = E[(\underline{x}-\underline{m})(\underline{x}-\underline{m})^T]$, as

$$\underline{m}_v = \begin{bmatrix} m_1 \\ m_2 \end{bmatrix} = H\,\underline{m} \pm \begin{bmatrix} 0 \\ \theta_0 \end{bmatrix} \qquad \text{(B.1-40)}$$

where

$$H \triangleq \begin{bmatrix} \underline{h}_1^T \\ \hline \underline{h}_2^T \end{bmatrix} \tag{B.1-41}$$

and

$$P_v = \begin{bmatrix} p_{11} & p_{12} \\ p_{12} & p_{22} \end{bmatrix} = H P H^T \tag{B.1-42}$$

The first nonlinearity (and its companion form, $\varphi_{10} = v_1 \sin v_2$) have been treated in Ref. 3 by considering the real and imaginary part of the function $v_1 \exp(jv_2)$, as follows: define

$$\varphi_8^* \triangleq v_1 e^{jv_2}$$

$$= v_1 (\cos v_2 + j \sin v_2) \triangleq \varphi_8 + j\varphi_{10} \tag{B.1-43}$$

The expected value of this complex function can be evaluated to be (Ref. 11)

$$E\left[\varphi_8^*\right] = e^{-\frac{p_{22}}{2}} (m_1 + j p_{12}) (\cos m_2 + j \sin m_2) \tag{B.1-44}$$

From this expression, the required ridis are available by inspection:

$$E[\varphi_8] = \mathrm{Re}\left(E\left[\varphi_8^*\right]\right) = e^{-\frac{p_{22}}{2}} (m_1 \cos m_2 - p_{12} \sin m_2) \tag{B.1-45}$$

$$n_{r_1} = e^{-\frac{p_{22}}{2}} \cos m_2$$

$$n_{r_2} = -e^{-\frac{p_{22}}{2}} (m_1 \sin m_2 + p_{12} \cos m_2) \qquad \text{(B.1-45)(cont.)}$$

$$E[\varphi_{10}] = \text{Im}\left(E\left[\varphi_8^*\right]\right) = e^{-\frac{p_{22}}{2}} (m_1 \sin m_2 + p_{12} \cos m_2)$$

$$n_{r_1} = e^{-\frac{p_{22}}{2}} \sin m_2 \qquad \text{(B.1-46)}$$

$$n_{r_2} = e^{-\frac{p_{22}}{2}} (m_1 \cos m_2 - p_{12} \sin m_2)$$

The same approach is utilized in evaluating ridf's for φ_9; defining its companion form to be $\varphi_{11} = v_1^2 \cos v_2$ yields

$$\varphi_9^* = v_1^2 e^{jv_2} = v_1^2 (\cos v_2 + j \sin v_2)$$

$$\triangleq \varphi_{11} + j\varphi_9 \qquad \text{(B.1-47)}$$

yields

$$E\left[\varphi_9^*\right]\Big) = e^{-\frac{p_{22}}{2}} \left[\left(m_1^2 + p_{11} - p_{12}\right) + 2j m_1 p_{12}\right] (\cos m_2 + j \sin m_2) \qquad \text{(B.1-48)}$$

Thus the quasi-linear representation of φ_9 and φ_{11} require

$$E[\varphi_{11}] = \mathrm{Re}\left(E\left[\varphi_9^*\right]\right) = e^{-\frac{p_{22}}{2}}\left[\left(m_1^2 + p_{11} - p_{12}\right)\cos m_2 - 2m_1 p_{12} \sin m_2\right]$$

$$n_{r_1} = e^{-\frac{p_{22}}{2}}\left(2m_1 \cos m_2 - 2p_{12} \sin m_2\right) \qquad \text{(B.1-49)}$$

$$n_{r_2} = -e^{-\frac{p_{22}}{2}}\left[\left(m_1^2 + p_{11} - p_{12}\right)\sin m_2 + 2m_1 p_{12} \cos m_2\right]$$

$$E[\varphi_9] = \mathrm{Im}\left(E\left[\varphi_9^*\right]\right) = e^{-\frac{p_{22}}{2}}\left[2m_1 p_{12} \cos m_2 + \left(m_1^2 + p_{11} - p_{12}\right)\sin m_2\right]$$

$$n_{r_1} = e^{-\frac{p_{22}}{2}}\left[2p_{12} \cos m_2 + 2m_1 \sin m_2\right] \qquad \text{(B.1-50)}$$

$$n_{r_2} = e^{-\frac{p_{22}}{2}}\left[-2m_1 p_{12} \sin m_2 + \left(m_1^2 + p_{11} - p_{12}\right)\cos m_2\right]$$

This completes the exposition of the ridf's necessary for the statistical analysis of the missile-target intercept model treated in the present study.

B.2 RANDOM INPUT DESCRIBING FUNCTIONS USED IN SENSITIVITY ANALYSIS

In Section 5.2 we consider three nonlinearities, the limiter, power law nonlinearity, and sinusoidal operator, and portray the variation caused in ridf calculation by varying the probability density function (pdf) of the input. Seven quite different pdfs were studied, denoted $p_i(x)$, $i=1,2,\ldots,7$, as given in Eq. (5.1-4); each pdf leads to a describing function given by

$$n_{r_i} = \frac{1}{\sigma^2} \int_{-\infty}^{\infty} x\, f(x)\, p_i(x)\, dx \qquad \text{(B.2-1)}$$

where x is a zero-mean random variable with standard deviation σ.

Limiter — For this nonlinearity, all ridfs are a function of the ratio of the input standard deviation to the break point (Fig. 5.1-2), here denoted by

$$\mu = \sigma/\delta$$

In terms of this parameter, we have

$$n_{r_1} = 1 - \left(1 + \frac{1}{\sqrt{2}\mu}\right) e^{-\frac{\sqrt{2}}{\mu}} \qquad \text{(exponential)}$$

$$n_{r_2} = 2\,\mathrm{PI}\left(\frac{1}{\mu}\right) - 1 \qquad \text{(gaussian)}$$

$$n_{r_3} = \begin{cases} 1, & \mu \le \dfrac{1}{\sqrt{6}} \\ 1 - \dfrac{(\sqrt{6}\,\mu+1)}{36\,\mu^4}\,(\sqrt{6}\,\mu-1), & \dfrac{1}{\sqrt{6}} < \mu < \infty \end{cases} \qquad \text{(triangular)}$$

$$n_{r_4} = \begin{cases} 1, & \mu \le \dfrac{\sqrt{5}}{3\sqrt{3}} \\ \dfrac{5}{144\mu^4} - \dfrac{\sqrt{5}}{8\sqrt{3}\,\mu^3} + \dfrac{9\sqrt{3}}{8\sqrt{5}\,\mu} - \dfrac{1}{80}, & \dfrac{\sqrt{5}}{3\sqrt{3}} < \mu \le \dfrac{\sqrt{5}}{\sqrt{3}} \\ \dfrac{13\sqrt{3}}{12\sqrt{5}\,\mu} - \dfrac{\sqrt{5}}{12\sqrt{3}\,\mu^3}, & \dfrac{\sqrt{5}}{\sqrt{3}} < \mu < \infty \end{cases} \qquad (p_4)$$

$$n_{r_5} = \begin{cases} 1, & \mu \le \dfrac{1}{\sqrt{3}} \\ \dfrac{9\mu^2 - 1}{6\sqrt{3}\,\mu^3}, & \dfrac{1}{\sqrt{3}} < \mu < \infty \end{cases} \qquad \text{(uniform)}$$

$$n_{r_6} = \begin{cases} 1, & \mu \le \dfrac{\sqrt{7}}{2\sqrt{6}} \\ \dfrac{7}{72\mu^4} - \dfrac{\sqrt{42}}{18\mu^3} + \dfrac{4\sqrt{2}}{\sqrt{21}\,\mu} - \dfrac{1}{7}, & \dfrac{\sqrt{7}}{2\sqrt{6}} < \mu \le \dfrac{\sqrt{7}}{\sqrt{6}} \\ \dfrac{\sqrt{6}}{\sqrt{7}\,\mu} - \dfrac{7}{72\mu^4}, & \dfrac{\sqrt{7}}{\sqrt{6}} < \mu < \infty \end{cases} \qquad (p_6)$$

$$n_{r_7} = \begin{cases} 1, & \mu \le \dfrac{5}{3\sqrt{6}} \\ \dfrac{25}{72\mu^4} - \dfrac{5}{2\sqrt{6}\,\mu^3} + \dfrac{9\sqrt{6}}{10\mu} - \dfrac{31}{50}, & \dfrac{5}{3\sqrt{6}} < \mu \le \dfrac{5}{2\sqrt{6}} \\ -\dfrac{25}{72\mu^4} + \dfrac{5}{6\sqrt{6}\,\mu^3} + \dfrac{11}{5\sqrt{6}\,\mu} + \dfrac{1}{50}, & \dfrac{5}{2\sqrt{6}} < \mu \le \dfrac{5}{\sqrt{6}} \\ \dfrac{2\sqrt{6}}{5\mu}, & \dfrac{5}{\sqrt{6}} < \mu < \infty \end{cases} \qquad (p_7)$$

Random input describing functions are quite complicated when both the pdf and nonlinearity are comprised of several linear segments, as is the case for p_4, p_6 and p_7.

Power Law Nonlinearity — The nonlinearity

$$f(x) = x^2 \text{ sign } (x)$$

leads to particularly convenient ridf's for the pdf's chosen in this study.

$$n_{r_1} = \frac{3}{\sqrt{2}}\sigma = 2.12\,\sigma \qquad \text{(exponential)}$$

$$n_{r_2} = \frac{4}{\sqrt{2\pi}}\sigma = 1.60\,\sigma \qquad \text{(gaussian)}$$

$$n_{r_3} = \frac{3\sqrt{6}}{5}\sigma = 1.47\,\sigma \qquad \text{(triangular)}$$

$$n_{r_4} = \frac{9\sqrt{3}}{5\sqrt{5}}\sigma = 1.39\,\sigma \qquad (p_4)$$

$$n_{r_5} = \frac{3\sqrt{3}}{4}\sigma = 1.30\,\sigma \qquad \text{(uniform)}$$

$$n_{r_6} = \frac{9\sqrt{6}}{7\sqrt{7}}\sigma = 1.19\,\sigma \qquad (p_6)$$

$$n_{r_7} = \frac{54\sqrt{6}}{125}\sigma = 1.06\,\sigma \qquad (p_7)$$

Sinusoidal Operator — For the nonlinearity

$$f(x) = \sin x$$

the following ridf's are obtained:

$$n_{r_1} = \frac{1}{\left(1+\frac{\sigma^2}{2}\right)^2} \qquad \text{(exponential)}$$

$$n_{r_2} = e^{-\frac{\sigma^2}{2}} \qquad \text{(gaussian)}$$

$$n_{r_3} = \frac{1}{3\sigma^4}\left[2(1-\cos x_3) - x_3 \sin x_3\right]; \qquad x_3 = \sqrt{6}\,\sigma \qquad \text{(triangular)}$$

$$n_{r_4} = \frac{5}{12\sigma^4}\left[2(\cos x_4 - \cos(3x_4)) + x_4(\sin x_4 - 3\sin(3x_4))\right]; \qquad x_4 = \sqrt{0.6}\,\sigma \qquad (p_4)$$

$$n_{r_5} = \frac{1}{3\sigma^4}\left[x_5 \sin x_5 - x_5^2 \cos x_5\right]; \qquad x_5 = \sqrt{3}\,\sigma \qquad \text{(uniform)}$$

$$n_{r_6} = \frac{7}{3\sigma^4}\left[x_6(\sin x_6 - \sin(2x_6)) - (1 - 2\cos x_6 + \cos(2x_6))\right]; \qquad x_6 = \sqrt{\frac{6}{7}}\,\sigma \qquad (p_6)$$

$$n_{r_7} = \frac{25}{3\sigma^4}\left[x_7\left(2\sin(2x_7) - \frac{3}{4}\sin x_7 - \frac{3}{4}\sin(3x_7)\right)\right.$$

$$\left. + 2(\cos(2x_7) - \cos x_7 - \cos(3x_7))\right]; \qquad x_7 = \frac{\sqrt{6}}{5}\,\sigma \qquad (p_7)$$

The ridf's for the three nonlinearities considered here are plotted in Figs. 5.1-2 (limiter), 5.1-4 (power law), and 5.1-6 (sinusoidal operator).

APPENDIX C

THE COVARIANCE ANALYSIS DESCRIBING FUNCTION TECHNIQUE (CADET)

The Covariance Analysis DEscribing function Technique (CADET) is a method for the direct determination of the statistical properties of a nonlinear system with random inputs, recently conceived and developed at The Analytic Sciences Corporation (Refs. 1, 2, and 3). The principal advantage of this technique is that it obviates monte carlo simulations, thereby achieving substantial savings in computer processing time. We first motivate the discussion by reviewing the covariance analysis method for linear systems; then we develop an analogous procedure (CADET) for the nonlinear case.

C.1 COVARIANCE ANALYSIS FOR LINEAR SYSTEMS

The dynamics of a linear continuous-time stochastic system can be represented by a first-order vector differential equation in which $\underline{x}(t)$ is the system state vector and $\underline{w}(t)$ is a random forcing function vector,

$$\dot{\underline{x}}(t) = F(t)\,\underline{x}(t) + G(t)\,\underline{w}(t) \qquad \text{(C.1-1)}$$

Figure C.1-1 illustrates the equation. The state vector is composed of any set of variables sufficient to completely describe the behavior of the system. The forcing function vector $\underline{w}(t)$ represents disturbances as well as control inputs that may act upon the system. In what follows the forcing function $\underline{w}(t)$ is assumed to be composed of a mean value $\underline{b}$ and random component $\underline{u}$, the latter being comprised of elements which are uncorrelated in time; that is, $\underline{u}(t)$ is "white" noise

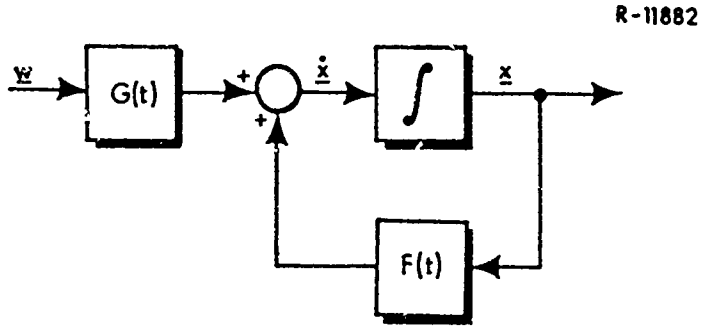

Figure C.1-1 Continuous Representation of the Linear Dynamic System Equations

having the spectral density matrix Q(t); thus $\underline{w}(t)$ is specified by*

$$E[\underline{w}(t)] = \underline{b}(t)$$

$$E[\underline{u}(t)\,\underline{u}^T(\tau)] = Q(t)\,\delta(t-\tau) \qquad \text{(C.1-2)}$$

Similarly, the state vector has a mean component $\underline{m}(t)$, and a random part $\underline{r} = \underline{x} - \underline{m}$; $\underline{x}$, then, may be described statistically by its mean and covariance matrix,

$$\underline{m}(t) \triangleq E[\underline{x}(t)]$$

$$P(t) \triangleq E[\underline{r}(t)\,\underline{r}^T(t)] \qquad \text{(C.1-3)}$$

The equation for the propagation of the mean vector and covariance matrix for the system described by Eq. (C.1-1) can be written as (Ref. 7).

*E denotes ensemble expectation, or average value; T denotes the matrix transpose.

$$\dot{\underline{m}} = F(t)\ \underline{m} + G(t)\ \underline{b}$$

$$\dot{P}(t) = F(t)\ P(t) + P(t)\ F(t)^T + G(t)\,Q\,G^T(t) \qquad \text{(C. 1-4)}$$

The elements of $\underline{m}(t)$ represent the effects of deterministic initial conditions and biases due to the system inputs ($\underline{b} \neq 0$). The diagonal elements of P(t) are the mean square values of the random components of the state variables; the off-diagonal elements represent the degree of correlation between the random components of the various state variables.

Equation (C. 1-4) provides a direct method for analyzing the statistical properties of $\underline{x}(t)$. This is to be contrasted with the monte carlo method, where many sample trajectories of $\underline{x}(t)$ are calculated from computer-generated random noise, or random numbers in the case of a digital computer, using Eq. (C. 1-1). If q such trajectories are generated -- denoted by $\underline{x}_k(t)$, $k = 1, \ldots, q$ -- then $\underline{m}(t)$ and P(t) are given approximately by

$$\underline{m}(t) \cong \hat{\underline{m}}(t) \triangleq \frac{1}{q} \sum_{k=1}^{q} \underline{x}_k(t)$$

$$P(t) \cong \hat{P}(t) \triangleq \frac{1}{q-1} \sum_{k=1}^{q} \hat{\underline{r}}_k(t)\, \hat{\underline{r}}_k^{\,T}(t) \qquad \text{(C. 1-5)}$$

where $\hat{\underline{r}}_k \triangleq \underline{x}_k - \hat{\underline{m}}$. In the limit as q approaches infinity, we are assured that

$$\lim_{q \to \infty} \hat{\underline{m}}(t) = \underline{m}(t)$$

$$\lim_{q \to \infty} \hat{P}(t) = P(t) \qquad \text{(C. 1-6)}$$

Note that Eq. (C. 1-4) provides exact solutions for $\underline{m}(t)$ and P(t), to within computer integration accuracy, whereas the monte carlo method yields approximate solutions for a finite value of q. Furthermore, Eq. (C. 1-4) need be solved only once over the time interval of interest, whereas Eq. (C. 1-1) must be solved repeatedly using the monte carlo technique; consequently the direct analytical method is not only exact, but is also generally the most efficient technique for analyzing linear systems. Our purpose here is to describe a procedure whereby the statistics of a nonlinear system can be computed approximately using a recursion relationship similar in form to Eq. (C. 1-4).

C. 2 COVARIANCE ANALYSIS FOR NONLINEAR SYSTEMS

The nonlinear counterpart of Eq. (C. 1-1) is

$$\dot{\underline{x}}(t) = \underline{f}(\underline{x}(t)) + G\underline{w}(t) \qquad \text{(C. 2-1)}$$

as depicted in Fig. C. 2-1. In order to develop a covariance analysis method similar to that used for linear systems, it is desirable to approximate $\underline{f}(\underline{x})$ in Eq. (C. 2-1) as a linear operation on $\underline{x}(t)$. The success of CADET in achieving its goals -- providing an efficient and accurate means for the direct statistical analysis of system performance -- depends on how well $\underline{f}(\underline{x})$ can be approximated. Thus, consider approximating the nonlinear function $\underline{f}(\underline{x})$ in Fig. C. 2-1 by a linear function, in the sense suggested by Fig. C. 2-2. The approximating output, $\underline{f}_a(\underline{x})$, is comprised of the sum of two terms, one linearly related to $\underline{m}$ and the other linearly related to $\underline{r}$. The gain matrices, N_m and N_r, are chosen to minimize the generalized mean-square error between the actual and approximate outputs defined by $E[\underline{e}^T S \underline{e}]$ when S is any symmetric positive definite matrix. This is often referred to as a quasi-linear approximation technique and N_m and N_r are called generalized describing function matrices.

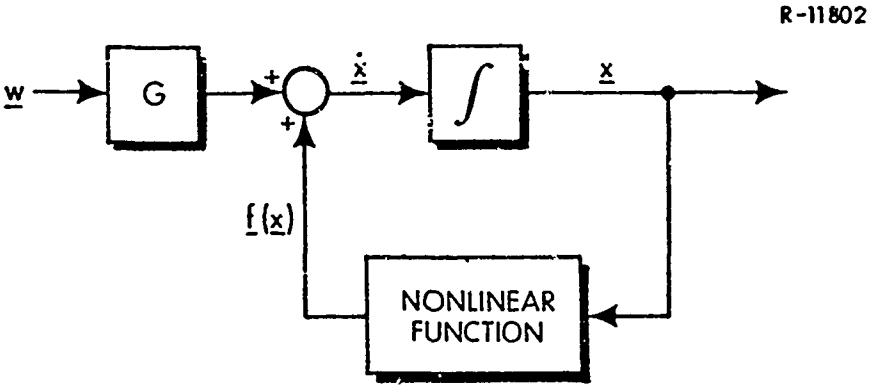

Figure C. 2-1 Nonlinear System Block Diagram

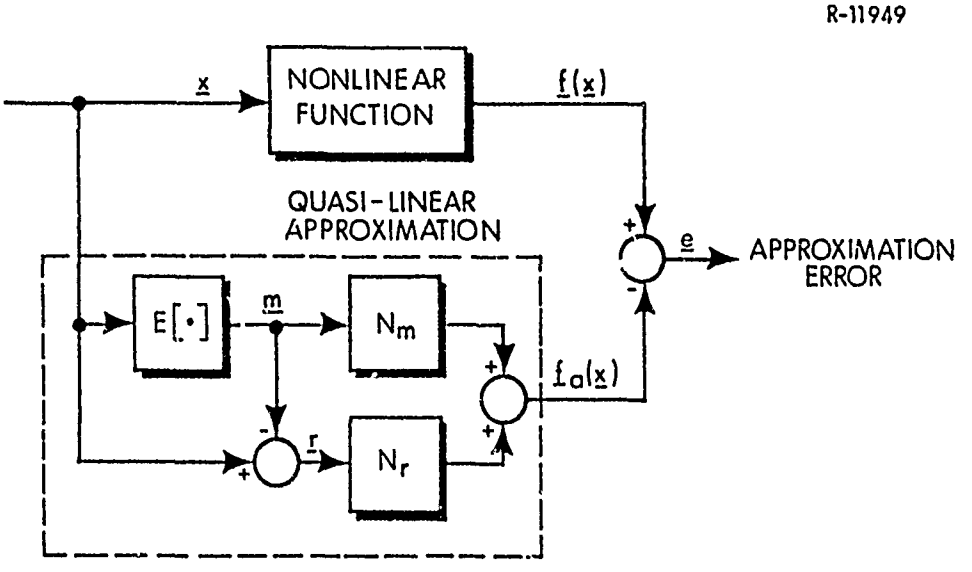

Figure C. 2-2 Quasi-Linear Approximation

Calculation of N_m and N_r is readily accomplished. Note first from Fig. C.2-2 that

$$\begin{aligned} \underline{e} &= \underline{f}(\underline{x}) - \underline{f}_a(\underline{x}) \\ &= \underline{f}(\underline{x}) - N_m \underline{m} - N_r \underline{r} \end{aligned} \tag{C.2-2}$$

Formally, it can be shown that $E[\underline{e}^T S \underline{e}]$ is minimized if N_m and N_r satisfy (Ref. 1)

$$\begin{aligned} N_m \underline{m}\,\underline{m}^T &= E[\underline{f}(\underline{x})]\,\underline{m}^T \\ N_r E[\underline{r}\,\underline{r}^T] &= E[\underline{f}(\underline{x})\,\underline{r}^T] \end{aligned} \tag{C.2-3}$$

The second relation directly defines N_r,

$$N_r = E[\underline{f}(\underline{x})\underline{r}^T]\, P^{-1} \tag{C.2-4}$$

since a unique P^{-1} always exists. Rather than attempting to solve for N_m -- which requires a pseudo inverse since $(\underline{m}\,\underline{m}^T)$ is always singular -- simply note that

$$N_m \underline{m} \triangleq \hat{\underline{f}} = E[\underline{f}(\underline{x})] \tag{C.2-5}$$

This result is all that is required to solve the problem at hand, as shown below.

Evaluating the expectations in Eqs. (C.2-4) and (C.2-5) requires an assumption about the probability density function of $\underline{x}(t)$. Most often a gaussian density is assumed, although this need not be the case from a theoretical point of view. However, the gaussian assumption leads to the significant computational simplification discussed in Section C.4. In addition, it is often physically reasonable

to assume that $\underline{x}$ is gaussian, because the superposition effect created by the linear part of the system dynamics tends to transform the nongaussian outputs of the nonlinearities into approximately gaussian state variables, by the central limit theorem (Ref. 9).

C.3 DEVELOPMENT OF THE MEAN AND COVARIANCE EQUATIONS

Replacing the nonlinear function of Fig. C.2-1 by the describing function approximation given in Fig. C.2-2 results in the quasi-linear system model illustrated in Fig. C.3-1. The quasi-linear system model consists of two parts; one part to propagate the mean or deterministic portion of the signal, and the other to propagate the random portion. Due to the nonlinearity of the system, the two loops are coupled through the describing function matrices; under the gaussian assumption, both matrices are functions only of the mean and covariance. The differential equation for the propagation of the mean vector for the quasi-linear system of Fig. C.3-1 is

$$\dot{\underline{m}} = N_m(\underline{m}, P)\,\underline{m} + G\underline{b} = \hat{\underline{f}} + G\underline{b} \qquad \text{(C.3-1)}$$

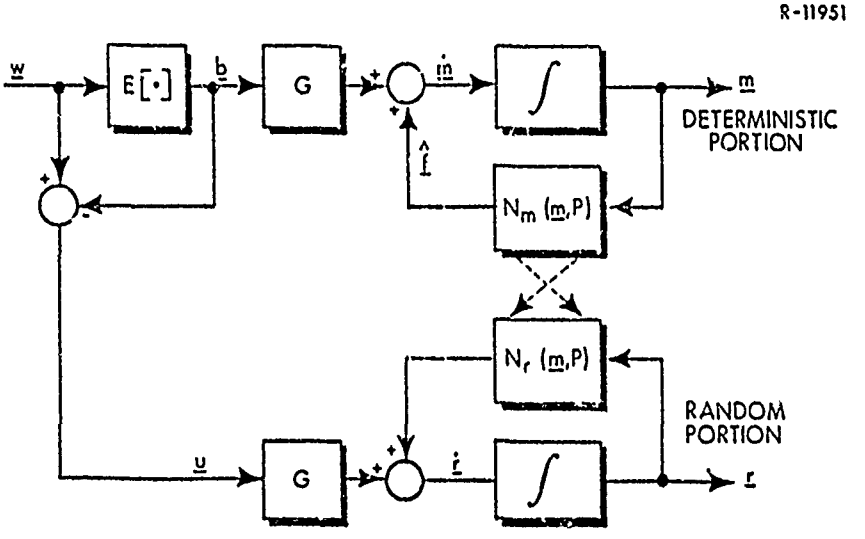

Figure C.3-1 Quasi-Linear System Model

The system covariance propagation equation is obtained by computing the covariance of the random signal component, $\underline{r}$, using linear system covariance analysis as discussed in Section C. 1. The resulting matrix covariance equation is

$$\dot{P} = N_r(\underline{m}, P)\, P + P N_r^T(\underline{m}, P) + GQG^T \qquad \text{(C. 3-2)}$$

These equations are nonlinear and coupled through the mean and random component describing function matrices, N_m and N_r, respectively. Initialization requires only the initial condition statistics,

$$\begin{aligned} \underline{m}(0) &= E[\underline{x}(0)] \\ P(0) &= E[\underline{r}(0)\underline{r}^T(0)] \end{aligned} \qquad \text{(C. 3-3)}$$

Equations (C. 3-1) and (C. 3-2) together with Eqs. (C. 2-4) and (C. 2-5) are the key equations of CADET.

C. 4 SPECIAL RELATIONSHIPS

A few special relationships are worth noting. First, we observe that when the system is linear [$\underline{f}(\underline{x}) = F\underline{x}$], Eqs. (C. 2-4) and (C. 2-5) immediately lead to the result $N_m = N_r = F$. Hence, Eqs. (C. 3-1) and (C. 3-2) reduce to the familiar equations for the propagation of the mean and covariance in linear systems, indicated in Eq. (C. 1-4). For a nonlinear system, computation of the describing function matrices in Eqs. (C. 2-4) and (C. 2-5) requires an assumption about the form of the probability density of the input signal to the nonlinearity. This, it should be noted, is the only assumption required in the CADET formulation. The assumption of a jointly gaussian probability density functio for the elements of $\underline{x}$ is most attractive from two viewpoints. First, the calculation of N_m and N_r tends to be simplest under this assumption. In addition,

many dynamic system models tend to contain more linear than nonlinear elements. This is advantageous, since low-pass linear filtering is necessary to insure that nongaussian nonlinearity outputs result in nearly gaussian nonlinearity inputs as signals propagate through the system. This so-called "filter hypothesis" is common to all describing functions analyses (Ref. 8).

One result of the gaussian assumption is that N_r can be directly computed (Ref. 16) from the relationship

$$N_r(\underline{m}, P) = \frac{d}{d\underline{m}} E[\underline{f}(\underline{x})] = \frac{d}{d\underline{m}} [N_m \underline{m}] \qquad \text{(C. 4-3)}$$

This is indeed a useful relationship, since calculating $N_m \underline{m}$ is required in any case for the propagation of the mean (Eq. (C. 3-1)). It is, in practice, much easier to employ Eq. (C. 4-3) than to solve Eq. (C. 2-4) for $N_r(\underline{m}, P)$. A direct result of Eq. (C. 4-3) is the fact that N_m and N_r can be formed by first replacing the individual nonlinear elements of $\underline{f}(\underline{x})$ by the appropriate scalar describing function gains. This is an extremely powerful property since a large number of describing functions have been catalogued in Ref. 8; consequently N_m and N_r can be formed directly from inspection of the system equations or block diagram, in many cases.

REFERENCES

1. Gelb, A. and Warren, R.S., "Direct Statistical Analysis of Nonlinear Systems: CADET," AIAA Journal, Vol. 11, No. 5, May 1973, pp.689-694.

2. Price, C.F. and Warren, R.S., "Performance Evaluation of Homing Guidance Laws for Tactical Missiles," The Analytic Sciences Corp., Report No. TR-170-4, January 1973.

3. Warren, R.S. and Siegel, J., "SAM-D Performance Analysis Using CADET," The Analytic Sciences Corp., Report Nos. TR-286-1 and TR-286-2, December 1972 and August 1973.

4. Bucy, R.S., Hecht, C. and Senne, K.D., "An Engineer's Guide to Building Nonlinear Filters," Seiler Research Lab. Report No. SRL-TR-72-0004 (USAF Systems Command), May 1972.

5. Bowker, A.H. and Lieberman, G.J., Engineering Statistics, Prentice-Hall, Inc., Englewood Cliffs, N.J., 1959.

6. Abramowitz, M. and Stegun, I.A. (editors), Handbook of Mathematical Functions with Formulas, Graphs, and Mathematical Tables, No. 55 in National Bureau of Standards Applied Mathematics Series, U.S. Department of Commerce, Washington, D.C., 1964.

7. Jazwinski, A.H., Stochastic Processes and Filtering Theory, Academic Press, New York, 1970.

8. Gelb, A. and Vander Velde, W.E., Multiple-Input Describing Functions and Nonlinear System Design, McGraw-Hill Book Co., New York, 1968.

9. Papoulis, A., Probability, Random Variables, and Stochastic Processes, McGraw-Hill Book Co., New York, 1965.

10. Peirce, B.O. and Foster, R.M., A Short Table of Integrals (Fourth Ed), Oxford University Press, London, 1956.

11. Gradshteyn, I.S. and Ryzhik, I.M., Table of Integrals, Series, and Products, Academic Press, New York, 1965.

12. Skolnik, M.I., Introduction to Radar Systems, McGraw-Hill, New York, 1962.

13. Goldstein, H., Classical Mechanics, Addison-Wesley, Reading, Mass., 1950.

14. Price, C.F., "Adaptive Control and Guidance for Tactical Missiles," The Analytic Sciences Corp., Report No. TR-170-1, June 1970.

15. Gibson, J.E., Nonlinear Automatic Control, McGraw-Hill, New York, 1963.

16. Phaneuf, R.J., "Approximate Nonlinear Estimation," Ph.D. Thesis, Dept. of Aeronautics and Astronautics, M.I.T., Cambridge, Mass., May 1968.